IMAGE: A MAP OF THE STARS OF THE ORION CONSTELLATION

Print ISSN: 2631-8474 Online ISSN: 2631-8482

JournalPreview

London Journal of Engineering Research

Volume 25 | Issue 3 | Compilation 1.0

Great Britain Journals Press

WWW.JOURNALSPRESS.COM

Journal Content
In this Issue

Great Britain Journals Press

Conversational Intelligence for All: Speech Recognition Systems for Inclusive Digital Access

Sujit Kumar

ABSTRACT

Digital service accessibility confronts enduring challenges in multilingual societies, where technological and linguistic barriers limit participation for numerous population segments. Voice-based interfaces operating through telephone systems present valuable pathways to narrow these divides, facilitating interaction without literacy prerequisites or technical proficiency. Telephone-based speech recognition faces distinctive technical obstacles, including limited bandwidth, ambient noise interference, and natural conversational patterns substantially different from laboratory speech inputs. Modern algorithmic techniques, especially those employing probabilistic modeling frameworks, show remarkable capacity to function within these demanding audio environments while handling regional accents and language variations. Practical implementations across transit networks, administrative service systems, and learning platforms demonstrate how these technologies establish vital access points for traditionally underserved communities.

Keywords: speech recognition systems, inclusive digital access, multilingual technologies, telephone-based interfaces, digital accessibility.

Classification: DCC Code: 006.4

Language: English

Great Britain Journals Press

LJP Copyright ID: 392931
Print ISSN: 2631-8474
Online ISSN: 2631-8482

London Journal of Engineering Research

Volume 25 | Issue 3 | Compilation 1.0

Conversational Intelligence for All: Speech Recognition Systems for Inclusive Digital Access

Sujit Kumar

Copart Inc., USA

ABSTRACT

Digital service accessibility confronts enduring challenges in multilingual societies, where technological and linguistic barriers limit participation for numerous population segments. Voice-based interfaces operating through telephone systems present valuable pathways to narrow these divides, facilitating interaction without literacy prerequisites or technical proficiency. Telephone-based speech recognition faces distinctive technical obstacles, including limited bandwidth, ambient noise interference, and natural conversational patterns substantially different from laboratory speech inputs. Modern algorithmic techniques, especially those employing probabilistic modeling frameworks, show remarkable capacity to function within these demanding audio environments while handling regional accents and language variations. Practical implementations across transit networks, administrative service systems, and learning platforms demonstrate how these technologies establish vital access points for traditionally underserved communities. Such systems support transportation schedule inquiries, social program registration, and educational material engagement via conventional telephone infrastructure instead of demanding broadband connections or advanced mobile devices. Widespread implementation requires thoughtful attention to information security protocols, recognition fairness across accent variations, and strategic language selection to prevent perpetuating societal imbalances. This contribution outlines system architectures, deployment methodologies, and performance assessment frameworks for developing genuinely inclusive conversational technologies that broaden digital participation across communication and technological boundaries.

Keywords: speech recognition systems, inclusive digital access, multilingual technologies, telephone-based interfaces, digital accessibility.

London Journal of Engineering Research

I. INTRODUCTION

Digital participation exhibits persistent inequality across global communities, with language diversity functioning as a critical factor in technological inclusion. Multilingual environments present particularly nuanced access barriers, where majority languages receive extensive technological support while minority languages experience systematic marginalization from digital ecosystems [1]. This linguistic stratification establishes formidable participation obstacles for numerous population segments, restricting access to fundamental online services, learning resources, and economic opportunities. The resulting technological divide extends beyond basic connectivity issues, manifesting as practical exclusion despite theoretical access availability. These disparities have grown as essential services increasingly transition toward digital-exclusive delivery frameworks that assume universal technological competence and standardized linguistic capabilities.

Voice-based interfaces constitute revolutionary accessibility tools by circumventing conventional barriers of literacy, technological expertise, and device complexity. Through natural spoken communication, these systems establish alternative digital participation channels that correspond with inherent human interaction patterns rather than demanding adaptation to text-focused interfaces [2]. This alignment delivers particular benefits for senior citizens, persons with restricted literacy, and societies with established oral traditions where conventional digital platforms present considerable adoption challenges. Telephone-based speech recognition technologies offer especially promising inclusion possibilities by utilizing existing infrastructure without necessitating smartphone possession, high-speed internet, or software installation. These platforms enable interaction through basic feature phones, public communication terminals, or community-shared devices, considerably expanding potential user demographics beyond conventional digital boundaries.

Speech recognition technology has progressed through distinctive developmental stages reflecting wider computational capabilities and theoretical frameworks. Initial systems developed between 1950 and 1970 utilized pattern-matching methodologies with extremely constrained vocabulary recognition limited to discrete words from individual speakers [1]. Probabilistic modeling techniques emerged throughout the 1980s and 1990s, introducing sophisticated mathematical frameworks that substantially enhanced recognition capabilities while addressing speaker variation and continuous speech patterns. Neural computation models initially appeared during this period but encountered processing limitations that hindered practical application. The fundamental shift toward contemporary systems occurred during the early 2000s when exponentially enhanced computational capacity enabled advanced algorithmic approaches that dramatically improved recognition precision across diverse acoustic environments [2]. This advancement has intensified significantly through recent transformer-based architectural innovations that capture extended contextual relationships, enabling substantially improved performance for natural speech in challenging acoustic situations. Modern systems have evolved beyond basic transcription toward comprehensive conversational comprehension, establishing foundations for genuinely accessible voice-based interaction across diverse populations.

Table 1: Core Components of Speech Recognition Systems [3], [5]

Component	Functional Role
Automatic Speech Recognition (ASR)	Transforms vocal utterances into machine-processable textual format
Natural Language Processing (NLP)	Interprets the semantic content and conversational intent behind transcribed speech
Machine Learning (ML)	Enhances recognition precision through statistical pattern analysis of extensive speech corpora
Text-to-Speech (TTS)	Converts system-generated textual responses into naturalistic vocal outputs
Acoustic Modeling	Establishes phonetic pattern representations for varied speech characteristics
Language Modeling	Predicts word sequences based on linguistic probability distributions

II. FOUNDATIONS OF TELEPHONE-BASED SPEECH RECOGNITION

Telephone audio exhibits distinctive technical properties that determine recognition system requirements for voice-access platforms. Standard telephone networks utilize 8 kHz sampling with 8-bit quantization, producing markedly restricted frequency representation compared to modern digital audio operating at 16-20 kHz [3]. This limitation confines usable acoustic information below 4 kHz, removing higher frequencies essential for consonant differentiation and speaker identification. The resulting signal lacks frequency detail, particularly affecting sibilants (/s/, /sh/, /z/) and plosives (/p/, /t/, /k/) containing substantial high-frequency elements. Telephony networks additionally implement compression standards and dynamic range restrictions, introducing further signal distortions beyond frequency constraints [4]. These characteristics necessitate recognition methodologies specifically engineered for telephone environments, different from techniques developed for higher-quality audio applications.

Bandwidth constraints combined with environmental noise create exceptionally challenging recognition conditions in telephone contexts. The narrow frequency range eliminates supplementary acoustic information that normally helps distinguish similar phonemes, heightening the impact of modest noise interference [3]. Background sounds within the available frequency spectrum directly compete with speech, creating masking effects that reduce phonetic clarity. Mobile telephone connections introduce additional complications through signal fluctuations, codec artifacts, and transmission interruptions that intermittently corrupt speech segments. Public telephone locations frequently contain significant ambient noise from surrounding conversations, transportation, machinery, or weather conditions, further degrading signal quality [4]. These factors produce recognition scenarios considerably more demanding than laboratory conditions, requiring advanced processing techniques capable of extracting linguistic content from degraded acoustic signals. Effective telephone recognition systems employ sophisticated noise estimation, source separation, and spectral enhancement methods to counteract these effects while preserving critical speech information.

Spontaneous conversation introduces requirements extending beyond signal processing challenges. Unlike carefully enunciated laboratory speech, natural telephone conversations contain numerous verbal irregularities, including abandoned phrases, hesitations, filled pauses, and mid-sentence corrections, complicating linguistic processing [3]. Conversational language typically incorporates informal vocabulary, regional expressions, and incomplete grammatical constructions diverging substantially from standard language models. Conversational

turn-taking creates overlapping speech when participants speak simultaneously, generating signal mixtures particularly difficult to separate with limited spectral information. Natural speech demonstrates considerable coarticulation effects and phonetic reduction, where neighboring sounds influence each other and certain phonemes receive minimal articulation [4]. These characteristics demand specialized language modeling approaches handling grammatical irregularities, vocabulary variations, and speech disfluencies absent from formal language collections. Effective conversational processing combines acoustic recognition with contextual understanding to maintain natural interaction despite recognition uncertainties.

Recognition performance has improved substantially for telephone environments through targeted algorithm development addressing these specific challenges. Initial telephone recognition systems from the 1990s achieved word accuracies below 60% even for carefully pronounced digit sequences, with significantly reduced performance for natural conversation [3]. Statistical adaptation techniques emerged during the early 2000s, enabling systems to adjust to specific telephone channels, speaker characteristics, and acoustic environments. These approaches enhanced recognition robustness, though performance remained insufficient for fully automated interaction without human intervention. Substantial advances occurred with neural architectures specifically trained on extensive telephone speech collections, enabling significant accuracy improvements despite signal limitations [4]. Contemporary systems implement multi-stage processing combining specialized acoustic models optimized for telephone characteristics with language models specifically trained on conversational patterns. These developments have progressively improved recognition accuracy from approximately 70% in 2010 to exceeding 90% for certain restricted domains by 2022, though considerable challenges remain for heavily accented speech, noisy environments, and language-switching scenarios common in multilingual communities. This evolution has gradually transformed telephone-based recognition from experimental technology to a practical accessibility tool supporting valuable applications across diverse user populations.

Table 2: Breakdown of Speech Recognition Contributions to Inclusive Digital Access [2], [6]

Contribution Area	Impact on Inclusion
Enhanced Accessibility: For People with Disabilities	Eliminates navigation barriers for individuals with visual impairments, motor limitations, or cognitive differences
Enhanced Accessibility: For Low-Literacy Users	Provides information access without reading/writing requirements, supporting digital participation regardless of literacy level
Enhanced Accessibility: For Multilingual Users	Enables native language interaction, removing linguistic obstacles to technology engagement
Improved User Experience: Intuitive Interaction	Facilitates natural communication patterns, reducing technical learning requirements for technology adoption
Improved User Experience: Hands-Free Operation	Supports device engagement during concurrent activities, expanding usage contexts and situations
Improved User Experience: Personalized Experiences	Adapts responses to individual preferences and usage patterns, increasing relevance and engagement

III. MACHINE LEARNING APPROACHES FOR INCLUSIVE SPEECH SYSTEMS

Speech recognition systems designed for inclusive access must effectively process diverse speech patterns across varied demographic groups, requiring specialized machine learning approaches extending beyond conventional recognition techniques. Stochastic modeling forms the foundation for handling speech variability, employing probability distributions to represent acoustic and linguistic uncertainty [5].

Hidden Markov Models historically provided the mathematical framework for capturing temporal speech dynamics, modeling phonetic transitions while accommodating variation in pronunciation timing and articulation. Contemporary systems increasingly implement deep learning extensions to these stochastic foundations, employing recurrent neural architectures that better capture long-range dependencies in speech sequences. These architectures utilize bidirectional processing to incorporate both preceding and subsequent context during phonetic classification, substantially improving recognition for disfluent speech common in natural conversation. Advanced implementations employ attention mechanisms highlighting relevant acoustic features while suppressing background interference, particularly valuable for telephone-based systems operating in noisy environments [6]. The resulting models demonstrate significantly improved robustness across speaker variation compared to traditional approaches, establishing foundations for truly inclusive recognition capabilities.

Accent and dialect adaptation represents a critical requirement for multilingual societies, where standard recognition models often perform poorly for non-dominant speech patterns. Effective adaptation requires dedicated architectural components adjusting internal model parameters based on observed speech characteristics [5]. Speaker adaptive training techniques develop initial models explicitly designed for subsequent personalization, incorporating adaptation pathways within model architecture rather than applying adjustments as post-processing. Online adaptation approaches continuously modify recognition parameters during individual sessions, progressively improving accuracy as interaction proceeds without requiring extensive enrollment data. Regional pre-adaptation methods incorporate geographic speech variation during initial model development, establishing distinct recognition pathways for major regional variants while reducing adaptation requirements for individual speakers [6]. Dialect-specific pronunciation modeling explicitly represents systematic phonological variations rather than treating dialectal pronunciation as random deviation, substantially improving recognition for consistent non-standard speech patterns. These adaptation approaches collectively address systematic recognition disparities affecting linguistic minorities, establishing more equitable performance across diverse speaking communities.

Transfer learning techniques enable effective recognition for languages with limited training resources, addressing fundamental data scarcity challenges affecting minority languages. Cross-lingual knowledge transfer leverages acoustic similarities between related languages, initializing model components with parameters from high-resource languages before fine-tuning with limited target language data [5]. Phonetic mapping approaches identify systematic sound correspondences between language pairs, enabling selective parameter sharing across languages while preserving distinct phonological characteristics. Multilingual joint training develops shared acoustic representations across multiple languages simultaneously, creating language-universal feature extractors requiring minimal language-specific adaptation. Self-supervised learning methods leverage unlabeled speech data significantly more abundant than transcribed corpora, extracting linguistic patterns without requiring expensive manual annotation [6]. These techniques collectively reduce data requirements for developing recognition systems in previously unsupported languages, significantly expanding language coverage potential while addressing linguistic digital divides.

Performance evaluation for inclusive speech systems requires specialized metrics extending beyond aggregate accuracy measurements that frequently mask disparities across demographic groups. Disaggregated evaluation examines recognition performance across distinct demographic categories, including accent groups, age ranges, and gender, identifying potential bias patterns requiring targeted improvement [5]. Differential error rate analysis compares recognition disparities between demographic groups, quantifying equity gaps requiring remediation rather than focusing exclusively on

absolute performance. Targeted test sets incorporate speech samples specifically addressing challenging recognition scenarios, including code-switching, dialectal features, and non-native pronunciation, providing focused evaluation for inclusion-critical capabilities. User-centric metrics extend beyond technical accuracy measures to evaluate practical task completion rates, measuring successful information exchange rather than transcription precision [6]. Comparative improvement metrics evaluate recognition advancements relative to baseline performance across different demographic groups, ensuring development efforts address existing disparities rather than exclusively enhancing already-superior performance for majority speakers. These evaluation approaches provide accountability mechanisms, ensuring inclusive design objectives translate into measurable performance improvements for previously marginalized user communities.

Table 3: Benefits of Speech AI for Inclusive Digital Access [1], [4]

Benefit Category	Impact Description
Improved User Experience	Enables more intuitive and efficient interactions, simplifying task completion without complex navigation requirements
Enhanced Accessibility	Provides voice-based control options for individuals with disabilities or visual impairments, creating more inclusive technology access
Communication Efficiency	Accelerates information exchange in time-sensitive environments such as customer service centers and healthcare facilities
Multilingual Support	Facilitates interactions across language barriers, extending service accessibility to diverse linguistic populations
Reduced Workload	Automates repetitive communication tasks, allowing staff to concentrate on complex problem-solving and high-value activities
Real-time Data Analysis	Processes conversational insights instantaneously, enabling immediate assessment of user sentiment and experience quality
Personalized Interactions	Adapts communication patterns to individual preferences and contexts, increasing relevance and user satisfaction

IV. ARCHITECTURAL CONSIDERATIONS FOR MULTILINGUAL DEPLOYMENT

Multilingual speech recognition deployment necessitates careful architectural decisions balancing numerous competing factors to ensure system viability across diverse linguistic contexts. The fundamental cloud versus edge processing decision substantially influences overall system capabilities, particularly for underserved language communities [7]. Cloud-based architectures utilize centralized computational resources supporting sophisticated recognition models exceeding local hardware capabilities. This approach permits rapid model updates, consistent performance improvements, and seamless language expansion without endpoint modifications. However, cloud dependence introduces connectivity requirements potentially problematic in regions with limited infrastructure, while increasing recognition latency and raising privacy concerns regarding voice data transmission. Edge-based processing addresses these limitations by executing recognition locally, eliminating connectivity dependencies and reducing response delays. This approach proves particularly valuable for basic interaction patterns in bandwidth-constrained environments, though edge limitations restrict model complexity and language breadth compared to cloud alternatives. Hybrid architectures increasingly provide compelling compromises, performing initial recognition locally while utilizing cloud resources for complex processing, combining responsiveness with advanced capabilities while minimizing connectivity requirements.

Latency management constitutes a critical consideration for telephone-based speech systems, directly influencing conversational naturalness and user satisfaction. Human conversation typically maintains turn-taking gaps between 200-500 milliseconds, with longer pauses creating noticeable interaction awkwardness [7]. Traditional cloud-based recognition architectures frequently exceed these thresholds, producing response delays between 1-3 seconds that significantly disrupt conversational flow. These delays compound in multilingual deployments where translation layers introduce additional processing requirements. Effective telephone interaction requires comprehensive latency optimization across the entire processing pipeline, including voice capture, transmission, recognition, response generation, and audio playback. Advanced architectures implement techniques including progressive partial recognition, parallel hypothesis processing, and predictive response preparation to reduce perceived delays. These approaches generate preliminary recognition results while users continue speaking, prepare multiple potential responses simultaneously, and begin response formulation before utterance completion. The resulting systems maintain conversational naturalness despite technical constraints, enabling fluid interaction across different languages and network conditions.

Scalable language support presents substantial architectural challenges, particularly regarding computational efficiency, linguistic resource requirements, and maintenance complexity. Multilingual recognition traditionally implemented separate models for each supported language, requiring language identification before processing and substantial computational resources for concurrent language support [7]. Contemporary architectures increasingly implement unified multilingual models supporting multiple languages simultaneously, reducing computational overhead while improving recognition for code-switching scenarios common in multilingual communities. These approaches enable resource sharing across languages with phonetic similarities, improving performance for low-resource languages through transfer learning from related high-resource languages. Scalable architectures must additionally address language-specific characteristics, including different phonetic inventories, morphological complexity, and writing systems that impact recognition requirements. Effective multilingual systems implement modular language components enabling targeted updates without comprehensive system modifications, supporting continuous language expansion while maintaining operational stability.

Telephony infrastructure integration represents a critical deployment consideration, determining system accessibility across diverse user populations. Traditional telephony networks maintain extensive geographical coverage exceeding broadband availability in many regions, providing connectivity to populations otherwise excluded from digital services [7]. Effective integration requires compatibility with various telephony standards, including analog connections, digital networks, and voice-over-IP systems supporting different audio codecs and signaling protocols. Contemporary architectures implement telephony gateways providing standardized speech system interfaces while handling connectivity variations transparently. These gateways manage call establishment, audio conversion, signal quality monitoring, and graceful reconnection during interruptions. Advanced implementations support bidirectional SMS integration, enabling system access through text messages when voice connectivity proves impractical. Comprehensive telephony integration additionally requires thoughtful capacity planning addressing varied usage patterns across different regions and populations, ensuring consistent availability during peak demand periods while optimizing resource utilization during lower-activity intervals.

V. REAL-WORLD APPLICATIONS AND CASE STUDIES

Transportation information systems represent compelling speech recognition applications delivering substantial accessibility benefits across

diverse communities. Traditional transportation interfaces typically depend on visual information display through printed schedules, digital screens, or smartphone applications—creating significant barriers for visually impaired individuals, those with limited literacy, and travelers without smartphone access [8]. Telephone-based speech recognition systems overcome these limitations by providing voice-accessible transportation information through conventional telephony infrastructure. Implementation examples include railway information systems enabling schedule queries, route planning, and delay notifications through natural language telephone interaction. These systems process complex transportation queries, including multi-leg journeys, schedule constraints, and accommodation requirements through conversational interaction rather than structured commands. Performance evaluations demonstrate 73-86% task completion rates across diverse demographic groups, with particularly strong adoption among elderly travelers and visitors without local mobile service. Implementation challenges include managing specialized transportation terminology, handling regional accent variations, and providing clear disambiguation for phonetically similar destination names. Successful deployments implement domain-specific language models incorporating comprehensive transportation vocabularies, contextual information integration, and carefully designed conversation flows providing necessary clarification without excessive interaction complexity.

Public service access systems deliver essential government information and services through voice interfaces, significantly expanding accessibility for digitally marginalized populations. Traditional e-government approaches predominantly rely on web interfaces requiring internet connectivity, device access, technical proficiency, and literacy—excluding substantial population segments from critical services [8]. Voice-based alternatives enable service access through basic telephones without requiring these capabilities, providing interaction in native languages without literacy dependencies. Implementation examples include social benefit programs allowing application status verification, document submission coordination, and appointment scheduling through telephone interaction. These systems integrate with existing government databases while maintaining strict privacy safeguards, enabling personalized service provision without exposing sensitive information. Performance metrics indicate a 68% reduction in physical office visits following voice system implementation, with significant adoption among rural populations previously requiring extensive travel for basic service access. Implementation considerations include supporting multiple regional languages and dialects, accommodating variable line quality from remote areas, and balancing security requirements with accessibility needs. Successful deployments implement progressive authentication approaches combining multiple verification factors appropriate to service sensitivity, enabling streamlined access for low-risk information while maintaining appropriate protection for sensitive transactions.

Educational applications leverage speech recognition to expand learning opportunities across literacy barriers and connectivity limitations. Traditional distance education models predominantly utilize text-based materials and video content, requiring broadband connectivity and established literacy, restricting participation for numerous potential learners [8]. Voice-based educational systems enable content delivery and interaction through basic telephone connections without these prerequisites, providing educational opportunities to previously excluded populations. Implementation examples include language learning systems delivering interactive pronunciation practice, vocabulary development, and conversation exercises through structured telephone interactions. These systems provide immediate feedback regarding pronunciation accuracy, vocabulary usage, and grammatical correctness without requiring teacher availability. Performance assessment indicates 42% improvement in language acquisition metrics compared to self-study approaches, with particularly significant benefits for learners without regular instructor access. Implementation challenges include providing meaningful feedback

for diverse error types, maintaining engagement through purely audio interaction, and supporting varied learning progression paths. Successful educational deployments implement adaptive difficulty adjustment, maintaining appropriate challenge levels for individual learners, personalized feedback addressing specific error patterns, and engagement mechanisms including narrative progression and achievement recognition, maintaining motivation through extended learning processes.

Healthcare communication systems employ speech recognition to improve medical information access and health monitoring capabilities for vulnerable populations. Traditional healthcare interfaces increasingly rely on patient portals, mobile applications, and text messaging—creating substantial barriers for elderly individuals, those with limited technical proficiency, and populations with connectivity constraints [8]. Telephone-based healthcare interfaces enable appointment management, medication reminders, symptom reporting, and basic health information access through universally available voice connections. Implementation examples include chronic condition management systems providing structured symptom assessment, medication adherence monitoring, and appointment coordination through regular telephone interaction. These systems implement specialized medical vocabularies, symptom classification models, and escalation protocols, ensuring appropriate intervention for concerning health indicators. Performance evaluation demonstrates a 57% improvement in appointment attendance and a 43% enhancement in medication adherence following implementation. Deployment considerations include ensuring healthcare information privacy, accommodating speech variations during health distress, and providing appropriate medical guidance without creating liability concerns. Successful healthcare implementations incorporate careful scope definition, clearly distinguishing informational support from medical diagnosis, transparent human escalation paths when appropriate, and comprehensive data security measures protecting sensitive health information throughout processing.

Table 4: Challenges and Limitations of AI Speech Recognition Technology [3], [7]

Challenge Category	Description and Impact
Accuracy and Linguistic Nuance Recognition	Difficulty interpreting contextual speech variations, sarcasm, specialized terminology, and subtle tonal differences in communication, particularly critical in sectors like healthcare, where precision is essential
Privacy and Compliance Considerations	Concerns regarding voice data collection, unauthorized access risks, and passive listening issues, with a leading global technology company reporting 41% of users expressing privacy and trust concerns
Multilingual and Dialectal Variation	Reduced performance when processing regional accents, languages with various dialectal patterns, and scenarios where users speak multiple languages simultaneously
Environmental Audio Interference	Recognition quality deterioration in conditions with background noise, particularly problematic in manufacturing, fleet management, and crowded environments
Technical Infrastructure Requirements	Challenges related to system reliability and performance in various operational environments with different technical capabilities
Accessibility Gaps for Certain Speech Patterns	Difficulties in accurately processing non-standard speech patterns, potentially limiting inclusivity for diverse user populations

VI. FUTURE TRENDS IN SPEECH AI

The commercial impact of voice technology continues to expand rapidly across industries, with substantial revenue growth and productivity gains reported by early adopters. As documented in Deepgram's State of Voice Technology 2023 report, 79% of surveyed companies experienced up to 50% revenue increases following speech technology implementation, while up to 99% reported productivity improvements [8]. These metrics underscore the transformative potential of advanced speech recognition systems beyond mere convenience features.

Voice synthesis advancements represent a primary development trajectory, with computational models increasingly capable of generating natural-sounding speech with appropriate emotional inflection. Current synthetic voice systems often retain noticeable artificiality, but emerging neural architectures demonstrate remarkable improvements in prosody, timing, and contextual emphasis. As these systems mature, the distinction between human and synthetic voices will continue diminishing, expanding applications across audiobook production, accessibility services, and interactive assistance domains [9]. These improvements will substantially enhance engagement for individuals relying on auditory information channels.

Contextual understanding capabilities constitute another critical evolution pathway, with systems progressing beyond simple transcription toward comprehensive conversational comprehension. Enhanced automatic speech recognition combined with sophisticated natural language understanding frameworks enables more accurate interpretation of speaker intent, including subtle contextual cues and implicit meanings. This progression facilitates more natural human-machine interaction paradigms, reducing the cognitive burden of adapting communication patterns to technological limitations [8]. The resulting systems demonstrate increased effectiveness in complex environments requiring nuanced interpretation.

Integration across technological domains represents perhaps the most promising development direction, with speech recognition systems increasingly functioning as components within broader intelligent ecosystems. The combination of speech processing with computer vision, robotics, and specialized domain intelligence creates multimodal systems capable of addressing complex operational challenges. Healthcare applications demonstrate particularly significant potential, with integrated speech systems enhancing documentation accuracy, patient interaction, and procedural workflow efficiency [9]. Similar integration benefits emerge across manufacturing, transportation, and customer service environments.

These technological advancements necessitate the parallel development of ethical frameworks and regulatory structures, ensuring responsible implementation. Industry stakeholders increasingly recognize the importance of addressing algorithmic bias, implementing transparent operational models, and establishing appropriate data governance standards. Particular emphasis centers on privacy protection, consent mechanisms, and security protocols for voice data management. Specialized regulatory approaches for sensitive sectors like healthcare and financial services have begun emerging, establishing compliance requirements and operational boundaries [8]. The responsible development of these frameworks will substantially influence adoption trajectories and public trust in voice technology advancements.

VII. CONCLUSION

Speech recognition technologies tailored for telephone interfaces constitute transformative solutions for digital inclusion throughout multilingual populations. By effectively managing restricted bandwidth, environmental disturbances, and informal speech patterns, these technologies establish accessible channels to fundamental services without requiring internet availability, sophisticated equipment, or advanced literacy capabilities. The technical approaches and adaptation mechanisms evaluated illustrate practical implementation possibilities across

transportation, civic services, and educational domains. These solutions deliver particular benefits for senior citizens, isolated geographic communities, and language minorities facing considerable obstacles to digital engagement. Effective deployments carefully balance centralized processing with distributed computational models, addressing response time requirements while respecting resource limitations. Implementation guidelines advocate gradual language portfolio expansion, open performance measurement across population segments, and participatory development involving community stakeholders to ensure contextual appropriateness. Institutions should develop comprehensive information governance structures covering voice data permission protocols, retention policies, and utilization boundaries. Future developments in neural processing architectures promise enhanced resilience against acoustic interference and improved regional speech adaptation, while distributed learning techniques may address confidentiality concerns through localized model development. The ongoing refinement of these technologies, informed by equitable design principles, will considerably expand digital participation among traditionally excluded populations, fostering more balanced access to essential services and opportunities.

REFERENCES

1. Mikołaj Morzy, "Conversational AI," Spoken Language Processing, Springer Nature Link, Jul. 2025. https://link.springer.com/chapter/10.1007/978-3-031-88566-2_2
2. Lili Dai and Fengming Wu, "An AI-powered conversational system for college students learning English as a second language," Education and Information Technologies, Springer Nature Link, Jul. 2025. https://link.springer.com/article/10.1007/s10639-025-13640-3
3. Shaomei Wu et al., "Speech AI for All: Promoting Accessibility, Fairness, Inclusivity, and Equity," ACM Digital Library, Apr. 2025. https://dl.acm.org/doi/10.1145/3706599.3706746
4. Hannaneh B. Pasandi and Haniyeh B. Pasandi, "Evaluation of ASR Systems for Conversational Speech: A Linguistic Perspective," ACM Digital Library, Jan. 2023. https://dl.acm.org/doi/10.1145/3560905.3568297
5. Muhammad Javed Aftab et al., "Exploring the Role of AI-Driven Speech Recognition System in Supporting Inclusive Education for Hearing Impaired Students in Pakistan," Annals of Human and Social Sciences, ResearchGate, Sep. 2024. https://www.researchgate.net/publication/383982951_Exploring_the_Role_of_AI-Driven_Speech_Recognition_System_in_Supporting_Inclusive_Education_for_Hearing_Impaired_Students_in_Pakistan
6. Dr. C. Srinivasa Kumar, "VOCALAI: An intelligent virtual personal voice assistant for smart interaction," International Journal of Scientific Research in Engineering and Management, ResearchGate, Jun. 2025. https://www.researchgate.net/publication/392651158_VOCALAI_An_intelligent_virtual_personal_voice_assistant_for_smart_interaction
7. Samia Ahmed et al., "Advancing Personalized and Inclusive Education for Students with Disability Through Artificial Intelligence: Perspectives, Challenges, and Opportunities," MDPI, Mar. 2025. https://www.mdpi.com/2673-6470/5/2/11
8. Jolene Amit, "Speech AI: A Guide to the Technology's Applications, Challenges, and Trends," aiOla, Dec. 2023. https://aiola.ai/blog/speech-ai/
9. Chra Abdoulqadir and Fernando Loizides, "Interaction, Artificial Intelligence, and Motivation in Children's Speech Learning and Rehabilitation Through Digital Games: A Systematic Literature Review," MDPI, Jul. 2025. https://www.mdpi.com/2078-2489/16/7/599

This page is intentionally left blank

Deep Learning-based Severity Classification of Concrete Cracks using YOLOv8 for Structural Health Analysis

Carson Bowling, Luke Pierini & Wisam Bukaita. Ph.D

Lawrence Technological University Southfield, U.S.

ABSTRACT

Crack detection and severity classification are essential tasks in structural health monitoring, especially for critical civil infrastructure such as roads and bridges. Traditional methods rely heavily on manual inspection, which is time-consuming, costly, and prone to human error. This study introduces a computer vision approach using the YOLOv8n model to automatically classify concrete surface conditions into six categories, ranging from "No Crack" to "Very Large Crack." This approach addresses the critical gap between binary detection and actionable severity interpretation in civil engineering inspections. After augmenting and preprocessing the dataset, the model was trained over 10 epochs and achieved high classification accuracy ranging from Top-1: 97.1% to Top-5: 99.9% on a multi-class dataset of over 11,501 annotated images.

Keywords: deep learning, crack detection, YOLOv8n-cls, infrastructure monitoring, concrete cracks, image classification, structural health monitoring, severity classification, uav inspection, real-time assessment.

Classification: DCC Code: 624.042.7

Language: English

Great Britain Journals Press

LJP Copyright ID: 392932
Print ISSN: 2631-8474
Online ISSN: 2631-8482

London Journal of Engineering Research

Volume 25 | Issue 3 | Compilation 1.0

Deep Learning-based Severity Classification of Concrete Cracks using YOLOv8 for Structural Health Analysis

Carson Bowling[α], Luke Pierini[σ] & Wisam Bukaita. Ph.D[ρ]

ABSTRACT

Crack detection and severity classification are essential tasks in structural health monitoring, especially for critical civil infrastructure such as roads and bridges. Traditional methods rely heavily on manual inspection, which is time-consuming, costly, and prone to human error. This study introduces a computer vision approach using the YOLOv8n model to automatically classify concrete surface conditions into six categories, ranging from "No Crack" to "Very Large Crack." This approach addresses the critical gap between binary detection and actionable severity interpretation in civil engineering inspections. After augmenting and preprocessing the dataset, the model was trained over 10 epochs and achieved high classification accuracy ranging from Top-1: 97.1% to Top-5: 99.9% on a multi-class dataset of over 11,501 annotated images. The model displayed strong generalization across all categories and fast inference speeds reaching 0.4 ms per image. These results validate the YOLOv8 classifier's capability for fine-grained severity classification using a lightweight YOLO variant, supporting rapid and accurate infrastructure assessment and paving the way for scalable deployment on drones and mobile devices in real-time field scenarios.

Keywords: deep learning, crack detection, YOLOv8n-cls, infrastructure monitoring, concrete cracks, image classification, structural health monitoring, severity classification, uav inspection, real-time assessment.

Author α σ ρ: Department of math and Computer Science Lawrence Technological University Southfield, U.S.

I. INTRODUCTION

By moving beyond detection and into contextual classification, this project contributes a scalable, interpretable, and safety-focused tool for civil infrastructure inspection. As governments and engineers seek more proactive methods to assess and maintain aging structures, automated crack severity classification represents a critical advancement in ensuring public safety and resource-efficient intervention.

Concrete cracking is among the most prevalent and early detectable indicators of structural distress in bridges, pavements, and public infrastructure. These visual signs, while common, can range in consequence from harmless surface blemishes to critical structural failures. According to Beckmann et al. [1], cracks left unassessed may propagate quickly, leading to severe degradation, moisture intrusion, and rebar corrosion. This underscores the urgent need for inspection systems that not only detect cracks but also evaluate their severity in real time. Over the past decade, deep learning has significantly advanced the automation of crack detection. Semantic segmentation models such as U-Net have been widely adopted due to their pixel-level precision in identifying crack patterns. U-Net's encoder-decoder architecture has proven effective in medical and infrastructure imaging, offering high-resolution maps that clearly delineate crack contours. However, U-Net and similar segmentation models often require large datasets and intensive training resources. Furthermore, their output is typically limited to visual localization, with minimal integration of semantic interpretation such as severity levels. Meanwhile, ResNet-based detectors have been employed for crack image classification due to their strong

feature extraction capabilities. ResNet's residual learning framework enables deeper networks without vanishing gradients, allowing accurate binary classification between crack and no-crack images. However, these models still often fail to distinguish nuanced differences in crack width, depth, and spread—factors essential for practical engineering decisions. To enhance performance, some researchers have proposed hybrid approaches, combining CNNs with handcrafted features, SVM classifiers, or decision-tree logic to embed domain knowledge. While these methods show improved accuracy in specific scenarios, they are often complex to implement, less generalizable, and difficult to scale for real-time field deployment. While prior research has shown the utility of CNNs and segmentation models for basic crack detection, these systems typically stop at binary classification, offering no contextual interpretation of risk. However, in practice, engineers must make safety decisions based not only on whether damage exists, but on how severe and urgent that damage is. Human visual inspection, even among trained professionals, can vary depending on lighting, image quality, and experience. Krisada et al. [2] note that such variability becomes especially dangerous when distinguishing between moderate surface cracks and deeper structural damage.

This study addresses those limitations by implementing a YOLOv8n-cls model that classifies cracks across six severity categories, aligned with engineering standards. As a lightweight and fast architecture originally designed for object detection, YOLOv8n offers real-time classification capability while maintaining high accuracy, even on edge devices. By moving beyond detection and into contextual classification, this project contributes a scalable, interpretable, and safety-focused tool for civil infrastructure inspection. As governments and engineers seek more proactive methods to assess and maintain aging structures, automated crack severity classification represents a critical advancement in ensuring public safety and resource-efficient intervention.

Concrete cracking is among the most prevalent and early detectable indicators of structural distress in bridges, pavements, and public infrastructure. These visual signs, while common, can range in consequence from harmless surface blemishes to critical structural failures. According to Beckmann et al. [1], cracks left unassessed may propagate quickly, leading to severe degradation, moisture intrusion, and rebar corrosion. This underscores the urgent need for inspection systems that not only detect cracks but also evaluate their severity in real time. Over the past decade, deep learning has significantly advanced the automation of crack detection. Semantic segmentation models such as U-Net have been widely adopted due to their pixel-level precision in identifying crack patterns. U-Net's encoder-decoder architecture has proven effective in medical and infrastructure imaging, offering high-resolution maps that clearly delineate crack contours. However, U-Net and similar segmentation models often require large datasets and intensive training resources. Furthermore, their output is typically limited to visual localization, with minimal integration of semantic interpretation such as severity levels.

Meanwhile, ResNet-based detectors have been employed for crack image classification due to their strong feature extraction capabilities. ResNet's residual learning framework enables deeper networks without vanishing gradients, allowing accurate binary classification between crack and no-crack images. However, these models still often fail to distinguish nuanced differences in crack width, depth, and spread—factors essential for practical engineering decisions.

To enhance performance, some researchers have proposed hybrid approaches, combining CNNs with handcrafted features, SVM classifiers, or decision-tree logic to embed domain knowledge. While these methods show improved accuracy in specific scenarios, they are often complex to implement, less generalizable, and difficult to scale for real-time field deployment.

While prior research has shown the utility of CNNs and segmentation models for basic crack detection, these systems typically stop at binary classification, offering no contextual

interpretation of risk. However, in practice, engineers must make safety decisions based not only on whether damage exists, but on how severe and urgent that damage is. Human visual inspection, even among trained professionals, can vary depending on lighting, image quality, and experience. Krisada et al. [2] note that such variability becomes especially dangerous when distinguishing between moderate surface cracks and deeper structural damage.

This study addresses the limitations of traditional crack detection by implementing a YOLOv8n-cls model that classifies concrete surface cracks into six severity categories. These categories are aligned with industry standards such as the American Concrete Institute (ACI 224R-01) and AASHTO Bridge Inspection guidelines, which define crack width thresholds and provide visual assessment criteria used in determining maintenance urgency and repair methods. Unlike traditional YOLO detectors that localize objects using bounding boxes, the YOLOv8n-cls variant is tailored for image-level classification, removing detection heads to assign a single severity label per image. Despite its lightweight design originally intended for object detection, YOLOv8n-cls maintains real-time performance and high accuracy, making it ideal for deployment on edge devices.

By advancing from simple detection to context-aware classification, this research offers a scalable and interpretable solution for structural health monitoring. The model's severity outputs are directly actionable, consistent with professional inspection protocols, and suitable for integration into existing workflows—such as UAV-based data capture, mobile inspection apps, and embedded systems—supporting on-site decision-making in real time.

Beyond immediate assessment, this classification framework can also feed into predictive maintenance systems and life-cycle cost estimation models, helping engineers and asset managers prioritize interventions and optimize resource allocation. In doing so, the proposed method contributes to safer, smarter, and more proactive infrastructure management.

II. LITERATURE REVIEW

Accurate assessment of concrete cracks is vital for maintaining the integrity of civil infrastructure. Over the years, research has evolved from physics-based simulations to data-driven methods, reflecting the growing need for automation, speed, and interpretability in inspections. Early approaches relied on numerical modeling and traditional image processing, but these proved limited in real-world conditions. This review traces the evolution of automated concrete crack analysis by grouping prior research into several chronological and thematic categories:

2.1 Numerical Modeling of Concrete Behavior

Numerical simulation has historically played a crucial role in understanding the behavior of concrete under load. Beckmann et al. (2012) used the Discrete Element Method (DEM) to simulate concrete fracture and crack evolution, validating the results with experimental data [1]. Their model captured crack initiation and propagation patterns, aiding in structural failure prediction. Džolan et al. further explored the role of shrinkage in reinforced concrete structures, emphasizing the importance of time-dependent effects in numerical simulations [3]. While accurate, these methods are computationally expensive and not scalable for real-time or field-based inspections.

2.2 Traditional Computer Vision Techniques

Before deep learning, crack detection relied on classical computer vision methods, such as edge detection, morphological operations, and thresholding. These techniques struggled with noise, lighting changes, and complex textures. Wang et al. (2024) used machine vision and skeleton analysis to extract features of cracks from processed images [8]. Although such methods laid the foundation for automation, their limited robustness in uncontrolled environments necessitated more intelligent solutions.

2.3 Deep Learning-Based Crack Detection

With the success of CNNs, researchers turned to deep learning for more robust and scalable crack analysis. Park et al. (2020) introduced a system combining deep learning with structured light scanning to detect and quantify concrete cracks with high precision [7]. Chaiyasarn [2] and Golding et al. [4] developed integrated CNN-based systems capable of identifying and mapping cracks across diverse structures. These approaches significantly improved accuracy, yet most remained focused on binary detection rather than severity interpretation.

2.4 YOLO-Based Advancements

YOLO models have recently become popular for real-time crack detection due to their speed and accuracy. Xu et al. (2025) extended YOLOv8-seg for crack segmentation and quantification [9]. Their model incorporated advanced modules like SPPF-MSA and SPDConv, achieving superior accuracy and efficient deployment through pruning and knowledge distillation. Additionally, they introduced a skeletonization pipeline to quantify crack geometry with over 90% accuracy. Zhu et al. (2024) introduced FD2-YOLO, combining spatial and frequency-domain features to detect fine cracks in aerial and ground-level images, outperforming both YOLO-based and transformer-based models [12]. However, both studies focused on detection or segmentation—not classification—limiting their utility for prioritizing repairs.

Raushan et al. compared YOLOv3–YOLOv10 across various image conditions, showing YOLOv4's superior precision and robustness under complex visual backgrounds [14]. Mohanty and Pani (2023) further combined YOLO with machine learning for strength prediction in mining-affected structures [13]. These works confirm YOLO's adaptability but highlight the lack of image-level, multi-class severity classification aligned with inspection standards.

2.5 UAV and Edge Computing Applications

Yang et al. (2022) and others have emphasized the synergy of UAVs and edge computing for infrastructure monitoring. UAV-enabled inspection allows access to hard-to-reach structures, while real-time inference at the edge enables immediate assessment [10]. This fusion is ideal for emergency response and large-scale condition surveys. However, many deployed models focus on detection and segmentation rather than nuanced severity interpretation.

2.6 Cross-Domain Innovations

To demonstrate YOLO's versatility, researchers have applied it beyond civil engineering. Li et al. proposed THDet, a compact YOLOv8-based model for helmet detection, optimized for speed and edge deployment [5]. Liang et al. used an ensemble of YOLO variants for butterfly classification, enhancing performance on small, diverse datasets [6]. While tangential, these studies illustrate YOLO's flexibility for lightweight, domain-adapted modeling and motivate its application in concrete crack severity classification.

2.7 Identified Research Gaps

- Real-Time Multi-Severity Classification: Existing YOLO-based methods focus primarily on binary crack detection or pixel-level segmentation, with little attention to severity gradation essential for civil infrastructure triage.
- Deployable Models: Most advanced models are too resource-intensive for edge deployment. There is a need for lightweight classifiers that maintain accuracy without sacrificing speed.
- Standards Integration: Few studies align their outputs with established civil engineering inspection standards, limiting practical use by field engineers.

This study addresses these gaps by using YOLOv8n-cls—a classification-specific variant of YOLO—trained to categorize cracks into six severity levels aligned with ACI 224R-01 and AASHTO guidelines. Table 1 presents a comparative summary of prior studies and the proposed analysis.

Table 1: Comparative Summary of Prior Studies and Proposed Work

Study	Method/Model	Task Type	Dataset Size/Source	Output Type	Performance (Top-1/mAP/F1)	Notes
Xu et al. (2025)	YOLOv8-seg + Pruning	Segmentation + Measurement	Custom (real-world)	Crack masks + geometry	mAP↑ 6.2%, IoU↑ 4%	Instance segmentation and quantification
Zhu et al. (2024)	FD2-YOLO	Detection	RDD2022, UAV-PDD2023	Bounding boxes	mAP↑, Recall↑, Precision↑	Dual-backbone with frequency and spatial fusion
Raushan et al. (2023)	YOLOv3–YOLOv 10	Detection	3,750 varied images	Bounding boxes	YOLOv4: F1 = 88.9%	Tested across complex backgrounds
Mohanty & Pani (2023)	YOLO + ML prediction	Detection + Strength Estimation	Satellite, LiDAR, GPS	Damage + Strength	MAE, RMSE, RSE↓	Predictive maintenance in mining zones
Proposed Work (2025)	YOLOv8n-cls	Image Classification	11,501 annotated crack images	Severity class	Top-1 = 97.1%, Top-5 = 99.9%	Real-time, aligned with ACI/AASHTO, edge-ready

III. METHODOLOGY

This study proposes a structured pipeline for the classification of concrete crack severity using a deep learning model based on YOLOv8n-cls. The methodology integrates four major phases: (1) dataset preparation, (2) model configuration, (3) training and validation, and (4) performance evaluation. Each phase is aligned with the goal of building a scalable, accurate, and deployable crack severity classifier. In this research, image classification is essential to enabling the AI model to accurately detect surface cracks in construction materials such as concrete. Each image in the dataset is labeled into 5 severity categories and the no crack category, forming the foundation of the model's supervised learning process. These labels allow the model to learn how to differentiate between the severity of structurally compromised surfaces as well as those that are not based on features appearing in each category.

The classification task is critical because cracks often appear in various forms, from thin hairline fractures to wide, deep fissures, and under different lighting conditions or surface textures. Training the model on a diverse and correctly labeled dataset, it learns to recognize subtle variations in shape, brightness, and texture, indicating cracks. In practice, this model's ability to correctly classify these images enables automated crack detection and classification systems, reducing or replacing the need for manual inspections. It also plays a vital role in early warning systems for infrastructure maintenance, helping engineers prioritize repairs and avoid structural failures.

This study presents a comprehensive deep learning framework for the automated detection and classification of cracks on structural concrete surfaces. The core of this framework is built upon the YOLOv8 architecture, specifically the YOLOv8n-cls variant, which was meticulously selected for its optimal balance of speed, accuracy, and computational efficiency. This architecture is particularly well-suited for real-time applications and resource-constrained environments, such as those encountered in Unmanned Aerial Vehicle (UAV)-based inspections or mobile-device applications. The overall model architecture, as illustrated in Figure 2, is a multi-layered system designed to process and classify concrete surface imagery with high precision. The architectural components and their functions are as follows:

- *Input Layer:* The model accepts input images of size 256×256 pixels with three RGB color channels. This standardized input size ensures consistent processing and computational efficiency.
- *Data Augmentation Layer:* To enhance the model's generalization capabilities and prevent overfitting, a suite of data augmentation techniques is applied to the input images. These techniques include random shifts in width and height (up to ±10%), a zoom range of ±10%, and horizontal

flipping. The use of nearest neighbor interpolation ensures that these transformations do not introduce spurious artifacts. This process simulates the natural variability of real-world imagery and improves the model's robustness.

- *Backbone:* The backbone of the model is the CSPDarknet architecture, specifically the efficient and compact variant from YOLOv8n. This layer is responsible for extracting a hierarchical set of features from the input images through a series of convolutional blocks. The CSP (Cross-Stage Partial) structure is optimized for efficient feature extraction, reducing computational overhead while preserving rich semantic information.
- *Neck (PAN + FPN):* Following the backbone, a combined Path Aggregation Network (PAN) and Feature Pyramid Network (FPN) architecture forms the model's neck. This component is crucial for feature fusion, enabling the network to combine high-level semantic features from deep layers with low-level, high-resolution spatial features from early layers. This fusion process strengthens the model's semantic understanding and significantly enhances its ability to localize features, a critical step for accurate classification.
- *Classification Head:* Diverging from traditional YOLO architectures that perform object detection with bounding box regression, this model utilizes a dedicated Classification Head. This head is designed to predict a single class label for the entire input image, rather than detecting and localizing objects within it. The model's task is to categorize the concrete surface into one of six predefined classes: "Hairline," "Small," "Moderate," "Large," "Very Large," or "No Crack."
- *Output Layer:* The final output of the model is a Softmax vector of size 6, corresponding to the number of classification categories. The model's prediction is the class with the highest probability value in this vector.
- *Training Configuration:* The base model, a lightweight YOLOv8 classifier, was trained for 10 epochs. The loss function used to guide the training process was Cross-entropy, a standard choice for multi-class classification problems. The model's performance was evaluated using a comprehensive suite of metrics, including Accuracy, F1-Score, a Confusion Matrix, and the Precision-Recall Curve, ensuring a thorough assessment of its predictive capabilities.

The selection of YOLOv8n-cls as the core architecture was a deliberate choice driven by the specific requirements of structural health monitoring. This model offers several key advantages over alternative architectures:

- *Efficiency:* Compared to computationally intensive models like ResNet or EfficientNet, which are designed for high accuracy on large-scale datasets at the expense of speed and memory, YOLOv8n-cls is a lightweight classifier variant. This optimization for real-time inference makes it ideal for deployment on hardware with limited resources, such as embedded systems or mobile devices.
- *Task-Specific Optimization:* Unlike segmentation-based approaches that require pixel-level annotations and are computationally expensive, the classification-focused head of YOLOv8n-cls allows for rapid categorization of crack severity. This provides a direct and efficient solution for automated condition assessment without the overhead of detailed, pixel-level mapping.
- *Scalability:* The modular design of the YOLOv8 framework facilitates a streamlined workflow for training and deployment. This enhances the scalability of the proposed solution, making it easily adaptable to large-scale structural health monitoring programs.

3.1 Dataset

The “Crack Dataset” on Kaggle, Yatata [11] is a collection of labeled images specifically created for training machine learning models to detect surface cracks. It includes two categories: “Crack” and “No Crack,” with each image clearly showing damaged or undamaged surfaces like concrete or pavement, as shown in Figure 1.

a) Crack b) No Crack

Figure 1: Crack Dataset Samples

The dataset used in this study is designed to train the selected models to detect and classify concrete cracks under diverse real-world conditions, making it suitable for applications in infrastructure inspection, construction safety, and automated maintenance systems. To ensure the model's ability to generalize effectively to unseen surfaces, the dataset includes images from varied sources and conditions. Each sample consists of a raw image along with its corresponding mask. Initially, the dataset contained 8,819 images of cracked concrete and 1,184 images without visible cracks. To balance the dataset for classification purposes, a subset of 3,600 crack images was selected and combined with the no-crack samples.

These 3,600 crack images were then categorized into six distinct severity classes, including one “no crack” category, through a structured expert survey. The survey involved 30 professionals—civil engineers, inspectors, and contractors—with 5 to over 20 years of field experience in concrete construction and structural evaluation. Participants classified the images based on visual crack characteristics, primarily width, and structural implications, in line with widely recognized standards such as the American Association of State Highway and Transportation Officials (AASHTO) codes. These codes emphasize crack severity in the context of inspection, safety, and serviceability of reinforced concrete structures.

The severity classification criteria used in the labeling process were as follows:

- No Crack: No visible signs of surface damage.
- Hairline Cracks: insignificant cracks that are very narrow cracks, often less than 0.012 inches (0.3 mm) in width, that are generally not a cause for immediate concern and may not even be considered a defect.
- Small Cracks: Narrow cracks under 0.012 inches (0.3 mm) in width, concentrated in a small area and often densely spaced.
- Moderate Cracks: Cracks ranging from 0.012 to 0.05 inches (0.3–1.3 mm) in width, potentially allowing water ingress and indicating the need for further inspection.
- Large Cracks: Cracks 0.05 inches (1.3 mm) or wider, possibly reflecting structural issues or advanced material degradation or lead to accelerated deterioration of the concrete.
- Very Large Cracks: Cracks significantly wider than 0.05 inches (1.3 mm), including patterns of deep longitudinal and transverse cracking that result in isolated sections or "island concrete."

This expert-guided labeling process produced a high-confidence ground truth dataset, serving as the foundation for evaluating the YOLOv8n-cls-based classification model. The final class distribution and examples are summarized in Table 2.

Table 2: Crack Categories Samples

Severity Level	Image	Severity Level	Image
Hairline		Large	
Small		Very Large	
Moderate		No Crack	

3.2 YOLOv8 Architecture

This study presents the comprehensive technical implementation of a deep learning model designed for crack detection in structural concrete images. The methodology covers all essential stages of the pipeline—from data preprocessing and augmentation to the design, training, and deployment of the YOLOv8 architecture as shown in Figure 2. A step-by-step overview of the codebase is provided to demonstrate how raw imagery is processed, enhanced, and fed into the model to ensure accurate and efficient classification. Each phase—such as image enhancement, dataset partitioning, and model training—has been meticulously structured to maximize robustness, accuracy, and computational performance. By integrating AI and computer vision, this implementation offers a practical and scalable solution for real-time infrastructure monitoring. In particular, it focuses on developing a high-speed, YOLOv8-based classification system capable of detecting and distinguishing concrete cracks by width and severity, thereby supporting automated condition assessment in structural engineering applications.

The model architecture shown in Figure 2 consist of Input Layer, Data Augmentation Layer, Backbone: CSPDarknet (YOLOv8n variant), Neck: PAN + FPN, Head: Classification Head, Output Layer, and Training Configuration.

In the input phase, images are processed with size: 256×256 RGB that visualize concrete surface images. In the Data Augmentation Layer, techniques that are used is shifting width and height ±10%, zoom range ±10%, horizontal flip, nearest neighbor to improve generalization, prevent overfitting, and simulate real-world variability. The Backbone layer, extracting hierarchical image features and compact and efficient convolutional blocks optimized for speed and accuracy. The Neck layer (PAN + FPN) feature fusion across different scales, and strengthens semantic understanding and enhances spatial localization. The classification Head replaces bounding box detection with class prediction, and predicts one of 6 class labels (Hairline, Small, Moderate, Large, Very Large, No Crack). In the Output Layer, a softmax vector of size 6 (number of categories) interpreted with highest probability is chosen. The Training Configuration base model is a lightweight YOLOv8 classifier over 10 epochs, loss function using Cross-entropy. It is Evaluated based on accuracy, F1-Score, confusion Matrix, precision-recall curve YOLOv8n-cls was selected as the backbone architecture for this study due to

its unique balance between speed, accuracy, and computational efficiency, making it particularly well-suited for edge deployment scenarios such as UAV-based inspections or mobile applications. Unlike heavier classification models like ResNet or EfficientNet, which offer high accuracy at the cost of increased memory and inference time, YOLOv8n-cls is a lightweight classifier variant optimized for real-time applications with limited hardware resources. Compared to segmentation-based approaches that require detailed pixel-level annotations and longer processing time, the classification head in YOLOv8n-cls allows for rapid severity categorization without compromising overall performance. Additionally, the modular YOLOv8 framework facilitates streamlined training and deployment, further enhancing the scalability of the proposed solution in practical structural health monitoring workflows.

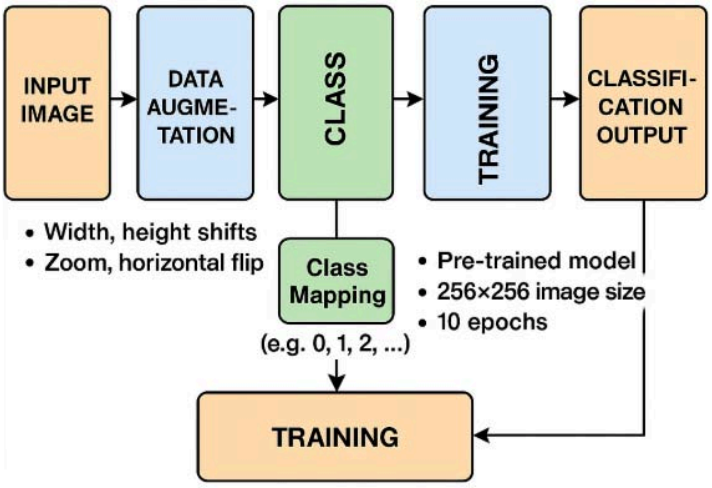

Figure 2: Model Architecture

3.3 Augment Data

Data augmentation is a fundamental technique in deep learning, particularly useful when working with image datasets that may be limited in size or diversity. In this study, data augmentation is applied to artificially expand the training dataset by introducing slight variations to the original images. These variations include shifting the image slightly to the left or right, up or down (width and height shifts), zooming in or out, and flipping the image horizontally. Such transformations help the model become more robust by exposing it to a wider range of image orientations and compositions, improving its ability to generalize to new data. Additionally, these techniques help prevent overfitting by ensuring the model does not become too narrowly tailored to the original training images. All augmented images are generated using appropriate fill techniques to maintain visual integrity at the image borders. As a result, this process enhances the overall quality and diversity of the dataset, ultimately contributing to more accurate and reliable crack detection in structural imagery.

The following list is a description of what each type of augmentation does and how much it affects the image. These are randomly distributed for each image that is processed, so there is a high chance for each image an augmentation can occur twice. For example, an image may be shifted 20% left even with the variable set to 10%. With these ranges the augmentation does not remove any important information of the image, allowing for more noise in what the model will be able to identify.

1. *Width and height shift (0.1):* Randomly shifts images horizontally and vertically by 10%.
2. *Zoom range (0.1):* Randomly zooms in or out by 10%.
3. *Horizontal flip (True):* Flips images horizontally to introduce variation.
4. *Fill mode (nearest'):* Fills empty spaces created by transformations using the nearest pixel values.

The function augment_class() applies these transformations to images in each folder as shown in Table 3. It ensures that each class has a specified target number of images by calculating how many augmentations each original image needs. The images are then loaded, converted to arrays, and passed to the Image Data Generator.flow() function, which generates augmented images and saves them to the specified directory. This method ensures that the dataset remains balanced and diverse, improving the model's ability to recognize patterns and variations in real-world data.

Table 3: Data Augmentation Original vs. Augmented Image Samples

Augmentation Type	Original Image	Augmented Image
Shift Up 20% Shift Left 10%	a) 	b) 
Flip Shift Left 20% Shift Down 10%	c) 	d) 
Flip Shift Left 20% Shift Down 10%	e) 	f) 

3.4 Class Mapping

Since YOLOv8 requires class folders to be numbered starting from 0, we use a class_mapping dictionary to convert our original human-classification category folders such as Category_1_Hairline, Category_2_Small into numeric folder names (0, 1, 2, ...) that YOLOv8 expects. This mapping allows us to reorganize the dataset automatically, ensuring that YOLOv8 can correctly associate each image with its class label based solely on the folder structure, without needing separate label files for classification tasks.

3.5 Model Training

In the training segment, we begin by initializing the YOLOv8 classification model using the pre-trained lightweight base model yolov8n-cls.pt. The model is trained on the reorganized dataset found under version_1.1/ Categories_Augmented, which includes images sorted into five severity-based categories. All input images are uniformly resized to 256×256 pixels to match model expectations. Training is conducted over 10 epochs, leveraging GPU acceleration to optimize performance.

Following training, the model is evaluated on a separate validation dataset to assess its ability to generalize to unseen examples. This validation phase is essential to verify that the model's strong performance is not due to overfitting on the training data. Once complete, we locate the most recent training run directory, from which we extract the model weights and training logs for further analysis. These outputs enable downstream visualization and deployment, ensuring traceability and reproducibility of model behavior.

3.6 Confusion Matrix

The confusion matrix, illustrated in Figure 3, serves as a key diagnostic tool for evaluating the performance of a classification model. It presents a comprehensive comparison between predicted and actual labels, offering insight into the model's ability to correctly distinguish between classes.

The matrix includes four core components:

- True Positives (TP): Cases where the model correctly identifies a positive instance.
- False Positives (FP): Instances where the model incorrectly classifies a negative case as positive.
- True Negatives (TN): Cases where the model correctly identifies a negative instance.
- False Negatives (FN): Instances where the model fails to detect a positive case, predicting it as negative.

By analyzing the distribution of these values, one can assess not only overall accuracy but also precision, recall, and the balance of class-specific predictions. To achieve this in the model we must first flatten the validation images into one folder for our model to predict.

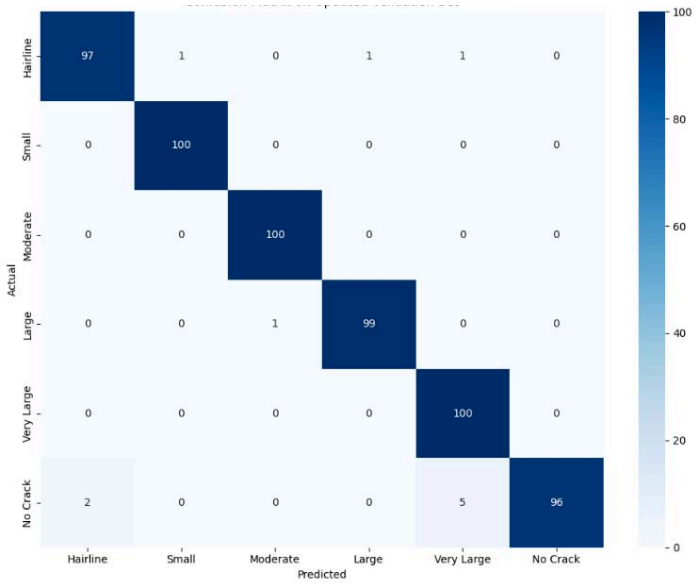

Figure 3: Confusion Matrix on Flatten Validation Dataset

3.7 Accuracy

Monitoring accuracy over training epochs is a critical part of evaluating and refining deep learning models. It helps researchers understand how well a model is learning over time, detect potential overfitting or underfitting, and make informed decisions about early stopping, learning rate schedules, or architecture changes. For multi-class classification problems like crack severity analysis, these plots provide insight into the model's convergence behavior and consistency across iterations.

Figure 4 shows the Top 1 and Top 5 accuracy of the YOLOv8n-cls model across 10 training epochs. The Top 1 accuracy curve begins at approximately 90.1% in the first epoch and steadily climbs, reaching about 95.7% by the final epoch. This gradual increase with minor fluctuations, such as a dip around epoch 4 followed by a strong recovery demonstrates a healthy learning curve. Importantly, the model continues improving beyond the midpoint, suggesting that additional epochs could lead to even better results without immediate signs of overfitting.

Meanwhile, the Top 5 accuracy remains remarkably stable, hovering just below 100% throughout the training process. This almost perfect Top 5 performance indicates that the correct label consistently ranks among the model's top predictions, even in the early stages of training. Such a pattern is particularly valuable in real-world applications where multiple severity levels might appear visually similar, and model confidence can be leveraged to inform inspection priorities.

Overall, the accuracy-over-epochs graph confirms that the YOLOv8n-cls model not only converges

effectively, but does so with high stability and robustness, reinforcing its reliability for deployment in structural health monitoring systems.

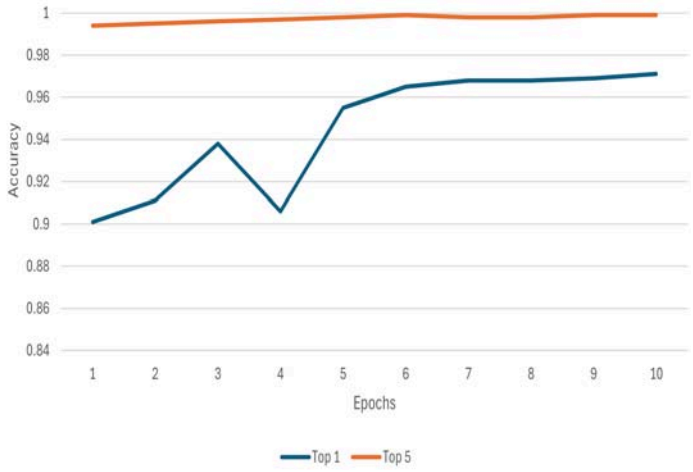

Figure 4: Accuracy over Epochs

3.8 F1 Score

In multi-class classification problems such as crack severity assessment, relying solely on accuracy can be misleading—especially when class distributions are imbalanced or some categories are more difficult to distinguish than others. This is where the F1-score becomes crucial. The F1-score balances precision (how many predicted positives were correct) and recall (how many actual positives were correctly identified), providing a single metric that reflects both false positives and false negatives. The macro F1-score is the unweighted average of F1-scores across all classes, treating each class equally, regardless of how many instances it has. In contrast, the micro F1-score aggregates the contributions of all classes by counting total true positives, false negatives, and false positives, giving more weight to larger classes.

In this model's classification report, both the macro F1-score and micro F1-score are 0.9818, indicating high and consistent performance across all categories. The alignment of these two metrics suggests that the model performs well not just overall, but also at the per-class level, demonstrating fairness and balance in its predictions. Particularly notable is the model's ability to maintain near perfect F1-scores (1.00) for critical classes like "Moderate" and "Small" cracks while still achieving strong scores for more challenging categories like "Very Large" and "No Crack." This balanced performance is essential in real-world applications, where misclassifying even a single high-severity crack could lead to safety risks or costly maintenance delays. Thus, strong and closely aligned macro and micro F1-scores confirm the model's robustness and reliability in structural health monitoring tasks.

3.9 Precision-Recall (PR) Curve

The Precision-Recall (PR) curve shown in Figure 5 illustrates the model's ability to balance precision and recall across all six classes (five severity categories and no crack) in the crack classification task. In this curve, each class, Hairline, Small, Moderate, Large, Very Large, and No Crack, is plotted with a nearly flat line at the top of the graph, with average precision (AP) values of 1.00 for every class. This outcome strongly suggests near-perfect performance, where the model maintains both high recall and high precision throughout the range of thresholds.

This is particularly significant in real-world scenarios where false positives and false negatives have serious implications. For instance, high precision ensures that when the model predicts a "Very Large" or "Corrosive" crack, it is almost always correct, minimizing unnecessary repairs. Conversely, high recall ensures that critical damage is not overlooked. The ability to consistently perform well in both dimensions across all categories, including the often

misclassified "No Crack" class, demonstrates a robust and well-calibrated model.

Another key takeaway from this PR curve is the stability of model confidence. The flat segments near the top indicate that the model sustains its high performance across a wide range of threshold values. This is valuable for deployment in varying operational conditions where confidence thresholds might need to be adjusted to favor either sensitivity or specificity depending on safety requirements.

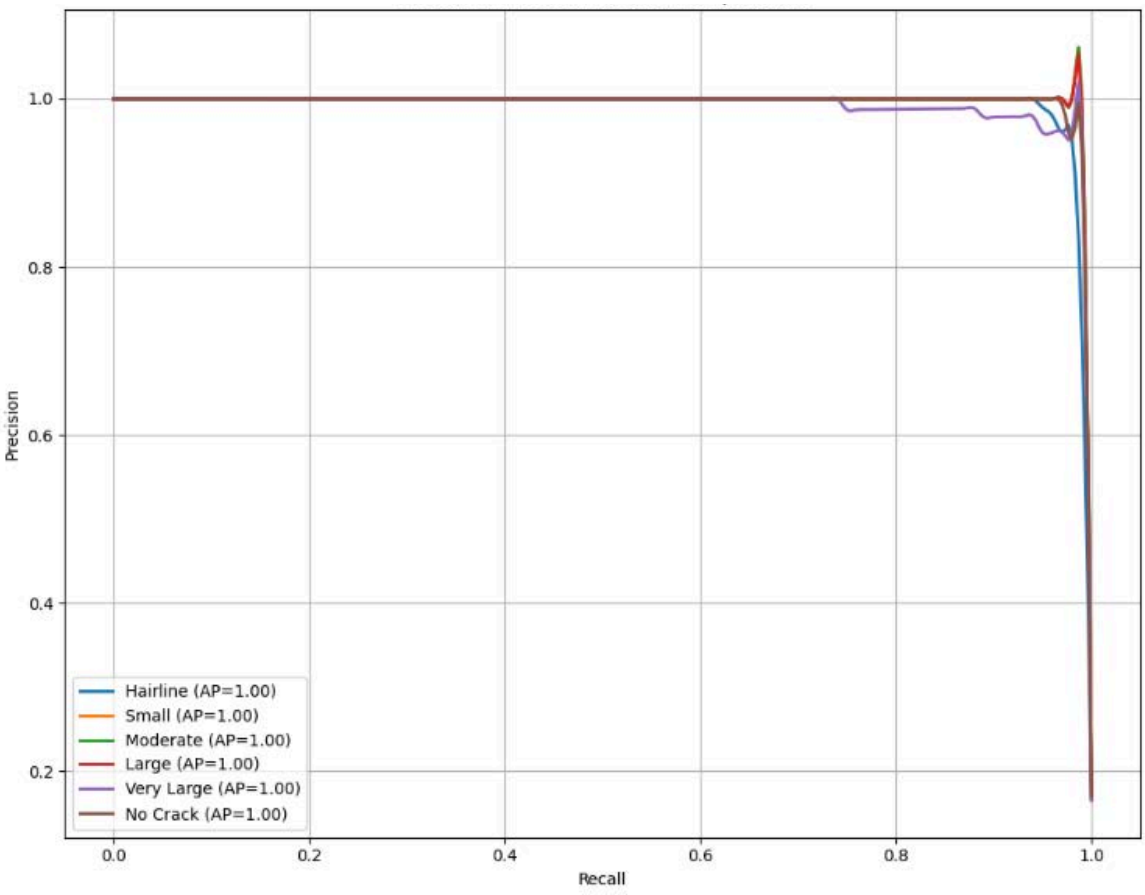

Figure 5: Smoothed Precision-Recall Graph for Each Class

IV. CONCLUSION

This research presents a comprehensive and highly accurate approach to classifying concrete crack severity using the YOLOv8n-cls model. Starting from foundational convolutional neural network-based detection, the project evolved to encompass multi-class classification aligned with engineering standards. The dataset was carefully curated and reorganized into six distinct categories, with labels reflecting real-world structural implications.

The model was trained in an augmented dataset of over 11,000 images and validated on 1,600 additional samples. It achieved accuracy of 99.9%, reflecting strong generalization and class-wise performance. The precision-recall curve confirmed outstanding reliability, with Average Precision (AP) of 1.00 for each of the six main crack classes. These results point to a model that maintains high confidence and prediction stability across a range of decision thresholds, an essential trait for real-world deployment. The model's inference speed of 0.4 milliseconds per image supports applications in embedded systems, UAV inspection, and real-time structural monitoring environments.

The evolution from basic crack detection to contextual classification marks a critical advancement in infrastructure safety assessment. By embedding engineering relevance into each decision, the model helps bridge the gap between

AI perception and civil engineering priorities. This research offers a deployable, interpretable, and efficient solution for automated crack severity assessment, enabling faster, safer, and more objective evaluations of structural health.

LIST OF REFERENCES

1. Beckmann, Birgit, Kai Schicktanz, Dirk Reischl, and Manfred Curbach. 2012. "DEM Simulation of Concrete Fracture and Crack Evolution." Structural Concrete 13 (4): 213–20. https://doi.org/10.1002/suco.201100036.
2. Chaiyasarn, Krisada, Apichat Buatik, and Suched Likitlersuang. 2021. "Concrete Crack Detection and 3D Mapping by Integrated Convolutional Neural Networks Architecture." Advances in Structural Engineering 24 (7): 1480–94. https://doi.org/10.1177/1369433220975574.
3. Džolan, Ante, Mladen Kožul, Alen Harapin, and Dragan Ćubela. 2020. "Analysis of the Concrete Shrinkage Effects on the Real Behavior of the Spatial Concrete and Reinforced Concrete Structures Using the Thermal Analogy." Engineering Computations 37 (4): 1451–72. https://doi.org/10.1108/EC-04-2019-0187.
4. Golding, Vaughn Peter, Zahra Gharineiat, Suliman Munawar Hafiz, and Fahim Ullah. n.d. "Crack Detection in Concrete Structures Using Deep Learning." Sustainability 14 (13): 8117. https://doi.org/10.3390/su14138117.
5. Li, Yi, Huiying Xu, Xinzhong Zhu, Xiao Huang, and Hongbo Li. 2024. "THDet: A Lightweight and Efficient Traffic Helmet Object Detector Based on YOLOv8." Digital Signal Processing 155. https://doi.org/10.1016/j.dsp.2024.104765.
6. Liang, Bohan, Shangxi Wu, Kaiyuan Xu, and Jingyu Hao. "Butterfly Detection and Classification Based on Integrated Yolo Algorithm." Advances in Intelligent Systems and Computing, 2020, 500–512. https://doi.org/10.1007/978-981-15-3308-2_55.
7. Park, Song Ee, Seung-Hyun Eem, and Haemin Jeon. 2020. "Concrete Crack Detection and Quantification Using Deep Learning and Structured Light." Construction and Building Materials 252. https://doi.org/10.1016/j.conbuildmat.2020.119096.
8. Wang, Rui, Xinxin Guo, Jiaxuan Liu, Wan Yu, and Bang Yeon Lee. n.d. "Concrete Crack Skeleton Analysis: A Machine Vision Approach to Feature Extraction." Advances in Civil Engineering 2024. https://doi.org/10.1155/2024/6942295.
9. Xu, Jiangbo, Shaowei Wang, Ruida Han, Xiong Wu, Danni Zhao, Xianglong Zeng, Ruibo Yin, Zemin Han, Yifan Liu, and Sheng Shu. 2025. "Crack Segmentation and Quantification in Concrete Structures Using a Lightweight YOLO Model Based on Pruning and Knowledge Distillation." Expert Systems with Applications 283. https://doi.org/10.1016/j.eswa.2025.127834.
10. Yang, Jianxi, Hao Li, Junzhi Zou, Shixin Jiang, Ren Li, and Xinlong Liu. 2022. "Concrete Crack Segmentation Based on UAV-Enabled Edge Computing." Neurocomputing 485: 233–41. https://doi.org/10.1016/j.neucom.2021.03.139.
11. Yatata. "Crack Dataset." Kaggle, June 3, 2023. https://www.kaggle.com/datasets/yatata1/crack-dataset.
12. Zhu, Weijie Li, Kaicheng Mu, Xue Zhang, Xuefeng Zhao. 2025. "An Automatic Arrival Time Picking Algorithm of Ultrasonic Waves for Concrete Crack Depth Detection." Engineering Structures 328. https://doi.org/10.1016/j.engstruct.2025.119729.
13. Mohanty, Surajit, and Subhendu Kumar Pani. 2024. "Empowering Structural Integrity: YOLO-Based Crack Detection and MLDriven Concrete Strength Prediction of Critical Infrastructure Caused due to Mining Operation." Journal of Electrical Systems 20 (5s): 2705–21.
14. Raushan, Rakesh, Vaibhav Singhal, and Rajib Kumar Jha. 2025. "Damage Detection in Concrete Structures with Multi-Feature Backgrounds Using the YOLO Network Family." Automation in Construction 170. https://doi.org/10.1016/j.autcon.2024.105887

Electrode Process with DC High Voltage and Electrochemical Plasma for Synthesis of Nanoparticle Solution and Wastewater Treatment

Nguyen Duc Hung

ABSTRACT

Conventional electrochemical processes with voltages of a few Volts only occur in an electrolyte solution, but with high DC voltage electrode reactions can still occur in non-aqueous electrolyte, even distilled water. Electricity not only converts to heat, which increases the temperature of the water environment, but also performs anodic electrochemical reactions such as dissolving metals or generating oxygen (Me → Men+ + ne; 2H2O → O2 + 4H+) and generating hydrogen gas on the cathode (2H2O → H2 + 2OH). The gaseous environment formed from the electrochemical reactions on the electrodes with high electric, magnetic and suitable temperature conditions will appear plasma on the electrodes – the ionized state of materials. The reactions in the plasma state will generate many strong reactive agents such as electrons, atoms of H, O, O3 as well as free radicals H•, O•, OH•...Simultaneous dispersion into solution of agents formed by eletrochemical processes with DC high-voltage and plasma reactions creates a variety of application possibilities.

Keywords: DC high voltage electrochemical reation, electrochemical plasma, free radicals, nano metal solution, enviromentally friendly watertreatment.

Classification: LCC Code: TP 250–261

Language: English

Great Britain Journals Press

LJP Copyright ID: 392933
Print ISSN: 2631-8474
Online ISSN: 2631-8482

London Journal of Engineering Research

Volume 25 | Issue 3 | Compilation 1.0

Electrode Process with DC High Voltage and Electrochemical Plasma for Synthesis of Nanoparticle Solution and Wastewater Treatment

Nguyen Duc Hung

ABSTRACT

Conventional electrochemical processes with voltages of a few Volts only occur in an electrolyte solution, but with high DC voltage electrode reactions can still occur in non-aqueous electrolyte, even distilled water. Electricity not only converts to heat, which increases the temperature of the water environment, but also performs anodic electrochemical reactions such as dissolving metals or generating oxygen ($Me \rightarrow Men^{+} + ne$; $2H_2O \rightarrow O_2 + 4H^{+}$) and generating hydrogen gas on the cathode ($2H_2O \rightarrow H_2 + 2OH$). The gaseous environment formed from the electrochemical reactions on the electrodes with high electric, magnetic and suitable temperature conditions will appear plasma on the electrodes – the ionized state of materials. The reactions in the plasma state will generate many strong reactive agents such as electrons, atoms of H, O, O_3 as well as free radicals $H^{\cdot}$, $O^{\cdot}$, $OH^{\cdot}$.. Simultaneous dispersion into solution of agents formed by eletrochemical processes with DC high-voltage and plasma reactions creates a variety of application possibilities.

The reaction between the nascent hydrogen from the cathode and the metal ion soluted from the anode will form a nonvalence metal and metal nanoparticle ($mMe^{n+} + mn/2H_2 \rightarrow mMe^{o} \rightarrow$ MeNPs. Solution of metal nanoparticles such as AgNPs, CuNPs, FeNPs, AuNPs are prepared by electrochemical method with DC high voltage in distilled water without using reducing agent, so they are very pure, do not contain salts generated from reducing agents and do not need stabilizers. The presence of electrochemical plasma will increase the rate and thereby increase the concentration of metal nanoparticle in solution. The reaction of strong oxidizing-reducing agents, wich is generated from electrochemical plasma reactions and disperses into the aqueous medium, with pollutants with persistent structures such as methylene blue, 2,4-D or 2, 4.5-T is still inorganicized into CO_2 and H_2O. In addition, the presence of Fe^{2+} from electrode dissolution and UV from plasma also contribute Fenton catalyst or photocatalyst for redox radical generation reactions. With a combination of the possibilities the reagents generated from the high-voltage DC reaction and electrochemical plasma can also treat NH_4^{+} contaminated water to N_2. The water treatment with DC high voltage and electrochemical plasma without chemicals and materials, so it can be considered environmentally friendly.

Keywords: DC high voltage electrochemical reation, electrochemical plasma, free radicals, nano metal solution, enviromentally friendly watertreatment.

Author: Department of environmentally friendly technology Institute of environmental technology Vietnam academy of science and technology 18 Hoang Quoc Viet, Cau Giay, Hanoi, Vietnam.

Institute of Chemistry - Materials, MSTI, 17 Hoang Sam, Cau Giay, Hanoi, Vietnam, Institute of Environmental Technology, VAS, 18 Hoang Quoc Viet, Cau Giay, Hanoi.

I. INTRODUCTION

Electrochemical methods have created many possibilities in both research and applications.[1,2] Conventional electrochemical reactions must use electrolyte solutions and low voltage DC power sources.[3]

Figure 1 shows that the electron-donating oxidation reaction is carried out directly on the metal anode or indirectly to create an oxidizing agent from the reaction on the electrode:

$$Me - ne \rightarrow Me^{n+} \quad (1)$$

$$2H_2O - 2e \rightarrow O_2 + 4H^+ \quad (2)$$

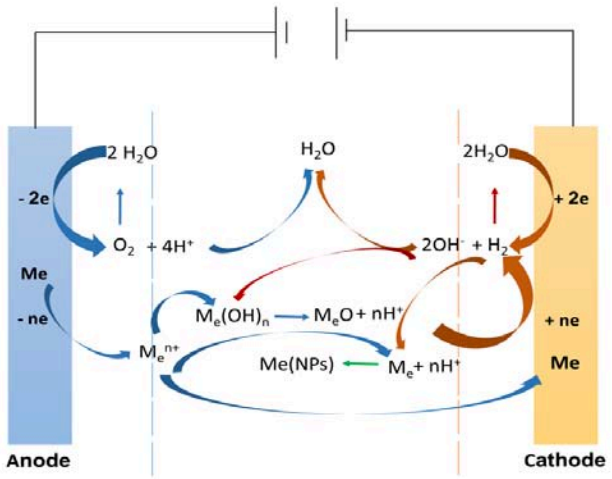

Figure 1: Schematic diagram of common electrochemical reactions

At the same time, on the cathode, the electron-donating electrode performs a direct reduction reaction or creates an indirect reducing agent:

$$Me^{n+} + ne \rightarrow Me \quad (3)$$

$$2H_2O + 2e \rightarrow H_2 + O \quad (4)$$

In the electrolyte solution, redox reactions take place:

$$Me^{n+} + nH_2 \rightarrow Me + 2nH^+ \quad (5)$$

or neutralization reactions between substances that have been generated from the electrodes:

$$H^+ + OH^- \rightarrow H_2O \quad (6)$$

Silver nanosolutions (AgNPs) were produced from reaction (3) in an electrolyte solution of 5×10^{-3}mol/L $AgNO_3$ 0.2M/L sodium dedocylsulfonate[4] or precipitated into Al_2O_3 pore size.[5] Reaction (5) is also applied to prepare AgNPS, CuNPs in DE-25 water solution with voltage up to 30 V[3] or by electrolyte solution with glycerol and polyvinylprolidone (PVP), combined with ultrasound.[6-8]

When the electrolyte solution with low voltage is not used, the electrochemical reactions as shown in Figure 1 cannot occur. However, when using DC high voltage even in twice distilled water environment, electrochemical processes (1) on the anode electrode and reaction (4) on the cathode still occur.[9] The formation of metal ions with a small concentration will gradually increase the conductivity of the aqueous environment[10] and the gas generated on the electrodes will be the condition for the appearance of plasma state - ionized state of matter.[11] This distinction between low voltage and high voltage electrochemistry will guide distinct research methods and difference applications.

II. ELECTROCHEMICAL PROCESS WITH DC HIGH VOLTAGE

2.1 Differences in Non-Electrolyte and Equipment

Use a non-electrolyte medium such as double distilled water with low conductivity 0.01 ÷ 0.5 mS/m[12] to eliminate the influence of the electrolyte composition in the products of the electrochemical process is different from the conventional electrochemical process. The device model for performing high-voltage electrochemical reaction (Figure 2) has the difference that: High-voltage source (a) to 20 kV with voltage stabilizer or current stabilizer mode is stepless controlled, displaying the following

values: value of voltage, current, amount of electricity and reaction time on control box a_1.

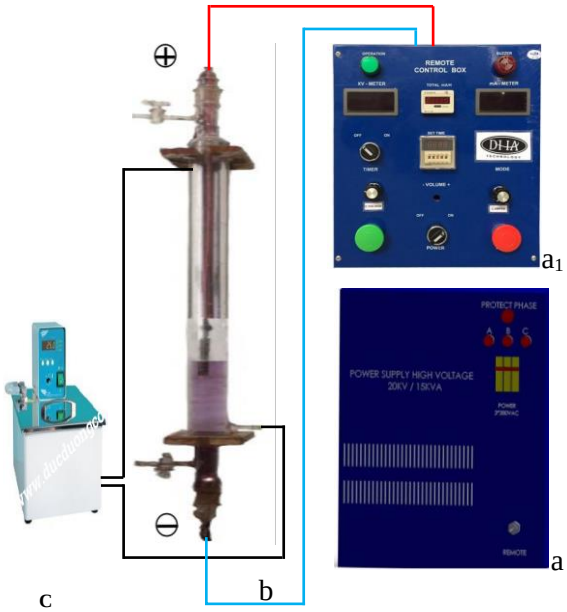

Figure 2: Model of DC high voltage equipment

The reaction vessel (b) shall be insulated with water made of plastic[13] but preferably made of heat-resistant glass such as a condenser. The cathode (b_1) is installed at the bottom of the reactor so that the H_2 gas formed is dispersed from the bottom up. The anode (b_2) is mounted on top; The liquid oulet valve (b_3) is on the cathode side and the air outake valve (b_4) is on the anode side. Cooling water with a specified temperature is supplied from the thermostat (c) by circulating pump into the insulation layer from below. Using this device it is possible to control electrochemical reaction processes by: 1) Changing voltage or current; 2) Change the distance between anode and cathode; 3) Change the nature of the environment 4) Change the cooling temperature; 5) Change the area and metallic nature of the electrodes.

2.2. Electric Energy Distribution with Electrochemical Reaction DC High Voltage

The power from the source (a) supplied to the reaction system of the device (b) has been determined (Q) to be balanced with the total heating energy of the entire electrolyte solution (Q_1) as well as the cooling water (Q_2) and perform an electrochemical reaction on the electrodes (Q_3).[14,15] The amount of heat lost by evaporation and heating the atmosphere below 100°C is negligible, so it can be ignored, so:

$$Q = Q_1 + Q_2 + Q_3 \quad (7)$$

Power supplied from the source is determined:

$$Q = U \times I \times t \quad \text{(Wh)} \quad (8)$$

The electrical energy that heats the solution and the cooling water is determined by Joule-Lenz's law:

$$Q_1 \,\&\, Q_2 = m \times C \times \Delta T \quad \text{(Wh)} \quad (9)$$

So the electricity to carry out the electrochemical reaction will be:

$$Q_3 = Q - (Q_1 + Q_2) \quad (10)$$

With the device diagram in Figure 2, it is possible to determine the parameters: potential (U, V), current (I, A), quantity of cooling distilled water (m_1, kg) and distilled water of reacion solution (m_2, kg) with heat specific capacity (C = 1,163 Wh/kg°C) with temperatures before (T_1, °C) and after (T_2, °C) after reaction time (t, h).

Table 1 presents the electricity ratio of DC high voltage supplied at different electrode distances, time and initial temperature.

Table 1: Value of electrical energy (Wh) converted to heat and electrochemical reaction at different of electrode distances (H_{A-C}), reaction time (t) and initial temperature (T)

	H_{A-C}, mm			t, min			T, °C		
	500	750	950	15	50	80	15	20	55
Q	615	785	980	424	718	867	408	349	336
Q_1	13.5	23	32	16	24	23	16	16	16
%	2.3	2.9	3.3	3.8	3.3	2.7	4.0	4.5	4.7
Q_2	595	665	707	335	670	800	335	316	316
%	96.7	84.7	72.1	79.0	93.4	923	82	91	94
Q_3	6.5	97	241	73	24	43	57	16	4
%	1.0	12.3	24.6	17.2	3.3	5.0	14	4.5	1.3

From the results in Table 1, it can be seen that the percentage of electricity converted into heat is used from 75% to 99%, the remaining to carry out the electrochemical reaction is the highest only 25%. This ratio decreases as the reaction time as well as the initial temperature of the cooling water and reaction solution increases, but increases sharply when the distance between the anode - cathode increases.

2.3 Electrochemical Reactions with DC High Voltage

Figure 3 shows the anode of the electrode when electrochemically reacting with high DC voltage in dissolved twice-distilled water. The amount of metal dissolved after 50 minutes is determined by weighing method (m_W):

$$m_W = m_T - m_S \quad (11)$$

and calculated by Faraday's law (m_F) where (k) is the electrochemical equivalent of the metal:

$$m_F = k \times I \times t \quad (12)$$

at different anode - cathode (H_{A-C}) electrode distances are presented in Table 2.

The results of Figure 3 and Table 2 show that with DC high-voltage the anodic dissolution reaction according to equation (1) still occurs in non-conductive double-distilled water.

Table 2. Mass of Ag anode dissolved after DC high voltage reaction after 50 minutes calculated according to Faraday, weight loss of anode and ratio.

H_{A-C}, mm	500	700	950
m_F, mg	213	211.5	195.8
m_W, mg	98	65	58
%	46.0	30.7	29.6

Figure 3: Ag anode is dissolved after DC high voltage reaction

However, the amount of dissolved metal weighed is always smaller than the amount calculated according to Faraday, showing that the gas escape process according to equation (2) also occurs at the same time with the rate up to 30% and will increase even more when the electrode distance between the electrodes is increased. anode and cathode decrease. Effect of initial temperature of cooling water as well as reaction medium (T) and DC high voltage electrochemical reaction time (t) on the amount of anodic dissolved metal at H_{A-C}: 650 mm determined by The loss of anode weight (m_W) and calculated according to Faraday's law (m_F) is presented in Table 3.

Table 3: Amount of anodic soluble Ag determined (m_W) and calculated (m_F) at different initial temperatures and times

T, °C.	5	15	25	35	55
m_W,mg	49	45	68	56	62
m_F, mg	107	108	174	215	261
%	45.8	41.7	39.1	26.0	23.8
t, ph.	5	15	25	35	50
m_W,mg	12	15	19	23	68
m_F, mg	21	56	103	146	216
%	57	26.8	18.4	15.8	31.5

The results from Table 3 also show that the amount of anodic soluble metal at DC high voltage calculated by Faraday's law is always larger than the amount determined by the anode electrode weight loss with a decreasing trend with increasing initial temperature of the cooling water as well as reaction time. It also proves that the gaseous reaction according to equation (2) accounts for a significant proportion in the anodic processes of DC high voltage electrochemistry.

Simultaneously with the metal dissolution on the anode, on the cathode, strong gas escape (Figure 4) occurs according to the reaction of equation (4).

The measured gas volumes (V_D) as well as those calculated according to Faraday's law (V_F) are presented in Table 4. This shows that in addition to electrochemical reactions that follow Faraday's law, there are also reactions that do not follow Faraday's law.[16]

Table 4: Amount of gas determined (V_D) and calculated (V_F) released from the cathode at different electrode distances (H_{A-C}) and reaction times (t)

H_{A-C}, mm	500	700	850
I, mA	93.4	112.6	119.3
V_F, mL	14.7	17.6	22.5
V_D, mL	63,0	110	80
V_D/V_F	4.3	6.3	3.6
t, phút	18	30	35
I, mA	119.3	115.7	106.7
V_F, mL	22.5	36.4	39.1
V_D, mL	80	150	250
V_D/V_F	3.6	4.1	6.4

Figure 4: Gas escapes strongly from the cathode and disperses into solution

The rate of electrochemical and non-electrochemical reaction with DC is high with changing reaction conditions such as electrode distance, time will also be different, especially the reaction time increases the non-Faraday rate with a marked increase. Because the amount of gas released on the cathode is high and strong, the metal precipitation reaction according to equation (3) does not occur with DC high voltage, so the cathode weight does not change after the reaction. The products from the DC high-voltage electrochemical reaction corresponding to equations (1), (2) and (4) create Men^+, H^+ and OH^- ions dispersed into the aqueous medium, thus increasing the electrical conductivity of the environment (Table 5).

Table 5: Average conductivity of solution after DC high voltage reaction of Ag electrode with 50 min at different distances (HA-C)

H_{AC}, mm	400	500	600	700	800	900	1000
□, µScm^{-1}	91.3	71.2	74.7	72.8	72.1	80.8	102.8

The results from Table 5 show that the conductivity of the medium after the DC high-voltage reaction has increased compared to the average value of 3.14 µS/cm of the original distilled water, but it is not large and does not change significantly when change the reaction conditions such as electrode distance, potential and time. It shows that in the solution, there have been oxidation - reduction reactions according to equation (5) or neutralization according to (6), reducing the amount of ions produced from reactions (1), (2), (4) and dispersed in solution.

III. SYNTHESIS OF METAL NANO SOLUTION

3.1. Silver Nano-Solutions and Characteristics

Silver nanoparticles (AgNPs) have good anti-viral effect[17], so they should be focused on preparing them by various methods such as physical,[18] physicochemical,[19] biology, green chemistry,[20] or chemical reduction.[21,22] Most methods use $AgNO_3$ and reducing agents such as γ-rays, bacteria, plant extracts or reducing agents. The reaction of $AgNO_3$ with $NaBH_4$ reducing agent to form AgNP occurs according to equation (13)[23] or (14)[24]:

$$2AgNO_3 + 2NaBH_4 \rightarrow 2Ag + B_2H_6 + 2NaNO_3 + H_2 \quad (13)$$

$$\text{or: } 2AgNO_3 + 2NaBH_4 + 6H_2O \rightarrow$$

$$2Ag + 2B(OH)_3 + 2NaNO_3 + 7H_2 \quad (14)$$

AgNPs solution products prepared from $AgNO_3$ with reducing agents always contain salts of NO_3^- ions and other products, which are difficult to remove, limiting their applicability.

Apply DC high voltage electrochemical reaction to generate Ag^+ from anode as equation (3) and reducer H_2 from cathode as equation (4) to carry out reaction (5) in solution to form AgNP:

$$\text{on the anode: } Ag - e \rightarrow Ag^+ \quad (15)$$

$$\text{on the cathode: } 2H_2O + e \rightarrow H_2 + 2OH^- \quad (16)$$

$$\text{inside the solution: } 2Ag^+ + H_2 \rightarrow 2Ag^0 + 2H^+ \quad (17)$$

Ag^0 atoms are acted upon by Van der Walls forces to form AgNPs that change the color of the solution:

$$nAg^0 \rightarrow AgNPs \quad (18)$$

Thus, summarizing the equations from (15) to (18), we have a general equation for the process of forming AgNPs by DC high-voltage (DC_{HV}) in H_2O from solid Ag electrode (Ag_{El}):

$$nAg_{Eletrode}. + (DC_{HV} + H_2O) \rightarrow AgNPs \quad (19)$$

Figure 5 shows the evolution of AgNPs formation during electrochemical reaction with DC high voltage at 8 kV in double distilled water at 25°C with a distance between Ag electrodes of 850 mm.

From Figure 5 it can be seen that: with distilled water initially transparent (a), but after 5 min of reaction with DC high pressure it turned white color of air bubbles dispersed in water (b), after 15 min near the cathode turns brown (c), after 25 min the whole reaction solution has changed color: dark near the cathode electrode and light near the anode electrode (d) and by 50 min after the end of the reaction, the whole reaction has turned dark brown (e).

Typical characteristics of AgNPs solutions such as shape and particle size determined by TEM, particle size distribution determined by Laser scattering particle size distribution analyer Partica LA-950 (Horiba) and deeper by Nicomp 380/DLS (Nicom)) are presented in Figure 6 as like as those reported in the literature prepared by different methods.[25-27]

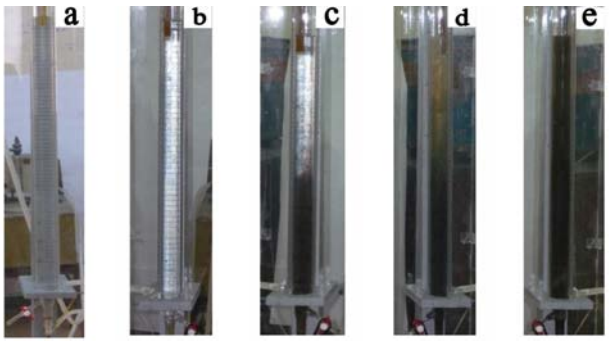

Figure 5: AgNPs formation at reaction times with DC high voltage in double distilled water

From TEM images with different high voltage DC reaction conditions: electrode spacing 350 mm (*H.6.1*) and 1000 mm (*H.6.2*) as well as after 15 min (*H.6.3*) and 50 min (*H.6.4*) the particles of AgNPs are all spherical in shape with sizes from 5.26 nm to 40.4 nm. Under the same reaction conditions with different electrode distances (*H.6.1* and *H.6.2*) the AgNP particle size did not change significantly, but when increasing the reaction time (*H.6.3*) and (*H.6.4*), the size of the AgNPs particle size increased from 2 to 3 times.

The particle size distribution determined by the two methods also shows that the AgNPs of the DC high-voltage (*H.6.7*) are not uniform but in Gaussian form similar to the chemically prepared AgNPs (*H.6.8*). Figure 6 also shows that the AgNPs solution is a polydisperse system, with at least 2 to 3 particle levels at the reaction electrode distances: 350 mm (*H.6.5*) as well as at 1000 mm (*H.6.6*). The method of determining Nicomp 380/DLS with sample of 1000 mm and 50 min (*H.6.9*) also determined the polydispersity of AgNPs system.

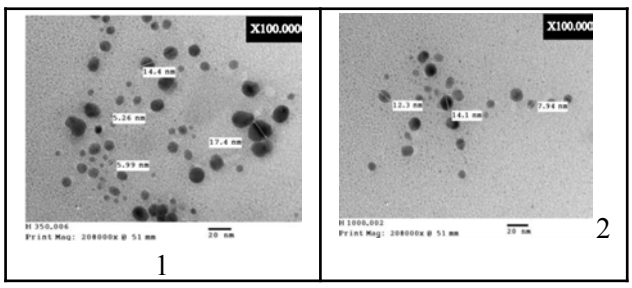

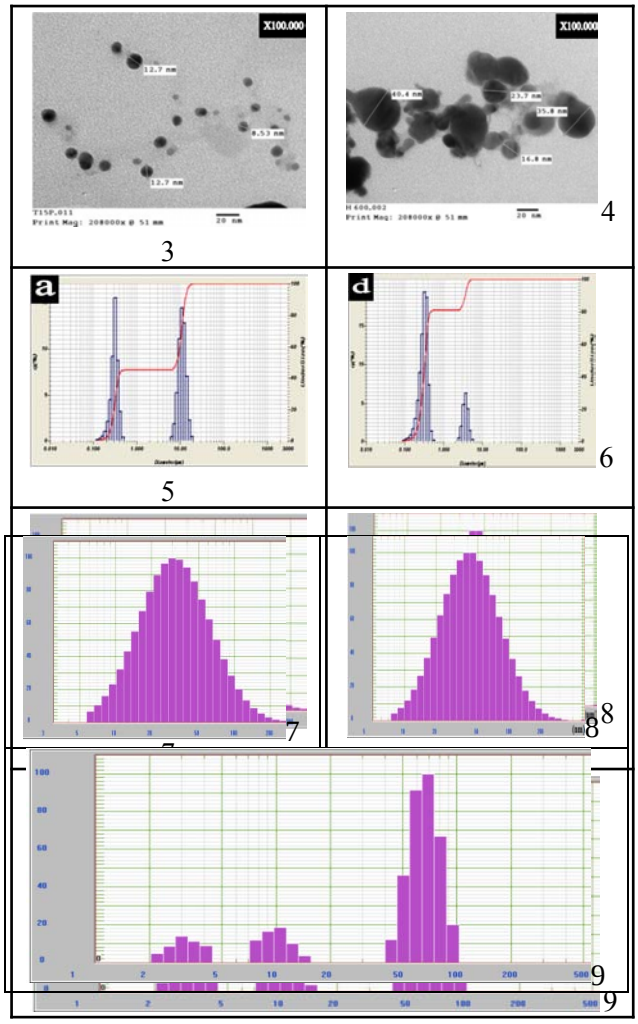

Figure 6: TEM image and particle size distribution of AgNPs

UV-Vis characteristics of AgNPs (Figure 7) prepared by DC high-voltage at different conditions such as time as well as anode size obtained a spectrum with a peak at about 420 nm like other methods.[26-28]

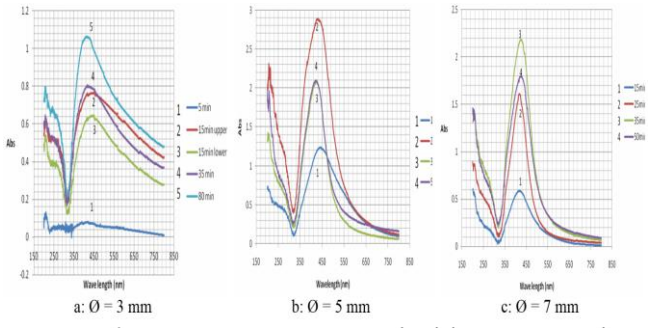

Figure 7: UV-Vis spectra of AgPNs prepared by DC high voltage with different anode diameters and times

The results from Figure 7 also show that the UV-Vis peak height trend increases as the reaction time increases.

The bactericidal properties of AgNPs prepared by high-voltage DC are shown in Figure 8.

The results of Figure 8 show that AgNPs obtained from DC high voltage are also effective against Gram+ and Gram- bacteria,[29-31] especially with *E.Coli*, only 0.24 ppm has achieved efficiency 99.9%.[32] Bacterial pathogens for shrimp (*H. 8*.d ÷ *8*.f) were also killed with concentrations ranging from 144.5 ppm to 96.23 ppm.[32,33]

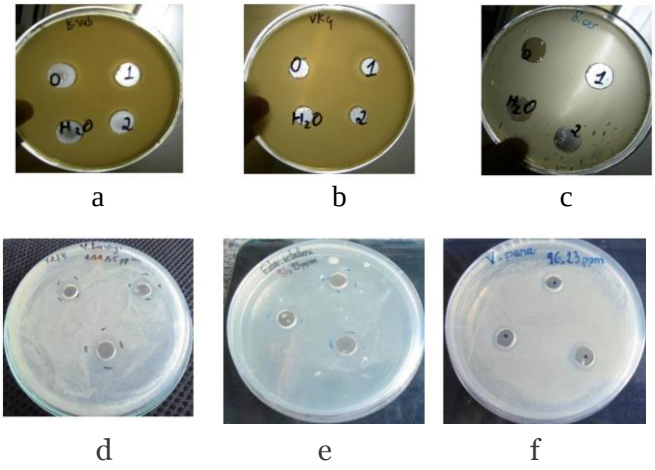

a b c d e f

Figure 8: The reactance loop of AgNPs solution prepared by DC high voltage: a) *Baclllus subtlls*, b) *Baclllus sp*, c) *Saccharomyces cerevlslae*, d) *Vibrio harveyi*, e) *Edwardsiella ictaluri*, f) *V. Parahaemolyticus*

The results of Figure 8 show that AgNPs obtained from high-pressure DC are also effective against Gram-positive and Gram-negative bacteria,[29-31] especially with E.Coli, only 0.24 ppm has an efficiency of 99, 9%.[32] Bacterial pathogens for shrimp (Figure 8d-8f) were also killed with concentrations ranging from 144.5 ppm to 96.23 ppm.[32,33]

3.2. Differences in the Characteristics of AgNPs Prepared from DC High Voltage

3.2.1 Conductivity

Table 6 presents a very clear difference between AgNPs solution prepared by high voltage DC electrochemical method as equation (19) and chemical method from $AgNO_3$ according to reaction (14) by reducing agent $NaBH_4$[34] or with sucrose reducing agent ($C_{12}H_{22}O_{11}$).[35]

From Table 6, it can be seen that the conductivity of AgNPs solution prepared by DC high Voltage is not much higher than distilled water and does not change significantly when the concentration increases from 127 ppm to 403 ppm. In contrast, the electrical conductivity of the AgNPs solution chemically prepared from $AgNO_3$ with different reducing agents has a very large value and increases greatly when the concentration of AgNPs increases.

The reason that the conductivity value of AgNPs prepared by DC high-Voltage is small and does not change significantly with different concentrations, which can be explained by the absence of NO_3^- Na+ ions well as the ions of the reduction products in the solution of AgNPs prepared by DC high-Voltage.

Table 6: Conductivity comparison of AgNPs solutions prepared by high-voltage DC and chemical reduction

Solution	c_{AgNPs}	□ , μScm^{-1}		
Dist.water	RO	10.2	10.4	10.3
	2 times	3.1	3.4	3.2
DC high Voltage	127 mg/L	56.6	55.9	57.1
	197 mg/L	71.2	70.9	71.3
	403 mg/L	72.8	72.4	73.6
$NaBH_4$	200 mg/L	1469	1465	1477
	500 mg/L	1872	1887	1880
	1000 mg/L	2800	2810	2820
$C_{12}H_{22}O_{11}$	50 mg/L	3960	3860	4110
	100 mg/L	9510	9460	9460

It also proves that the AgNPs solution prepared by DC high-Voltage does not have any ions other than the AgNPs colloid, so the purity is very high.

3.2.2 Zeta Potential

Figure 7 presents the zeta potential of AgNPs solution prepared by DC high-Voltage with spacing of 350 mm (a), 650 mm (Figure 7b), 1000 mm (Figure 7c) at 50 min as well as at 650 electrode spacing. mm with time of 5 min (Figure 7d), 15 min (Figure 7e), 50 min (Figure 7b) are different from the zeta potential of chemically prepared AgNPs solution (Figure 7g).[34]

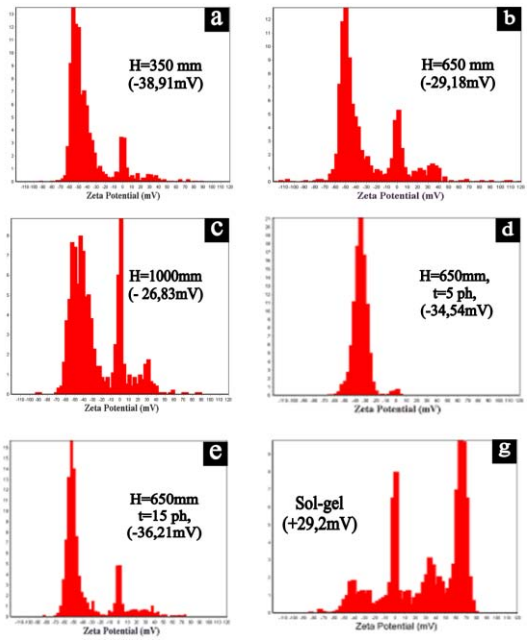

Figure 7: The zeta potential of the DC high-Voltage-prepared AgNPs solution after 50 min with different distances (a, b, c) and different times (d, e, b) compared with chemical AgNPs

The results from Figure 7 show that the difference between the zeta potentials of AgNPs prepared by the DC high-Voltage method has negative values from -26.83 mV to -38.91 mV while the products prepared by chemistry has a positive value of + 29.2 mV. The large zeta potential is enough to ensure that the AgNPs colloidal system prepared by DC high-Voltage is stable over time without using chitosan stabilizers as chemical methods. This is also a difference showing the advantage of AgNPs modulated byDC high Voltage.

3.2.3 Concentration Yield of AgNPs

The concentration of AgNPS solution prepared by chemical method is usually determined by the concentration of $AgNO_3$ salt performing the reaction or analyzed by AAS method, which still converts Ag^0 to Ag^+ evenly, assuming that Ag^+ is completely converted to AgNPs. This assumption is not completely reasonable because in the solution of AgNPs, there are still Ag^+ ions in completely unknown proportions. The difference to determine the concentration of AgNPs prepared by DC high-Voltage is that it can be used to determine the loss of the dissolved anode according to Equation (11) or calculated from Faraday's law when determining get the electrochemical reaction current and time according to equation (12). Table 7 presents the concentration of AgNPs prepared by high voltage DC determined by 3 methods: loss of anodic weight ($c_{\Delta m}$), calculation by Faraday's law (c_F) and analysis of AAS (c_{AAS}) when changing the distance. electrode or reaction time while other conditions were kept unchanged.

Table 7: AgNPs concentration determined by weight loss: $c_{\Delta m}$, by Faraday:c_F and by AAS: c_{AAS} with different distances and reaction times

$H_{A\text{-}C}$, mm	350	550	850	1000
c_F, mg/L	129.6	213.5	217.3	198.2
$c_{\Delta m}$, mg/L	112	82	66	59
$(c_F/c_{\Delta m})$%	86.42	38.1	30.4	29.8
c_{AAS}, mg/L	34.7	30.6	13.9	11.9
$(c_{\Delta m}/c_{AAS})$%	30.97	31.2	21.1	20.2
t, min	5	15	25	50
$c_{\Delta m}$, mg/L	34.3	42.9	55.4	194.3
c_F, mg/L	61.1	162.8	294.6	616.8
$(c_F/c_{\Delta m})$%	56.2	26.7	20	31.5

The results of Table 7 show that the concentration of AgNPs calculated according to Faraday's law has the largest value because the amount of electricity supplied to the anodic process is not only to carry out the reaction (15) to dissolve the anode but also to react (2) to drain oxygen. That makes the AgNPs generation efficiency change when the electrode distance as well as the reaction time change. Table 7 also shows that when increasing the electrode distance as well as the reaction time, the yield of AgNPs tends to decrease, similar to the trend of anodic dissolution in Table 3.

3.2.4 Plasma Contribution During the Formation of AgNPs

Figure 9 shows the process of DC high-Voltage reaction under suitable conditions with the appearance of a plasma state.

The results from Figure 9 show that the color turns yellow during the generation of AgNPs when there is a contribution of plasma formation which is different from Figure 5 which turns to dark brown color of the generation of AgNPs by DC high-Voltage without plasma.

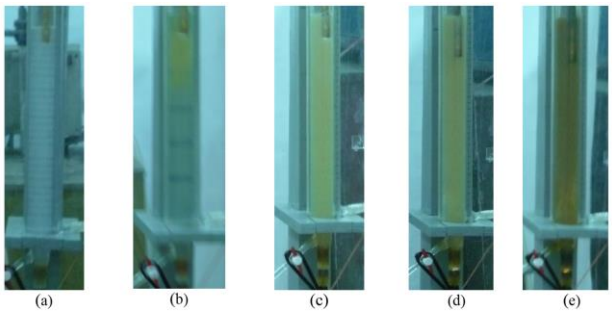

Figure 9: The process of generating AgNPs by DC high-Voltage with plasma appearing at U_{DC}: 6.15 kV, H_{AC}: 350 mm, i: 4.15 mA/mm²; (a) air release, (b) after 15 min. the anode solution turns yellow, (c) after 23 min. The Plasma glows on the anode, the entire solution turns yellow, (d) after 26 min; cathode plasma appears; (e) after 35 min the entire solution turned dark yellow.

According to Mizuno[36] a large amount of gas is released on the electrode and does not follow Faraday's law[16] as the results of Table 6 show that the plasma-based water decomposition has occurred on the electrodes:

Thus, the DC high-Voltage and plasma reactions provided the solution from equations (15) ÷ (18) and (20), (21): Ag^+, H^+, OH^-, H_2, O_2, H_2O_2 and AgNPs In the solution then the following reactions can also take place:

On the anode: $4H_2O \rightarrow 3H_2O + O_2 + H_2O_2$ (20)

On the cathode: $2H_2O \rightarrow 2H2 + O_2$ (21)

$2Ag^+ + 2OH^- \rightarrow Ag_2O + H_2O$ (22)

$2Ag^+ + O_2 \rightarrow Ag_2O_2$ (23)

$$Ag_2O + H_2 \rightarrow 2Ag^0 + H_2O \quad (24)$$

$$Ag_2O_2 + 2H_2 \rightarrow 2Ag^0 + 2H_2O \quad (25)$$

$$Ag_2O + H_2O_2 \rightarrow Ag_2O_2 + H_2O \quad (26)$$

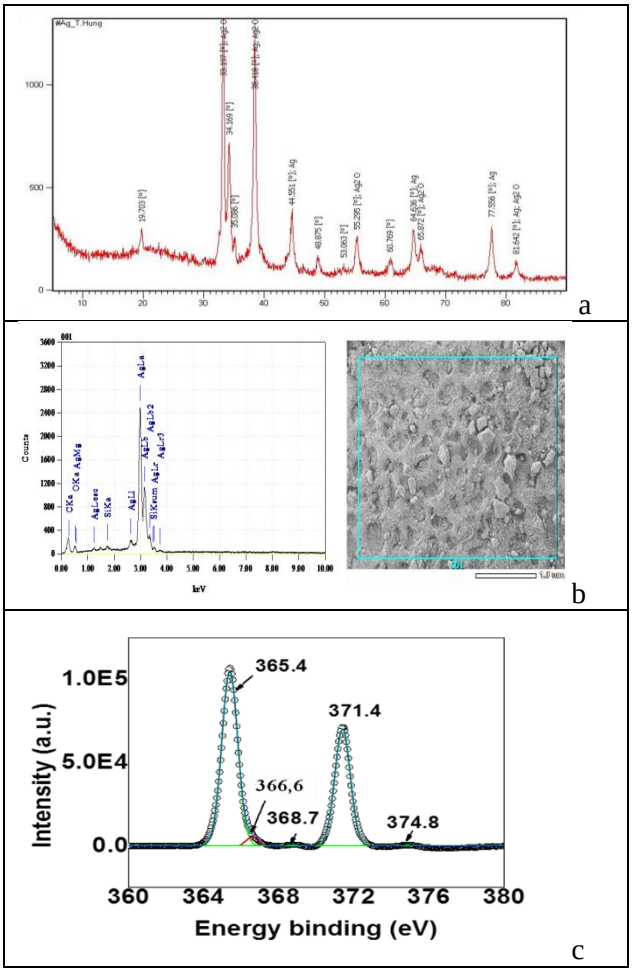

Figure 10: X-ray (a), EDX (b) and XPS (c) spectra of AgNPs prepared by DC high-Voltage with plasma.

Figure 10a shows that the Ronghen spectrum of AgNPs, the characteristic spectra of Ag also have a small amount of spectrum of Ag_2O with θ respectively: 32,709 for [111], 37,984 for [200], 54,794 for [220], 65,341 for [311] and 68,596 for [222]. EDX analysis results (Figure 10b) showed that the percentage of Ag element accounted for (89.18 ÷ 92.31)% and O element was (5.77 ÷ 9.6)%. This proves that Ag_2O is also formed to cover the AgNPs and is the reason why the fluorescence spectrum of AgNps solution prepared by high pressure DC with plasma (Figure 8) has a different color from that of AgNPs prepared by DC. with plasma (Figure 5). A special feature is that in the XPS spectrum (Figure 10c) of Ag 3d5/2 and Ag5d3/2 in AgNPs samples, there is no pick at the binding energy of 368.21 eV, which is typical for the chemical state of Ag^+ ion.[37] This also proves that, in the AgNPs solution obtained without Ag^+ ions, all silver atoms dissolved from the anode are converted into Ag_2O, AgO and Ag.[38] The presence of small amounts of oxide compounds also significantly affects the bactericidal effect of AgNPs.[39]

3.3 Preparation of Bimetallic Nanoparticle Solution

Combining good properties while reducing the amount of precious metals such as Au, Ag, etc. by bimetallic nanoforming is the trend of modern nanotechnology.[40,41] High-voltage DC method is

also used to Preparation of bimetallic nanoparticle (Cu/Ag)NPs solutions. Performing high-voltage DC process with Ag electrode followed by Cu electrode or in solution containing CuNPs will obtain (Cu/Ag)NPs.[42] Figure 11 presents the nanoparticle size (a) and zeta potential (b) distributions of AgNPs, CuNPS and (Cu/Ag)NPs.

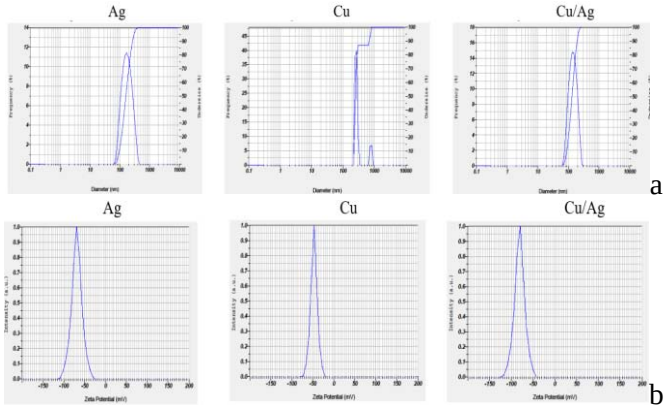

Figure 11: Nanoparticle size distribution (a) and zeta potential (b) characteristics of AgNPs, CuNPS and (Cu/Ag)NPs prepared by DC high-voltage at U_{DC}: 15 kV, H_{AC}: 200 mm and electric quantity Q: 25 mAh

From the results of Figure 11 it can be seen that the size and size distribution of bimetallic nanoparticles (Cu/Ag)NPs are the same as those of CuNPs and AgNPs, but the average particle size is slightly larger. Similarly, the zeta potential distribution of the bimetallic nanocolloid solution is the same as that of the monometals and all have negative values (-70.0 ÷ -80.6) mV, indicating that the colloidal system is stable without stabilizer.

Table 8: Metal content by Faraday c_{Far}, anodic weight loss $c_{\Delta m}$ and AAS analysis c_{AAS} of AgNPs, CuNPs and bimetallic (Cu/Ag)NPs nanosolutions prepared by DC high Voltage with a) Cu anode after Ag, b) Ag anode in 10 mg/L CuNPs solution

Điện cực		a) Cu_A/Ag_A	b) $CuNPs_{10mg/L}/Ag_A$
U_{DC}, kV		5	5
H_{AC}, mm		200	200
c_{Far}, mg/L	c^{Ag}	610.458	205.275
	c^{Cu}	15.906	
$c_{\Delta m}$, mg/L	c^{Ag}	54.671	118.333
	c^{Cu}	8.667	
c_{AAS}, mg/L	c^{Ag}	45.459	65.949
	c^{Cu}	0.321	3.214

From the results of Table 8 it can be seen that the rules of high-voltage DC electrochemical processes to prepare bimetallic nanosolutions (Cu/Ag)NPs are the same as those for the preparation of single-metal AgNPs or CuNPs, that is, the concentration obtained Faraday calculation is always greater than from anodic weight loss and minimum concentration calculated from AAS analysis. Table 8 also shows that the concentration of (Cu/Ag)NPs obtained can reach quite large values. The bactericidal ability of the solution (Cu/Ag)NPs with low concentration is also very good and the conductivity, UV-Vis spectra of the bimetallic nanoparticle (Cu/Ag)NPs solution are similar to that of the solution AgNPs.[42] Thus, the application of (Cu/Ag)NPs solution will be effective because it reduces the

amount of Ag and the ability to kill bacteria and adds Cu with better fungi and mold killing ability for crops in agriculture.

IV. ELECTROCHEMICAL PLASMA FORMATION

4.1 The Appearance of Plasma on the Electrodes

In section 2.3. showed that the DC high Voltage electrochemical reaction processes also have reactions that do not obey Faraday's law,[16] producing a large amount of gas. The gaseous environment created on the electrodes under conditions of high energy from electric and magnetic fields along with increasing temperature of the solution will appear glowing at the electrodes, which is a sign of a plasma state such as: mentioned in section 3.2.4.[36] Unlike arc-formed plasmas,[43-45] from microwaves,[46] from capacitance,[47.48] or gas powered,[49-51] plasmas are formed from gases by DC electrochemical reactions. The high voltage across the electrodes can be called an electrochemical plasma. The telltale sign of the presence of electrochemical plasma is not only the glow at the electrodes, but also the reaction rate – which increases sharply with time as shown in Figure 12. From the results of Figure 12, it can be seen that the electrochemical plasma appearance time will depend on the electrochemical reaction rate by DC on the electrodes. The greater the speed of the electrochemical reaction, the faster and more abundant the hydrogen and oxygen gas generated, especially when the conductivity is higher and the pH is farther from the neutral medium, the sooner the electrochemical plasma occurs.

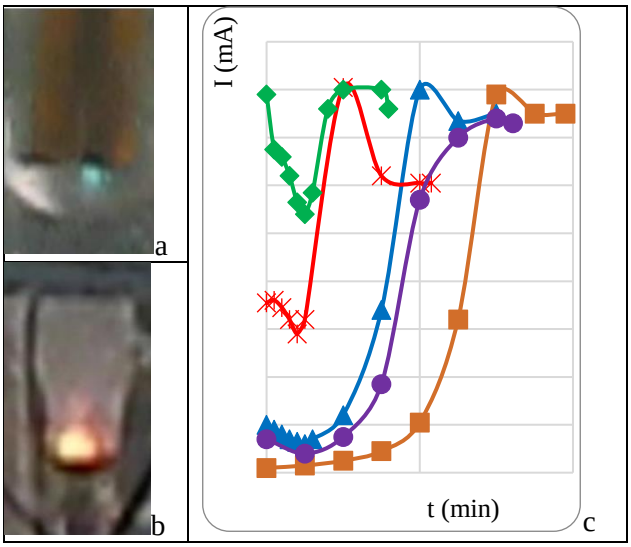

Figure 12: Electrochemical plasma heating sign on Ag electrode: a) glow on the anode; b) on the cathode, c) the current increases with time in the environment with different λ(μScm^{-1})/pH: 1) 2.6/6.9; 2) 12.4/6.3; 3) 21.8/6.0; 4) 80.7/5.1; 5) 143/4.3

The color of the electrochemical plasma on the different cathode and anode electrodes may be due to the different gaseous nature of the two electrodes according to processes (2) and (4). Of course, technological parameters affect the rate of electrochemical reactions by high voltage DC such as: voltage, electrode spacing, pH and conductivity as well as the initial temperature of the solution as well as the nature of the metal. of the electrode will also affect the electrochemical plasma appearance time (Table 9). The results from Table 9 also show that the faster the electrochemical plasma appears time as the

voltage, the higher the initial temperature as well as the increased conductivity or pH of the non-neutral medium. The shorter the distance between the anode and cathode electrodes, the sooner the plasma will appear.

Table 9: Electrochemical plasma appearance time (*t*, min) when performing DC high-Voltage reaction on Cu, Fe, W electrodes at the following values: potential (*U*, kV), anode-cathode distance (*H*, mm), pH-conductivity (χ , µScm-1) and initial temperature (*T*, °C) are different

Reaction conditions	Điện cực	Cu	Fe	W
U, kV (*H*: 200 mm; *T*: 30 °C; pH:7; χ : 1,4 µScm^{-1})	5	-	-	-
	10	55	40	20
	15	30	25	5
H, mm (*U*: 15 kV; *T*: 30 °C; pH: 7; χ : 1,4 µScm^{-1} ;)	200	30	20	7
	250	-	45	10
	300	-	-	20
pH/ χ , µScm^{-1} (*U*: 15 kV; *H*: 200 mm; *T*: 30°C)	4/120	3	2	1
	7/1.4	-	-	-
	11/150	3	2	1
T, °C (*U*: 15 kV; *H*: 200 mm; pH; 7; χ : 1,4 µScm^{-1})	30	-	70	20
	30	30	15	10
	40	25	5	3

On the electrode W, the time appears electrochemical plasma faster than Cu and Fe electrodes due to more electrochemicals, so it is difficult to dissolve and the air release reaction will prioritize more and faster than the favorable conditions to form the plasma earlier.

4.2 Plasma Reaction to Create Free Radicals

Plasma is formed from the electrochemical process that creates a gas environment with high voltage is a cold plasma state with different levels of ionization.[52,53] According to Lukes[54] and Ruma[49] plasma formed in a solution in the gas phase surrounding the electrode and liquid phase area in contact with the plasma area in the gas phase. Free radicals: $H^{\bullet}$, $O^{\bullet}$, $OH^{\bullet}$ H^+, H_3O^+, O^+, H^-, OH^- ions[55,56] as well as new molecules and molecules activities: H_2, O_2, H_2O_2[57-59] formed in the plasma area from the reaction:[60-62]

$$H_2O + e^- \rightarrow H^{\cdot} + OH^{\cdot} + e^- \quad (27)$$

$$H^{\cdot} + H^{\cdot} \rightarrow H_2 \quad (28)$$

$$OH^{\cdot} + OH^{\cdot} \rightarrow H_2O_2 \quad (29)$$

$$OH^{\cdot} + OH^{\cdot} \rightarrow O + H_2O \quad (30)$$

$$OH^{\cdot} + H_2O_2 \rightarrow HO_2^{\cdot} + H_2O \quad (31)$$

$$OH^{\cdot} + HO_2^{\cdot} \rightarrow H_2O + O_2 \quad (32)$$

$$OH^{\cdot} + H^{\cdot} \rightarrow H_2O \quad (33)$$

$$OH^{\cdot} + OH^{\cdot} \rightarrow O^- + H_2O \quad (34)$$

$$H_2O + e^- \rightarrow H_2O^+ + 2e^- \quad (35)$$

$$H_2O^+ + H_2O_2 \rightarrow H_3O^+ + OH^{\cdot} \quad (36)$$

$$H_2O + e^- \rightarrow H_2O^{\cdot} + e^- \quad (37)$$

$$H_2O^{\cdot} + H_2O \rightarrow H_2O + H^{\cdot} + OH^{\cdot} \quad (38)$$

$$H_2O^{\cdot} + H_2O \rightarrow H_2 + O^{\cdot} + H_2O \quad (39)$$

$$H_2O^{\cdot} + H_2O \rightarrow 2H^{\cdot} + O^{\cdot} + H_2O \quad (40)$$

The emission of UV rays when appearing plasma also contributes to the fracture of O-O into OH •:[63,64]

$$H_2O_2 + h\nu \rightarrow 2OH^{\cdot} \quad (41)$$

The equations (20), (29) show that H_2O_2 is formed when the state of electrochemical plasma appears. Although H_2O_2 is not durable and easy to participate in the correspondence (31), (36), it is still possible to determine quantitative by UV-Vis

method with yellow $TiO_2.H_2O_2$ complex at the wavelength: λ = 407 nm.[59,61,65]

$$Ti^{4+} + H_2O_2 + 2H_2O \rightarrow TiO_2.H_2O_2 + 4H+ \quad (42)$$

Figure 13 shows the standard line determining H_2O_2 with UV-Vis UH-5300, Hitachi with λ = 407 nm (A) and the defined H_2O_2 concentration on Cu, Fe, W electrodes at the condition of appearing plasma: T = 30°C, U = 15 kV, H = 200 mm, pH = 7 and χ = 1.4 µscm^{-1}.[66]

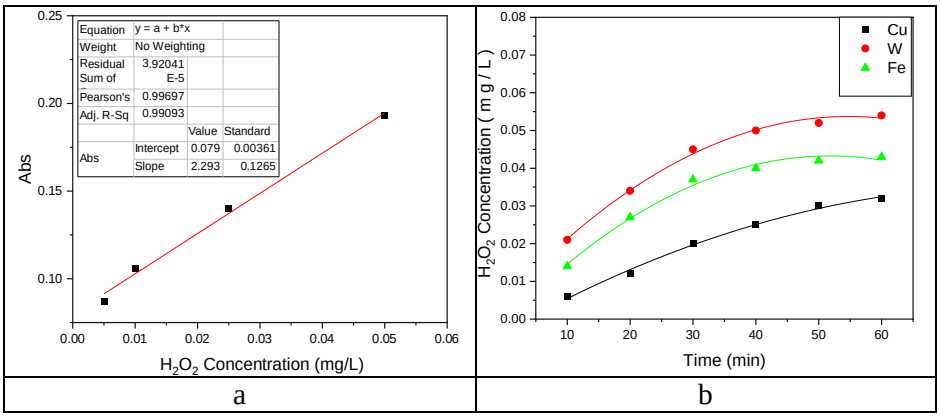

Figure 13: a) Standard line in the area 0.005 mg/L to 0.05 mg/L; b) The concentration of H_2O_2 formed on Cu, W, Fe electrodes depends on the time at U: 15 kV; H: 200 mm, T: 30°C with pH 7 and χ = 1.4 µscm^{-1}.

The result from Figure 13 shows that the H_2O_2 content was formed on the electrodes that increased rapidly in the first 30 minutes but then slowed down and reached balance with the reactions using H_2O_2. The amount of H_2O_2 formed on the electrodes decreased in order W > Fe > Cu corresponding to the 60 -minute gain: 0.054 mg/L > 0.043 mg/L > 0.032 mg/L.

The appearance of OH· radical at Equations 27, 36, 38, 41 on Fe electrode can also be determined by UV-Vis spectroscopy with salicylic acid complex (SA):[67-69]

OH• + SA 2,3 DHB (Dihydroxybenzoic) (43)

OH• + SA 2.5 DHB (Dihydroxybenzoic) (44)

The UV-Vis spectral absorption peaks are 290 nm for SA, 310 nm for 2.3 DHB and 330 nm for 3.5 DHB, respectively, as well as standard curves in the concentration range 1.0×10^{-4}M to 1.0×10^{-3}M respectively is shown in Figure 14 with equations (45), (46) and (47) respectively.[70,71]

$$Abs_{290nm}=2632.80_{[SA]} \pm 33.42 + 0.52 \pm 0.02 \quad (45)$$

$$Abs_{310nm}=2055.13_{[2,3\text{-}DHB]} \pm 58.23 + 0.72 \pm 0.03 (46)$$

$$Abs_{330nm}=2599.10_{[2,5\text{-}DHB]} \pm 115.99 + 0.23 \pm 0.07 (47)$$

The result of solving the system of equations can be obtained, the concentration value of OH· radical formed with electrochemical plasma on the iron electrode after 30 minutes is 3.0×10-4 M and after 60 minutes is 3.7×10-4 M.

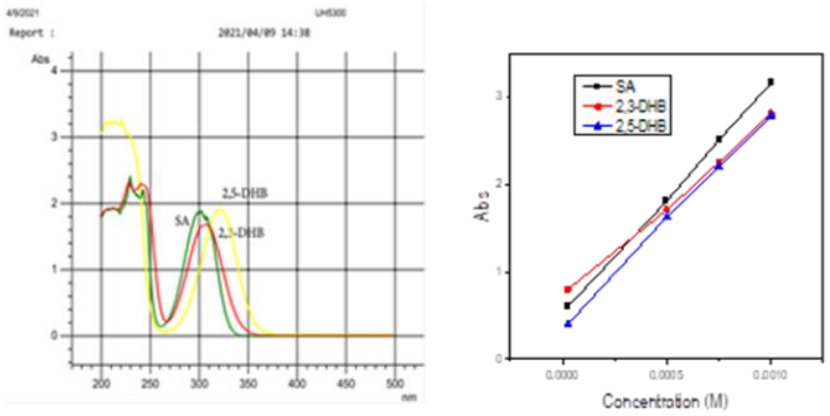

a b

Figure 14: Adsorption spectrum and SA calibration curve with (R^2=0.999) , 2.3DHB with (R^2=0.997) and 2.5 DHB (R^2=0.994) of complexes with $OH^{\cdot}$ radicals

4.3. Fenton Catalyst and Photocatalyst to form OH· Radicals

The reactions in the plasma state have created many strong reactive agents and free radicals with very short duration such as: $OH^{\bullet}$, O, H_2O_2, $HO_2^{\bullet}$ with similar oxidation potential values. response: 2.8 V; 2.42 V; 1.78 V and 1.7 V.[72] In order to increase the formation of $OH^{\bullet}$ free radicals in situ to increase the concentration as well as maintain a high activated state, the catalyst systems are commonly used as:[73] H_2O_2/UV;[74] Fenton system (H_2O_2/Fe^{2+});[75] or optical Fenton ($UV/H_2O_2/Fe^{2+}$).[76] When performing DC high Voltage electrochemical reaction on Fe electrode is Fenton catalyst system can be used:[77-79]

$$Fe^{2+} + H_2O_2 \rightarrow OH^{\cdot} + OH^{-} + Fe^{3+} \quad (48)$$

$$Fe^{3+} + H_2O_2 \rightarrow H^{+} + Fe^{2+} + HO_2^{\cdot} \quad (49)$$

$$Fe^{0} + O_2 + 2H^{+} \rightarrow Fe^{2+} + H_2O_2 \quad (50)$$

Thus, the use of Fe electrode to perform a DC high-voltage electrochemical reaction to generate plasma also creates a Fenton catalyst system that always maintains the reactions providing free radicals $OH^{\bullet}$, $HO_2^{\bullet}$ and H_2O_2 , wich. strong reactive agents can be applied to treat water pollution.

V. TREATMENT OF WATER ENVIRONMENTAL POLLUTION

Water is a very important environment for the life of all things and people.[80] However, human production and living activities discharge into the water environment many dissolved or dispersed substances that pollute the water environment, which have toxic effects on the life of organisms as well as human health.[81] Therefore, treatment of water pollutants is becoming more and more urgent to ensure the safety of life.[82] Often water pollutants are chemicals that can be oxidized, reduced, or coagulated and adsorbed to remove them from the environment.[83]

5.1 Oxidizes Difficult-to-Treat Pollutants

Water pollution from the textile and dyeing industry[84] such as methylene blue or from pesticides and herbicides,[85] including from Agent Orange that the US used during the Vietnam War such as $C_8H_6Cl_2O_3$: 2,4- dichlorophenoxyacetic (2,4-D) and $C_8H_5Cl_3O_3$: 2,4,5-trichlorophenoxy acetic (2,4,5-T) both contain persistent cyclic compounds that are difficult to handle.[86] The application of current treatment methods such as: burial, adsorption, combustion or the use of advanced oxidizing agents, although achieving certain efficiency, is still limited, such as using a lot of energy or materials and chemicals as well as land.[87-89] Moreover, the treatment processes are not really thorough, which can still pollute groundwater when burying or create other pollution products for the air from combustion or oxidation reactions.[90] Therefore, the study of highly effective water pollution treatment technologies including plasma technology is being

very noticeable.[91,92] With the electrochemical plasma state, strong reactive agents can be created, including strong oxidizing agents such as $OH^{\bullet}$, H_2O_2,... especially with Fenton's catalyst from the iron electrode, $OH^{\cdot}$-radical insitu can always be formed from the iron electrode stable concentration ensures the waste treatment process in the water environment.[93] Figure 15 shows the treatment efficiency of 2,4-D: 28.98 mg/L and 2,4,5-T: 30.22 mg/L on electrodes W, Cu, Fe (a) at: U_{DC}: 5 kV, H_{AC}; 300 mm, T: 30°C and χ = 38.8 µScm $^{-1}$, t: 60 minutes and (b) treatment results on Fe electrode with the same reaction conditions as (a) with other concentrations of pollutants together.

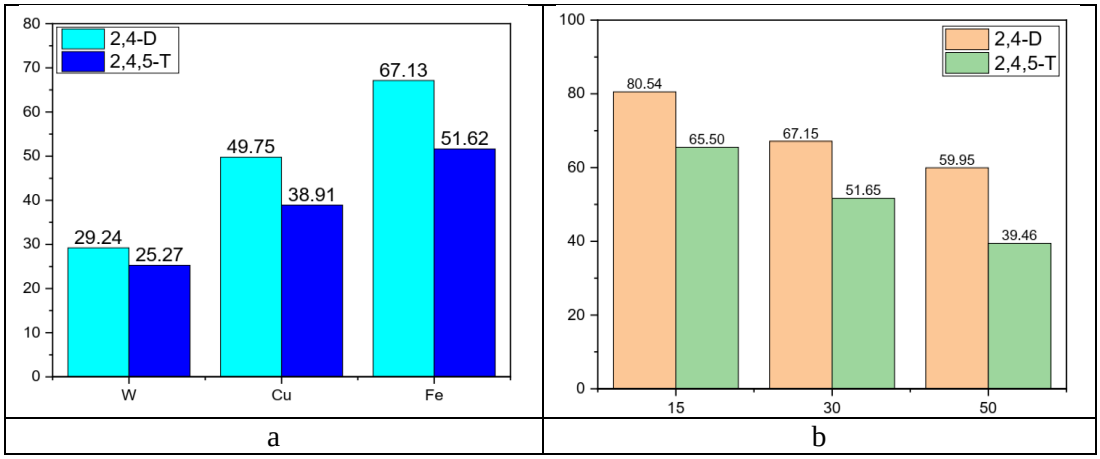

Figure 15: Effect of electrode material (a) and pollutant concentration on treatment efficiency of 2,4-D and 2,4,5-T on Fe electrode (b)

Figure 15(a) shows that the electrochemical plasma treatment efficiency on Fe electrode is much higher than that on Cu and W electrodes. This proves that Fenton catalysis plays a role. With a more complex molecular structure, the treatment efficiency of 2,4,5-T is always lower than that of 2,4-D. Figure 15(b) shows that when increasing the effective pollutant concentration, the effective pollutant concentration will also decrease because the ratio between oxidizing agents such as $OH^{\bullet}$, H_2O_2 in the solution to the substances to be treated in the solution decreases. Effect of high voltage, distance of anode-cathode electrodes, reaction time and ambient temperature on treatment efficiency of 2,4-D and 2,4,5-T by electrochemical plasma on Fe electrode presented in Table 10.

Table 10: Efficiency of treatment of pollution 2,4-D 28.89 mg/L and 2,4,5-T 30.33 mg/L by electrochemical plasma on Fe electrode when changing U_{DC}, t, T and H_{AC} with other general conditions unchanged at: U_{DC}=5 kV, H_{AC}=300 mm, t=60 min, T=30°C and χ =38.8 µScm^{-1}

Parameters change		2,4-D (28,89 mg/L)	2,4,5-T (30,22 mg/L)
U_{DC}, kV	2	25.85 %	20.96 %
	5	67.13 %	51.65 %
	10	93.57 %	88.68 %
t, min	30	47.94 %	36.96 %
	60	67.13 %	51.65 %
	120	86.62 %	71.18 %
T, °C	20	43.98 %	32.78 %
	30	67.13 %	51.65 %
	50	90.18 %	72.52 %
	250	75.92 %	63.55 %

H_{AC}, mm	350	53.22 %	42.74 %
	500	26.83 %	12.81 %

The results from Table 10 show that the treatment efficiency of 2,4-D and 2,4,5-T both increase with increasing DC high voltage, increasing reaction time as well as increasing ambient temperature, but vice versa, the treatment results will decrease sharply as the distance between the anode and cathode increases. That is related to the appearance and existence time of the electrochemical plasma on the iron electrode. The highest efficiency can be achieved at high voltage of 15 kV, distance of 2 electrodes 300 mm, temperature of 30°C, reaction time of 60 minutes and environmental conductivity of 38.8 µScm^{-1} respectively 93.57 % for 2,4-D and 88.68% for 2,4,5-T.

The results from Table 11 also show that the demand for oxidation of organic compounds (COD) as well as the total amount of carbon in water (TOC) decreased rapidly, indicating that the composition of organic substances decreased with increasing electrochemical plasma treatment time. It also shows that there is mineralization of difficult organic compounds such as 2.4-D and 2,4,5-T by oxidation with radicals such as OH$^{\cdot}$ and H_2O_2 to CO_2 and H_2O.

Table 11: Determination of COD and TOC in 2,4-D and 2,4,5-T solutions after different electrochemical plasma treatment times on Fe electrode at: U_{DC}=5 kV, H_{AC}=300 mm, T=30°C and and χ =38.8 µScm^{-1}

	t, phút	mg/L	%	mg/L	%
COD	0	196		57.0	
	30	40.2	62.1	30.2	47.0
	60	15.9	85.0	12.4	78.2
	90	6.8	93.6	8.9	84.4
TOC	0	6.1		4.6	
	30	4.7	22.9	3.7	19.5
	60	3.7	19.5	2.9	36.9
	90	2.8	54.1	2.4	47.8
	120	2.1	65.6	1.8	60.8

The results of GC-MS analysis of intermediate products formed during the reaction and after 120 min by electrochemical plasma are presented in Figure 16.

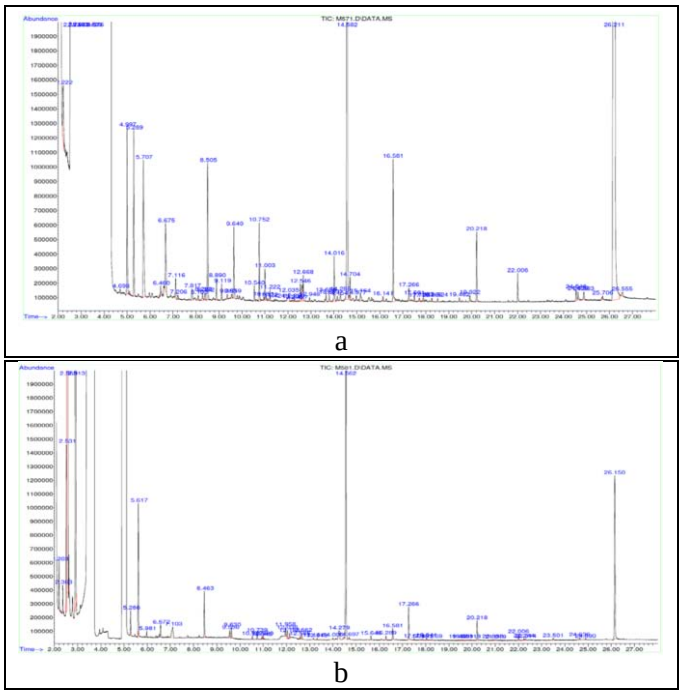

a

b

Figure 16: GC-MS spectrum of 2,4-D (a) and 2,4,5-T (b) decomposition products after 120 minutes of electrochemical plasma reaction at: U_{DC}=5 kV, H_{AC} =300 mm , T=30°C and χ =38.8 µScm^{-1}

Table 12 presents the intermediate organic compounds of 2,4-D and 2,4,5-T by electrochemical plasma that can be found by GC-MS spectroscopy.

Besides the formation of organic intermediates, the 2,4-D and 2,4,5-T process by electrochemical plasma also performs a dechlorination reaction that produces electrolytes that increase electrical conductivity. Figure 17 presents the conductivity change of the 2,4-D and 2,4,5-T solutions after the electrochemical plasma treatment times.

Table 12: Phenolic compounds and organic acids intermediates of 2,4-D and 2,4,5-T treatment determined by GC-MS

No.	Name of compound	t_{luu}, min
1	Phenol	6.839
2	4-chlorophenol-TMS este	10.233
3	1-chlorophenol	10.387
4	2,3-dichlorophenol	9.925
5	3,4-dichlorophenol	13.258
6	2,4-dichlorophenol	9.844
7	2,4,5-dichlorophenol	12.498
8	2,4,6-dichlorophenol	12.580
9	2,3,5-trichlorophenol	12.432
10	Axit formic-TMS este	2.198
11	Axit acetic-TMS este	2.911
12	Axit propanoic-TMS este	4.051
13	Axit propanoic, 2-methylTMS este	5.328
14	Axit pentanoic-TMS este	6.842
15	Axit propanoic, 2-[TMSoxi]-,TMS este	8.235
16	Axit hexanoic-TMS este	8.355
17	Axit pentanoic, 4-oxo-, TMS este	9.324

18	Axit succinic-TMS este	11.958
19	Axit oxalic-TMS este	12.038

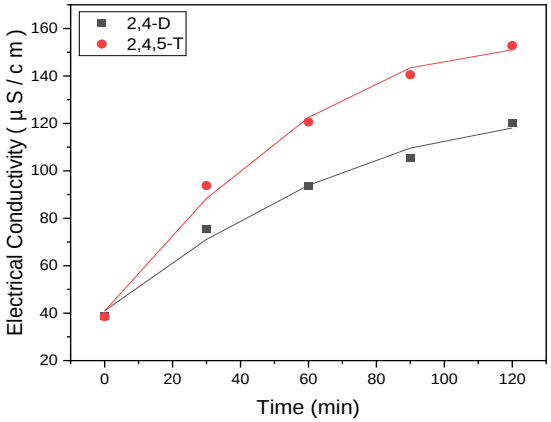

Figure 17: Change of conductivity of 2,4-D and 2,4,5-T solutions with time of electrochemical plasma treatment on Fe electrode at U_{DC}=5 kV, H_{AC}=300 mm, T = 30°C

From Figure 17 it can be seen that after 120 min of electrochemical plasma treatment on the Fe electrode, the conductivity of the solution increased from 38.8 μScm^{-1} up to 150 μScm^{-1} with 2,4-5-T and 110 μScm^{-1} with 2,4-D. Since 2,4,5-T contains 3 Cl^- more than 2,4-D contains only 2 Cl^-, the conductivity of the treated solution is always higher.

From the above results, it can be assumed that the oxidation of 2,4-D and 2,4,5-T by $OH^{\bullet}$ by electrochemical plasma will form phenol compounds and then open the ring into straight organic acids and continue to be mineralized into CO_2 and H_2O according to the following diagram:

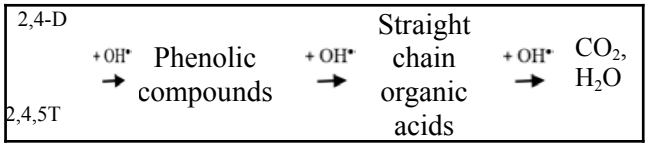

Thus, the process of treating difficult-to-treat pollutants with cyclic structures such as 2,4-D and 2,4,5-T by electrochemical plasma with forming $OH^{\bullet}$- radicals is not only highly efficient but also thoroughly mineralized.

Methylene blue dye: $C_{16}H_{18}ClN_3S$ - Phenothiazine-5-ium, 3,7-bis(dimethylamino)-, chloride is also easily treated by electrochemical plasma on the Fe electrode. Figure 16 shows the reduction of methylene blue concentration as well as total organic carbon (TOC) over time of the solution when treated with electrochemical plasma on the iron electrode at U_{DC}: 2.5 kV, H_{AC}: 300 mm, pH: 6.06.

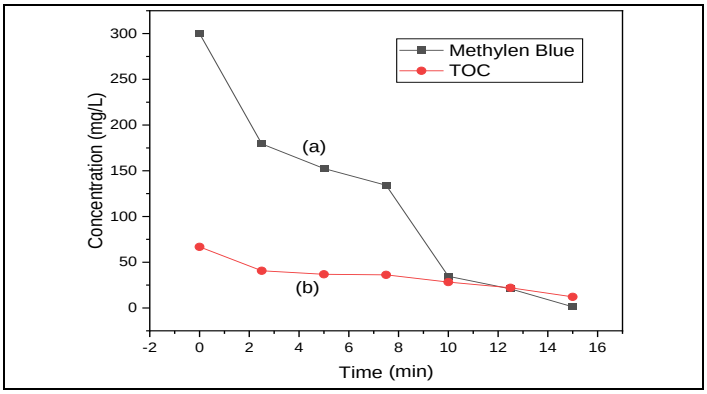

Figure 18: Remaining methylene blue concentration (a) and TOC (b) of solution after electrochemical plasma treatment on Fe electrode at U_{DC}=2.5 kV, H_{AC}=300 mm, pH=6.06

From Figure 18 it can be seen that the electrochemical plasma treatment of methylene blue on the Fe electrode also achieves very high efficiency and complete mineralization.

5.2 Combining Capabilities

In addition to strong oxidation free radicals, electrochemical plasma on Fe electrode also creates reducing agents and flocculation to be used to treat other difficult environmental pollutants.

Ammonium-contaminated water is always concerned by scientists because the existence in the water will turn into NO_3^- and NO_2^-, which is also toxic, easily converted to nitrosamines in the body, causing cancer. Therefore, according to QCVN 08-MT, 2015/BTNMT stipulates the limit value of ammonium in water is very low: 0.3 mg/L (level A) and 0.9 mg/L (b).[94] Ammonium treatment methods such as stripping chasing NH_3,[95,96] adsorbing,[97] flocculation,[98,99] advanced oxidation (AOPS)[100] or biotechnology[101] still limited as complex equipment, use a lot energy and chemicals as well as the effect are not as expected.[102,103] Therefore, the use of plasma to treat ammonium is also being noticed.[104]

Figure 19 shows that the ammonium concentration decreases quite rapidly with time (a) as well as increases the electrochemical plasma treatment DC voltage (b).

Figure 19a shows that from 800 mg/L concentration to 100 mg/L in 14 minutes of electrochemical plasma treatment at U_{DC}: 1.5 kV, H_{AC}: 350 mm, pH: 6.7. Processing efficiency after 8 minutes has reached 58%.

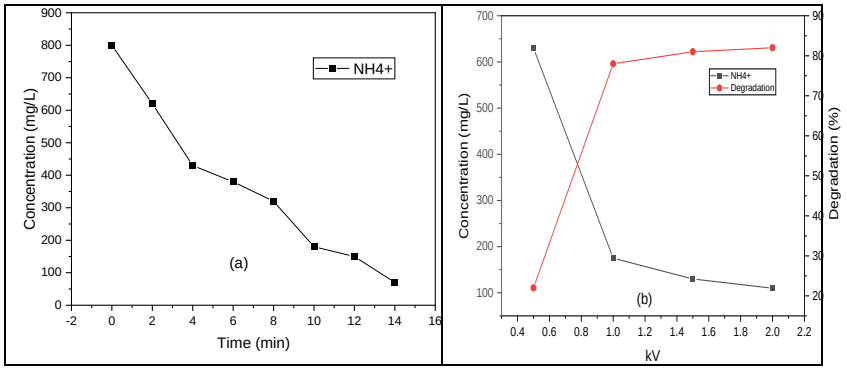

Figure 19: Ammonium concentration decreased with electrochemical plasma treatment time at U_{DC}: 1.5 kV, H_{AC}: 350 mm, pH: 6.7 (a) as well as with increasing DC voltage and corresponding efficiency also increased (b)

Figure 19b shows that at a DC voltage of 0.5 kV, the ability to remove ammonium is still low, but from 1.0 kV onwards, the ammonium concentration has decreased to nearly 100 mg/L after 10 minutes and the treatment efficiency has reached nearly 80% then more than 80% when the voltage is 1.5 kV.

With strong oxidizing agents such as H_2O_2, $OH^{\cdot}$ radicals are formed from electrochemical plasma, ammonia pollution can also be oxidized by the following reactions:

$$NH_4^+ + 5H_2O_2 \rightarrow NO_3^- + 7H_2O \quad (51)$$

$$NH_4^+ + 10OH^{\cdot} \rightarrow NO_3^- + 7H_2O \quad (52)$$

$$NH_4^+ + 4H_2O_2 \rightarrow NO_2^- + 6H_2O \quad (53)$$

$$NH_4^+ + 8OH^{\cdot} \rightarrow NO_2^- + 6H_2O \quad (54)$$

Figure 20 shows the variation of NH_4^+, NO_3^- and NO_2^- concentrations over time up to 240 min of electrochemical plasma treatment at U_{DC}: 0.5 kV, H_{AC}: 350 mm, pH: 6.7.

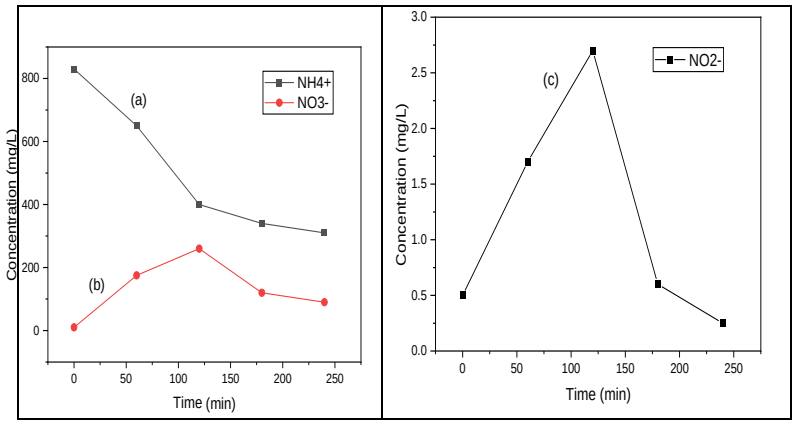

Figure 20: Concentrations of NH_4^+(a), NO_3^-(b) and NO_2^-(c) in ammonium wastewater treated with electrochemical plasma at U_{DC}: 0.5 kV, H_{AC}: 350 mm with time up to 240 minutes

From Figure 20 it can be seen that when increasing the electrochemical plasma treatment time at U_{DC}: 0.5 kV, the ammonia concentration decreased by more than 400 mg/L in 120 min (Figure 20a) while the NO_3^- concentration increased by nearly 250 mg /L (Figure 20b) and NO_2^- concentration increased by nearly 25 mg/L (Figure 20c). From the 120th minute, the concentration of NH_4^+ continued to decrease slightly while the concentration of NO_3^- and NO_2^- both decreased sharply to 150 minutes and then continued to decrease slightly to 240 minutes. The concentration of NO_3^- and NO_2^- increased correspondingly with the decrease of NH_4^+ concentration, indicating that the reactions (51) to (54) occurred when ammonia pollution was treated with electrochemical plasma. But after 120 minutes, the concentrations of NO_3^- (Figure 20b) and NO_2^- (Figure 20c) decreased again as the reaction time continued to increase, indicating that reduction occurred with H_2 gas formed from electrochemical plasma that can be simulated set according to the following reactions:

$$2NO_3^- + 6H_2 \rightarrow N_2 + 6H_2O \quad (55)$$

$$2NO_2^- + 4H_2 \rightarrow N_2 + 4H_2O \quad (56)$$

Thus, the combination of oxidizing and reducing agents caused by electrochemical plasma to produce ammonia pollution can be treated sparingly so as not to form intermediate products that still pollute the environment.

VI. CONCLUSION

The process of electrodes with high DC voltage to create electrochemical plasma on the electrodes will form many oxidizing and reducing substances in gaseous state, ions or radicals such as H_2, O_2, Ag^+, Fe^{2+}, $OH^{\cdot}$ etc in the aquatic environment for the production of metal nanomaterials or for the treatment of chemical substances that pollute the environment.

Characteristics as well as efficiency of manufatoring of metal nanoparticles as well as water pollution treatment can be controlled by high -voltage electrochemical reaction technology parameters such as: voltage, distance between the anode and cathode, the environmental temperature and the conductivity of the solution.

AgNPs or Cu/AgNPs solution is prepared by high pressure DC and electrochemical plasma with appropriate technological conditions will obtain a particle size, concentration as well as stability and ability to kill bacteria compare with other methods. The outstanding advantage is that the product is obtained without agents for reducing and stabilizers, so high purity promises to apply for medicine.

Strong oxidizing agents such as H_2O_2, $OH^{\bullet}$-radicals as well as Fenton catalysts supporting the generation of insitu radicals have been used to treat environmental pollutants such as 2,4-D as well as 2,5,5-T and methylene blue dye. Although these polluting chemicals have aromatic rings that are difficult to handle, by high voltage DC with electrochemical plasma they are all treated with a fairly thorough mineralization process to CO_2 and H_2O. The advantage of electrochemical plasma pollution treatment is that it does not use materials, chemicals and does not create polluting intermediate products, so it is considered an environmentally friendly method. Combining oxidizing and reducing agents and large amounts of gas from plasma water decomposition to treat ammonium contaminated water and intermediate products NO_3^- and NO_2^- also achieves high and thorough efficiency up to N_2. The advantage of the method is that it also does not use chemical materials as well as large areas, but the processing time is quite fast.

Conflict of interest: The authors declare that they have no competing interests.

ACKNOWLEDGMENTS

We acknowledge the support of the fund NAFOSTED and VAST for facilitating with the study as well as the PhD students and master students who have conducted research in this direction.

REFERENCES

1. Allen J. Bard, Larry R. Faulkner, Electrochemical Methods: Fundamentals and Applications, New York: Wiley, *2001*, 2nd ed.
2. AP O'Mullane, Electrochemistry, Elsevier Inc. *2013*.
3. Rashid A. Khaydarov, Renat R. Khaydarov, Olga Gapurova, Yuri Estrin, Thomas Scheper, Electrochemical method for the synthesis of silver nanoparticles, *J. Nanopart. Res.*, *2009*, *11*, 1193 – 1200.
4. Liang C. L., Zhong K., Liu M., Jiang L., Liu S. K., Xing D. D., Li H. Y., Na Y., Zhao W. X., Tong Y. X., Liu P., Synthesis of morphology-controlled silver nanostructures by electrodeposition Nano-*Micro Letters*, 2010, *2(1), 6-10*.
5. Nguyen Cong Phuc, Nguyen Duc Hung, Bactericidal activity of nano silver and nanocomposite Ag/Al_2O_3 using electrochemical deposition, Vietnam J. Chem., *2010*, *41(4)*, 409-413.
6. Doan Thi Kim Bong, Nguyen Nhi Tru, Preparation of silver nano-solutions by electrolysis combined with ultrasound, *Vietnam J. Chem.*, *2012*, *50(5A)*, 343-346.
7. San P.T., Khoa T.A., Hoang N., Electrochemical Method for Synthesis of Silver Nanoparticles, *Vietnam Journal of Science and Technology*, *2010*, *48(5A)*, 150 -154.
8. Vo Huu Thinh, Nguyen Nhi Tru, Preparation of copper nanoparticle solution by electrochemical technique, *Vietnam Journal of Science and Technology*, *2013*, *51(5B)*, 21 -26
9. Truong Anh Khoa, Phạm Trung San, Nguyen Hoang, Le Lan Anh, Research on the preparation of nano silver applied in medicine by electrochemical method, *Journal of analytical Sciences*, 2012, *17*, 35-40.
10. Nguyen Duc Hung, Mai Van Phuoc, Nguyen Minh Thuy, Conductivity of silver nanoparticle solution, *Journal of Military Science and Technology Research*, *2012*, *17(2)*, 96-101.
11. Nguyen Duc Hung, Electrochemical reaction at high voltage with electrode plasma, *Vietnam J. Chem.*, *2012*, *50(ĐB)*, 103-111

12. Vietnam standard, Water for analytical laboratory use - Specification and test methods, TCVN 4854-*1989* (ISO 3696:*1987*).
13. Nguyen Duc Hung, Method for preparation of metallic silver nanosolutions and equipment for implementing this method, Patent, No. 12229, *2013*, December 31.
14. Tadahiko Mizuno, Tadayoshi Ohakimoto, Akito Takahashi, Production of Heat during Plasma Electrolysis in Liquid, *The Japan Society of Applied Physis*, Part 1, *2000*, *10* .
15. Mai Van Phuoc, Nguyen Minh Thuy, Nguyen Duc Hùng, Energy balance in the process of creating silver nanoparticles using high-voltage electrochemical nanotechnology, *Vietnam J. Chem.*, *2014*, *52(6B)*, 183-186.
16. S. -K. Sengupta, R. Singh, A. -K. Srivastava, A Study on the Origin of Nonfaradaic Behavior of anodic Contact Glow Discharge Electrolysis, *J. Electrochem. Soc.*, *1998*, *145(7)*, 2209-2213.
17. Li Xu, Yi-Yi Wang, Jie Huang, Chun-Yuan Chen, Zhen-Xing Wang, Hui Xie, Silver nanoparticles: Synthesis, medical applications and biosafety, *Theranostics*, *2020*, *10(20)*, 8996-9031.
18. Kholoud M.M Abo El-Nour, Ala'a Eftaiha, Abdulrhman Al-Wrthar Reda A.A. Ammar, Synthesis and applications of silver nanoparticles, *Arabian Journal of Chemistry*, *2010*, *3*, 135-140.
19. Nasretdinova, Gulnaz R., Fazleeva, Rezeda R., Mukhitova, Rezeda K., Nizameev, Irek R., Kadirov, Marsil K., Ziganshina, Albina Y., Yanilkin, Vitaliy V., Electrochemical synthesis of silver nanoparticles in solution, *Electrochemistry Communications*, *2015*, *50*, pp. 69–72.
20. T. Sowmyya, G. Vijayalakshmi, Green synthesis and characterization of silver nanoparticles using Soymida febrifuga aqueous leaf extract, *World J. Pharm. Sci.*, *2016*, *5(1)*, 786-805.
21. Sukdeb Pal, Yu Kyung Tak, Joon Myong Song, Does the Antibacterial Activity of Silver Nanoparticles Depend on the Shape of the Nanoparticle? A Study of the Gram-Negative Bacterium *Escherichia coli*,*Applied and Environmental Microbiology, 2007, 73(6),* 1712-1720
22. Hayelom Dargo Beyene, Adhena Ayaliew Werkneh, Hailemariam Kassa Bezabh, Tekilt Gebregergs Ambaye, Synthesis paradigm and applications of silver nanoparticles (AgNPs), a review, *Sustainable Materials and Technologies*, *2017*, *13*, 18–23.
23. Xuan Hoa Vu, Thi Thanh Tra Duong, Thi Thu Ha Pham, Dinh Kha Trinh, Xuan Huong Nguyen, Van-Son Dang, Synthesis and study of silver nanoparticles for antibacterial activity against *Escherichia coli* and *Staphylococcus aureus*, *Adv. Nat. Sci.: Nanosci. Nanotechnol. 2018*, *9*, 025019 (7pp).
24. Atiqah Salleh, Ruth Naomi, Nike Dewi Utami, Abdul Wahab Mohammad, Ebrahim Mahmoudi, Norlaila Mustafa, Mh Busra Fauzi, The Potential of Silver Nanoparticles for Antiviral and Antibacterial Applications: A Mechanism of Action, *Nanomaterials 2020*, *10*, 1566 (20 pp).
25. Rama Koyyati, Vee babu Nagati, Rạu Nalvothula, Ramchander Merugu, Karunakar Rao Kudle, Paul Max, Pratap Rudra Manthur Padigya, Antibacterial activity of silver nanoparticles synthesized using *Amaranthus viridis* twig extract, *Int.J. Res. Pharm. Sci., 2014, 5(1),* 32-39.
26. S Elumalai, R Devika, Biosynthesis of silver nanoparticles using *curcuma longa* and their antibacterial activity, *Int. J. Pharm. Res. Sci., 2014, 02(1),* 98-103.
27. Ratyakshi, R.P. Chauhan, Colloidal Synthesis of Silver Nano Particles, *Asian Journal of Chemistry, 2009, 21(10)*, 113-116.
28. Guangyu Zhang, Yan Liu, Xiaoliang Gao, Yuyue Chen, Synthesis of silver nanoparticles and antibacterial property of silk fabrics treated by silver nanoparticles, *Nanoscale Research Letters, 2014, 9,* 216-224.
29. Amany A. El-Kheshen, Sanaa F. Gad El-Rab, Effect of reducing and protecting agents on size of silver nanoparticles and their anti-bacterial activity, *Der Pharma Chemica*, *2012, 4(1),* 53-65.
30. Zong-ming Xiu, Qing-bo Zhang, Hema L. Puppala, Vicki L. Colvin, Pedro J. J.Alvarez, Negligible Particle-Specific Antibacterial Activity of Silver Nanoparticles, *Nano Lett. 2012*, *12*, 4271-4275.

31. Ratan Das, Sneha Gang, Siddhartha Sankar Nath, Preparation and Antibacterial Activity of Silver Nanoparticles, *Journal of Biomaterials andNanobiotechnology*, *2011*, *2*, 472-475.
32. Nguyen Minh Thuy, Research on electrochemical dissolution reaction at the anode (anode) to create silver nano solution by high voltage, Military Academy of Science and Technology, Thesis of Ph. D, 2014.
33. Nguyen Minh Thuy, Nguyen Duc Hung, Nguyen Thị Ngoc Tinh, Nguyen Nhị Tru, Silver nano solution prepared by high-voltage electrochemical method: bactericidal ability and application in medicine and pharmacy. *Vietnam J. Chem., 2012, 50(5A)*, 134-138.
34. N.Q. Buu, T.T.N. Dung, N.H. Chau, D.T. Hieu, Studies on manufacturing of topical wound dressings based on nanosilver produced by aqueous molecular solution method, *J. Exp. Nanoscience*, *2011, 6(4)*, 409-421.
35. Nguyen Thi Huong, Nguyen Viet Hung, Preparation of silver nano colloidal solution with sucrose reducing agent, *Journal of Military Science and Technology*, *2011*, *10(15)*, 86-91.
36. Tadahiko Mizuno, Tadasi Akimoto, Kazuhisa Azumi, Tadayoshi Ohmori, Yoshiaki Aoki, AkitoTakahasi, Hydrogen Evolution by Plasma Electrolysis in Aqueous Solution, *Japanese Journal of Applied Physics*, *2005, 44(1A)*, 396-401.
37. Wenjing Zhang, Aijuan Zhang, Ying Guan, Yongjun Zhang, X. X. Zhu, Silver-loading in uncrosslinked hydrogen-bonded LBL films: structure change and improved stability, *J. Mater. Chem.*, *2011*, *21*, 548–555.
38. Carla Gasbarri, Maurizio Ronci, Antonio Aceto, Roshan Vasani, Gianluca Iezzi, Tullio Florio, Federica Barbieri, Guido Angelini, Luca Scotti, Structure and Properties of Electrochemically Synthesized Silver Nanoparticles in Aqueous Solution by High-Resolution Techniques, *Molecules*, *2021*, *26*, 5155.
39. X. Wang, H.F. Wu, Q. Kuang, R.B. Huang, Z.X. Xie, L.S. Zheng, Shape-dependent antibacterial activities of Ag_2O polyhedral particles, *Langmuir*, *2010*, *26(4)*, 2774-2778.
40. S. Link, Z. L. Wang, M. A. El-Sayed, Alloy formation of gold-silver nanoparticles and the dependence of the plasmon absorption on their composition, *J. Phys. Chem. B*, *1999*, *103(18)*, 3529-3533.
41. Z. Kiani, Y. Abdi, E. Arzi, Low temperature formation of silver and silver-copper alloy nanoparticles using plasma enhanced hydrogenation and their optical properties, *World Journal of Nano Science and Engineering*, *2012*, *2*, 142-147.
42. Nguyen Duc Hung, Tran Van Cong, Hoang Nhu Trang, Synthesis of bimetallic Cu-Ag nanoparticles prepared by DC high voltage electrochemical method, *Vietnam J. Chem.*, *2019*, *57(5)*, 609-614.
43. Tien D.C., Liao C. Y., Huang J. C., Tseng K. H., Lung J. K., Tsung T. T., Kao W. S., Tsai T. H., Cheng T. W., Yu B. S., Lin H. M., Stobinski L., Novel technique for preparing a nano-silver water suspension by the arc-discharge method, *Rev. Adv. Marter. Sci.*, *2008*, *18*, 750-756.
44. Kroesen G.M.W., Schram D.C., De Haas J.C.M., Description of cascade arc plasma, *Plasma Chemistry and Plasma Processing*, *1990*, *10(4)*, 531–551
45. B. Jiang, J.T. Zheng, S. Qiu, M.B. Wu, Q.H. Zhang, Z.F. Yan, Q.Z. Xue, Novel technique for preparing a nano-silver water suspension by the arc-discharge method, *Rev. Adv. Marter. Sci.*, *2008*, *18*,. 750-756.
46. Fang-Chia Chang, Carolyn Richmonds, R. Mohan Sankarana, Microplasma-assisted growth of colloidal Ag nanoparticles for point-of-use surface-enhanced Raman scattering applications, *J.Vac.Sci.Technol.A*, *2010*, *28(4)*, 5-8
47. Park J., Henins I., Herrmann H.W., Selwyn G.S., Hicks R.F., Discharge phenomena of an atmospheric pressure radio frequency capacitive plasma source, *Journal of Applied Physics*, *2001*, *89*,. 20.
48. Hopwood J., Review of inductively coupled plasmas for plasma processing, *Plasma Sources Science and Technology*, *1992*, *1(2)*, 109–116.
49. Ruma Hosano H., Sakugawa T., Akijama H., The Role of pulse voltage amplitude on

chemical processes incluced by streamer discharge at water surface, *Catalysts*, *2018*, *8*, 213, doi: 10.3390/cât18050213
50. Seong Cheol Kim, Sung Min Kim, Jung Wan Kim, Sang Yul Lee, Synthesis nanoparticles using solution plasma process and their various applications, *The 4th. International Workshop on Nanotechnology and Application*, Vung Tau, *2013*, 71-74.
51. Leroux F., Perwuelz A., Campagne C., Behary N., Atmospheric air-plasma treatments of polyester textile structures, *Journal of Adhesion Science and Technology*, *2006*, *20(9)*, 939.
52. Sugiarto A.T., Ohshima T., Sato M.. Advanced oxidation processes using pulsed streamer corona discharge in water, *Thin Solid Films*, *2002*, 407, 174-178.
53. Sunka P., Babicky V., Clupek M., Lukes P., Simek M., Schmidt J., Cernak M, Generation of chemically active species by electrical discharges in water, *Plasma Sources Sci. Technol*, *1999*, *8*, 258-265.
54. Lukes P., Locke B.R., Brisset J.L., Aqueous-phase chemistry of electrical discharge plasma in water and in gas-liquid environments, *2012*, WileyVCH Verlag GmbH & Co. KgaA, pp. 243-308.
55. Joshi A.A., Locke B.R., Arce P., Finney W.C., Formation of hydroxyl radicals, hydrogen peroxyde and aqueous electrons by pulsed streamer corona discharge in aqueous solution, *Journal of Hazardous Materials*, *1995*, *41*, 3-30.
56. Sahni M., Locke B.R., Quantification of hydroxyl radicals produced in aqueous phase pulsed electrical discharge reactors, *Ind. Eng., Chem. Res*, *2006*, *45*, 5819-5825.
57. T. Mizuno, T. Akimoto, K. Azumi, T. Ohmori, Y. Aoki, A. Takahashi, Hydrogen Evolution by plasma electrolysis in aqueous solution, *Japanese Journal of Applied Physics*, *2005*, *44*(1A), 396-401.
58. Kirkpatrick M.J., Locke B.R., Effects of platinum electrode on hydrogen, oxygen, and hydrogen peroxide formation in aqueous phase pulsed corona electrical discharge, *Ind. Eng. Chem. Res*, *2006*, *45*, 2138-2142.
59. Porter D., Poplin M.D., Holzer F., Finney W.C., Locke B.R., Formation of hydrogen peroxide, hydrogen, and oxygen in gliding arc electrical discharge reactors with water spray, *Transactions on industry applications*, *2009*, *45*, 623-629
60. Wang L., 4-Chlorophenol Degradation and Hydrogen Peroxyde Formation Induced by DC Diaphragm Glow Discharge in an Aqueous Solution, *Plasma Chem Plasma Process*, *2009*, *29*, 241-250.
61. Stara Z., Krcma F., The study of H_2O_2 generation by DC diaphragm discharge in liquids, *Czechoslovak Journal of Physics*, *2004*, *54*, 1050-1055.
62. Sayed M., Efficient removal of phenol from aqueous solution by the pulsed high-voltage discharge process in the presence of H_2O_2, *Chemistry International*, *2015*, *1(2)*, 81-86.
63. Peralta E., Roa G., Servin J.H., Romero R., Balderas P., Hydroxyl Radicals quantification by UV spectrophotometry, *Electrochimica Acta*, *2014,* http://dx.doi.org/10.1016/j.electacta.2014.02.047.
64. Anpilov A.M., Barkhudarov E.M., Bark Y.B., Zadiraka Y.V., Christofi M., Kozlov Y.N., Kossyi I.A., Kop'ev V.A., Silakov V.P, Taktakishvili M.I., Temchin S.M., Electric discharge in water as a source of UV radiation, ozon and hydrogen peroxyde, *Journal of Physic. D: Applied Physic*, *2001*, *34*, 993-999.
65. Tran Van Cong, Reseaching high voltage electrochemical engineering of applied electrodic plasma generation for decomposition of 2,4-dichlorophenoxyacetic acid and 2,4,5-trichlorophenoxyacetic acid in water environment, Thesis of Ph.D., Academy of Military Science and Technology, 2022.
66. Ronald S. Lankone, Alyssa R. Deline, Michael Barclay, D. Howad Fairbrother, UV-Vis quantification of hydroxyl radical concentration and dose using principal component analysis, *Talanta*, *2020*, *218*, 121148.
67. E. Peralta, G. Roa, J.A. Hernandez-Servin, R. Romero, P. Balderas, R. Natividad,Hydroxy Radicals quantification by UV spectrophotometry, *Electrochimica Acta*, *2014*, *129*, 137-141.

68. Chongchong Wu, Alex De Vischer, Ian Donald Gates, Reactions of hydroxyl radicals with benzoic acid and benzoate, *ASC Advances*., *2017*, *7*, 35776-35785.
69. Haiqian Zhao, Jihui Gao, Wei Zhou, Zhonghua Wang, Shaohua Wu, Quantitative detection of hydroxyl radicals in Fenton system by UV-Vis spectrophotometry, *Analytical Methods*, *2015*.
70. Manfred Saran, Karl H. Summer, Assaying for Radicals: Hydroxylated Teraphthalate is a Superior Fluorescence Marker than Hydroxylated Benzoate, *Free Rad. Res*., *1999*, *31*, 429-436.
71. Arthur L. Sagone, Mary Ann Decker, Rose Marie Wells, Charles Democko ,A new method for the detection of hydroxyl radiacal production by phagocytic cells, *Biochimica et Biophysica Acts*, *1980*, 628, 90-97.
72. Lukes P., Water treatmen by pulsed streamer corona discharge, Ph.D.Thesis, *2001*, Institute of plasma physics academy of sciences of the Czech Republic.
73. Lukes P., Clupek M., Babicky V., Sisrova I., Janda V., The catalytic role of tungsten electrode material in the plasmachemical activity of a pulsed corona discharge in water, *Plasma Sources Science and Technol*, *2011*, *20*, 1-11.
74. Ruzhong Chen and Joseph J. Pignatello, Role of Quinone Intermediates as Electron Shuttles in Fenton and Photoassisted Fenton Oxidations of Aromatic Compounds, *Environ. Sci. Technol. 1997*, *31*, 2399-2406.
75. F. Abdelmalek, R.A. Tores, E. Combet, C. Petrier, C. Pulgarin, A. Addou, Gliding Arc Discharge (GAD) assisted catalytic degradation of bisphenol a in solution with ferrous ions, *Separation and Purification Technology*, *2008*, *63*, 30-37.
76. Xiaolong Hao, Minghua Zhou, Qing Xin, Lecheng Lei, Pulsed discharge plasma induced Fenton-like reaction for the enhancement of degradation of 4-chlorophenol in water, *Chemosphere*, *2007*, *66*, 2185-2192.
77. Shunsuke Tomizawa, Meguru Tezuka, Kinetics and Mechnism of Organic Degradation in Aqueous Solution Irradiated with Gaseous Plasma, *Plasma Chem. Plasma Process*, *2007*, *27*, 486-495.
78. Jong K.I., Huyn S.S., Kyung D.Z., Perchlorate removal in Fe^0/H_2O_2 systems: Impact of oxygen availability and UV radiation, *Journal of Hazardous Materials*, *2011, 192*, 457- 464.
79. Xia Q., Jiang Z., Wang J., Yao Z., A facile preparation of hierarchical dendritic zero valent iron for Fenton-like degradation of phenol, *Catalysis Communications*, *2017*, *100*, 57-61.
80. Basil Amaka-Anolue, Agu Augustine, Agbo Christain, Water use efficiency and conservation in green building, *Journal of Environmental Management and Safety*, *2022*, *13*,1, 67-78.
81. Li Lin, Haoran Yang, Xiaocang Xu, Effects of Water Pollution on Human Health and Disease Heterogeneity: A Review, *Water and Wastewater Management*, *2022*, *10*, 1-20.
82. Arvaniti OS, Stasinakis AS, Review on the occurrence, fate and removal of perfluorinated compounds during wastewater treatment. *The Science of the Total Environment*, *2015*, *524–525*: 81–92.
83. A. Saravanan, P. Senthil Kumar, S.Jeevanantham, S.Karishma, b. Tajsabreen, P.R. Yaashikaa, B. Reshma, Effective water/wastewater treatment methodologies for toxic pollutants removal: Processes and applications towards sustainable development, *Chemosphere*, *2021*, *280*, 130595.
84. Reddy P.M.K., Raju B.R., Karuppiah J., Reddy E.L., Subrahmanyam. C., Degradation and mineralization of methylene blue by dielectric barrier discharge non-thermal plasma reactor, *Chemical Engineering Journal*, *2013*, *217*, 41-47
85. Lu Q., Yu J., Gao J., Degradation of 2,4-dichlorophenol by using glow discharge electrolysis, *J. of Hazardous Materials*, *2006*, *B1*,36, 526-531.
86. Reddy, P.M.K., Subrahmanyam, C., Green approach for wastewater treatment degradation and mineralization of aqueous organic pollutants by discharge plasma, *Ind. Eng. Chem. Res*, *2012*, *51*, 11097-11103.
87. Pasinszki, T., Krebsz, M., Synthesis and Application of Zero Valent Iron Nanoparticles in Water Treatment, Environmental

Remediation, Catalysis, and Their Biological Effects, *Nanomaterials*, *2020*, *10*, 917.
88. Li H.O.L., Kang J., Urashima K., Saito N., Comparison between the mechanism of liquid plasma discharge process in water and organic solution, *Journal of Institute Electrostat Janpan*, *2013*, *37*, 22-27.
89. Jiang B., Zheng J., Liu Q., Wu M., Degradation of azo dye using non-thermal plasma advanced oxidation process in a circulatory airtight reactor system, *Chemical Engineering Journal*, *2012*, *204-206*, 32-39.
90. Peyton, G.R., Glaze, W.H., Destruction of pollutants in water with ozone in combination with ultraviolet radiation. 3. Photolysis of aqueous ozone, *Environ. Sci. Technol*, *1998*, *22*, 761-767.
91. Jiang, B., Zheng, J., Qiu, S., Wu, M., Zhang, Q., Yan, Z., Xue, Q., Review on electrical discharge plasma technology for wastewater remediation, *Chemical Engineering Journal*, *2014*, *236*, 348-368.
92. Locke B.R., Thagard S.M., Analysis and review of chemical reactions and transport processes in pulsed electrical discharge plasma formed directly in liquid water, *Plasma Chem Plasma Process*, *2012*, *32*, 875-917.
93. Tran Van Cong, Nguyen Duc Hung, Ngoc Dung Tran Thi, Nguyen Van Hoang, Surya Veerendra Vattikuti, Nam Nguyen Dang, Electrochemical plasma for treating 2,4,5 trichlorophenoxyacetic acid in water environment using iron electrodes, *ÁCS Omega*, *2021*, *6*, 26329-26337.
94. QCVN 08-MT:2015/BTNMT, National technical regulation on surface water quality, Ministry of Natural Resources and Environment of Vietnam, *2015*.
95. Lennevey Kinidi, Ivy Ai Wei Tan, Noraziah Binti Abdul Wahab, Khairul Fikri Bin Tamrin, Cirilo Nolasco Hipolito, Shanti Faridah Salleh, Review Article: Recent Development in Ammonia Stripping Process for Industrial Wastewater Treatment, International Journal of Chemical Engineering, *2018*, Vol. *2018* | Article ID 3181087 | https://doi.org/10.1155/2018/3181087.
96. A. Bonmati, X. Flotats, Air stripping of ammonia from pig slurry: characterisation and feasibility as pre- or posttreatment to mesophilic anaerobic digestion, *Waste Management*, *2003*, *23*(3), 261–272.
97. Jianyin Huang, Nadeeka Rathnayke Kankanamge, Christopher Chow, David T. Welsh, Tianling Li, Peter R. Teasdale, Removing ammonium from water and wastewater using cost-effective adsorbents: A review, *Journal of environmental sciences*, *2017*, doi.org/10.1016/j.jes 2017.09.009.
98. X. Z. Li., Q. L. Zhao., X. D. Hao, Ammonium removal from landfill leachate by chemical precipitation, *Waste Management, China*, *1999*, *19*(6), 409 – 415.
99. Borojovich EJC, Münster M, Rafailov G, Porat Ze, Precipitation of Ammonium from Concentrated Industrial Wastes as Struvite: A Search for the Optimal Reagents, *Water Environment Research*, *2010*, *82*(7), 586-591.
100. D. Kanakaraju, B. D. Glass, M. Oelgemöller, Advanced oxidation process-mediated removal of pharmaceuticals from water: A review, *Journal of Environmental Management*, *2018*, *219*, 189–207.
101. Nicole D. Berge., Debra R. Reinhart., John Dietz and Tim Townsend, In situ ammonia removal in bioreactor landfill leachate, *Waste Management*, *2005*, *26*(1), 334 - 343.
102. Karri RR, Sahu JN, Chimmiri V. Critical review of abatement of ammonia from wastewater, *Journal of Molecular Liquids*. *2018*, *261*, 21-31.
103. V.K. Gupta; H. Sadegh; M. Yari; R. Shahryari Ghoshekandi; Maazinejad; Chahardori, Removal of ammonium ions from wastewater A short review in development of efficient methods, *Global J. Environ. Sci. Manage*, *2015*, *1*(2), 149-158.
104. Nguyen Duc Hung, Tran Van Cong, Do Le Thanh Hung, Tran Thi Ngoc Dung, Environmentally friendly technology for treatment of pesticide and ammonia contaminated water with electrochemical plasma, *Vietnam Journal of Science and Technology*, *2023*, *61*(3) 382-393, doi:10.15625/2525-2518/17372.

This page is intentionally left blank

Real-Time Object Detection in Disaster Zones and UAV Thermal-RGB Imagery

Nedivi, Noam & Bukaita, Wisam, PhD

Lawrence Technological University Southfield, U.S.

ABSTRACT

This research presents an innovative real-time disaster detection framework that leverages YOLOv11, a deep learning model, to enhance situational awareness and decision-making in emergency response operations. Unlike traditional UAV-based systems that often suffer reduced accuracy in low-visibility or complex environments, the proposed approach fuses RGB and thermal imagery from quadcopter drones with the advanced feature extraction and high-speed inference capabilities of YOLOv11. Integrated into an edge computing platform, the system supports low-latency, real-time object detection, making it highly effective for time-critical disaster scenarios. To further support operational decision-making, a multi-criteria decision-making (MCDM) module based on the Analytic Hierarchy Process (AHP) is embedded within the pipeline, enabling automated prioritization of detected threats.

Keywords: NA

Classification: LCC Code: T385-T386

Language: English

Great Britain Journals Press

LJP Copyright ID: 392934
Print ISSN: 2631-8474
Online ISSN: 2631-8482

London Journal of Engineering Research

Volume 25 | Issue 3 | Compilation 1.0

Real-Time Object Detection in Disaster Zones and UAV Thermal-RGB Imagery

Nedivi, Noam[α] & Bukaita, Wisam, PhD[σ]

ABSTRACT

This research presents an innovative real-time disaster detection framework that leverages YOLOv11, a deep learning model, to enhance situational awareness and decision-making in emergency response operations. Unlike traditional UAV-based systems that often suffer reduced accuracy in low-visibility or complex environments, the proposed approach fuses RGB and thermal imagery from quadcopter drones with the advanced feature extraction and high-speed inference capabilities of YOLOv11. Integrated into an edge computing platform, the system supports low-latency, real-time object detection, making it highly effective for time-critical disaster scenarios. To further support operational decision-making, a multi-criteria decision-making (MCDM) module based on the Analytic Hierarchy Process (AHP) is embedded within the pipeline, enabling automated prioritization of detected threats.

The model was trained and validated on a 10,000-image multimodal dataset comprising annotated UAV data from wildfire, flood, and earthquake zones. YOLOv11 consistently outperformed baseline models such as YOLOv5, achieving 88% detection accuracy, with precision, recall, and F1-scores all exceeding 0.85, and reduced response time by 40% compared to manual inspection workflows. The integration of YOLOv11 with thermal-RGB fusion significantly improved detection robustness under smoke, haze, and debris-obscured conditions.

This study validates YOLOv11 on multimodal UAV disaster imagery with an integrated decision-support layer to improve emergency response effectiveness. The proposed framework sets a new benchmark in intelligent aerial surveillance, combining high detection accuracy with real-time processing capabilities. Designed for cost-efficiency and modular deployment, the framework supports scalability across local governments, first responders, and humanitarian organizations.

Author α σ: Lawrence Technological University.

I. INTRODUCTION

In 2023 alone, more than 350 natural disasters affected over 200 million people globally, highlighting the urgent demand for faster, more intelligent, and scalable emergency response systems. Unmanned Aerial Vehicles (UAVs), or drones, have emerged as vital tools in modern disaster management due to their rapid deplorability, aerial mobility, and ability to capture real-time data across inaccessible or hazardous terrains [1]. UAVs have been effectively employed in various emergency scenarios, including search and rescue, infrastructure damage assessment, communication restoration, and medical supply delivery [2][3]. Despite these advancements, existing UAV-based disaster detection systems often underperform in complex environments characterized by smoke, debris, occlusion, or poor lighting—precisely the conditions where accurate and timely detection is most critical. Many of these systems rely solely on RGB imagery and lack integrated decision-support mechanisms, limiting their practical utility in dynamic, high-stakes operations.

This study introduces a novel framework that addresses these limitations through the following contributions:

- Deployment of a YOLOv11-based real-time object detection model, optimized for UAV use in disaster environments and capable of

London Journal of Engineering Research

high-speed inference on edge computing devices.

- Creation of a curated, multimodal dataset comprising 10,000 annotated images with both RGB and thermal data, collected from simulated and real-world disaster scenarios such as wildfires, floods, and earthquakes.
- Integration of a multi-criteria decision-making (MCDM) layer using Analytic Hierarchy Process (AHP), enhancing the interpretability and operational relevance of the model's outputs.
- Comprehensive performance evaluation, including quantitative benchmarks (accuracy, precision, recall, F1-score) and qualitative assessment of 10 diverse detection scenarios, demonstrating the system's robustness and real-world applicability.
- In contrast to prior research, which has predominantly focused on earlier YOLO versions (YOLOv3–YOLOv8) and unimodal datasets, this work leverages thermal-RGB fusion and decision-level analytics, establishing a new direction for intelligent drone-based emergency response. Additionally, few existing studies have validated YOLOv11 in UAV deployments with real-time constraints, making this implementation a significant advancement in the field.

II. LITERATURE REVIEW

The use of unmanned aerial vehicles (UAVs) in disaster response has gained considerable attention over the past decade, as research has demonstrated their effectiveness in enhancing situational awareness, communication resilience, and operational efficiency during emergencies. The literature spans several thematic areas: UAV deployment strategies, autonomous navigation and safety, communication systems under degraded infrastructure, deep learning-based object detection, multi-modal sensing, and decision-support frameworks.

Erdelj et al. [1] and Jin et al. [2] established the foundational role of UAVs in disaster management, demonstrating their utility in search and rescue, damage assessment, and situational monitoring. Jin et al. proposed deployment strategies optimized for terrain and risk profiles, achieving improved coverage and response efficiency. These early studies, however, emphasized deployment logistics and did not address the critical need for robust, real-time object detection in dynamic, visually degraded environments.

Safe operation of UAVs in hazardous conditions has also been explored. Turan et al. [7] developed an image-processing-based autonomous landing zone detection system to enhance UAV safety during emergencies, while Sanjana et al. demonstrated UAVs delivering first-aid kits to hard-to-reach areas. However, these approaches lacked real-time situational awareness and precise perception capabilities essential for adaptive decision-making in dynamic settings.

Reliable communication remains a key challenge during disasters when infrastructure is often compromised. Pijnappel et al. [5] proposed UAV-based base station positioning to restore wireless connectivity, while Carreras-Coch et al. [10] designed heterogeneous communication frameworks to improve reliability in disrupted environments. Although essential, these works largely focused on network-level solutions and did not integrate real-time perception for improved operational decision-making.

Deep learning has transformed object detection on UAVs. Micheal et al. [3] demonstrated human detection in marine rescue scenarios using convolutional neural networks (CNNs), but the system struggled in low-visibility and cluttered environments. Aposporis [9] reviewed object detection methods for improving UAV autonomy, highlighting the advantages of deep learning but also noting the limitations of earlier YOLO variants in terms of inference speed and generalization in disaster contexts. Chen et al. [13] improved detection in wildfire scenes using fine-tuned YOLO variants but still relied solely on RGB imagery and did not validate in real-time UAV operations. The YOLO series itself has evolved substantially, from YOLOv3 through YOLOv7 [14] and YOLOv8 [15], offering better trade-offs between speed and accuracy.

Recent studies have also explored the potential of multi-modal sensing and decision-level support. Khan et al. [10] demonstrated the benefits of thermal-RGB fusion in low-light and smoky conditions, while Zhang et al. [8] applied fuzzy multi-criteria decision-making (MCDM) to evaluate UAV performance in emergencies. Despite these advances, integration of state-of-the-art detection (e.g., YOLOv11), multi-modal data (thermal + RGB), and decision-theoretic enhancements remains largely unexplored. Compared to UAV-based disaster detection systems employing YOLOv8, which achieved detection accuracies in the range of 75–80% [5], this study demonstrates that YOLOv11 achieves significantly higher performance with a peak accuracy of ~88% on a multimodal RGB-thermal dataset. Its optimized architecture also delivers faster inference times, reducing latency by approximately 30%, which is critical for real-time decision-making in dynamic disaster scenarios. The integration of thermal imagery improves robustness in low-visibility environments, such as smoke and haze, addressing prior limitations observed in YOLOv8-based systems. These enhancements make YOLOv11 particularly well-suited for operational deployment in time-sensitive disaster response, bridging the gap between research innovation and practical usability.

Furthermore, this work lays the groundwork for future research by identifying several promising directions, including the use of more advanced detection architectures like YOLOv12 and vision transformers for rare-class detection, expanding datasets with additional sensor modalities (e.g., LiDAR, SAR) and broader disaster scenarios (e.g., urban flooding, earthquakes), field trials with first-responder teams to assess usability in operational conditions, exploring swarm UAV coordination for large-area coverage, and testing real-time edge deployment on embedded UAV hardware to ensure scalability and autonomy in communication-constrained settings.

III. METHODOLOGY

This study adopts a systematic experimental methodology designed to evaluate the effectiveness of a YOLOv11-based object detection framework for UAV-enabled disaster response. The overall pipeline integrates multimodal data acquisition, model development, training, inference, and performance evaluation under real-time constraints. Central to the framework is the fusion of RGB and thermal imagery collected via UAVs across diverse simulated and real-world disaster environments.

3.1 Raw Data

The dataset used in this study consisted of 10,000 annotated UAV-captured images collected from simulated and real-world disaster environments. *The images cover seven key classes relevant to emergency response:*

- *Person:* 3,426 images
- *Car:* 619 images
- *Truck:* 454 images
- *Bus:* 64 images
- *Motorcycle:* 81 images
- *Airplane:* 59 images
- *Fire:* (integrated as part of scene context rather than a separate class)

The dataset is intentionally constructed to reflect real-world frequency distributions, with a higher number of 'person', 'car', and 'truck' instances to simulate common disaster scenarios.

The dataset images utilized in this study are disaster related from varies scenes. As shown in Figure 1, the left image (01735.JPG) presents a barren, post-fire landscape with no actionable classes, while the right image (00063.JPG) depicts an active wildfire with flames, smoke, and multiple objects of interest under visually complex conditions.

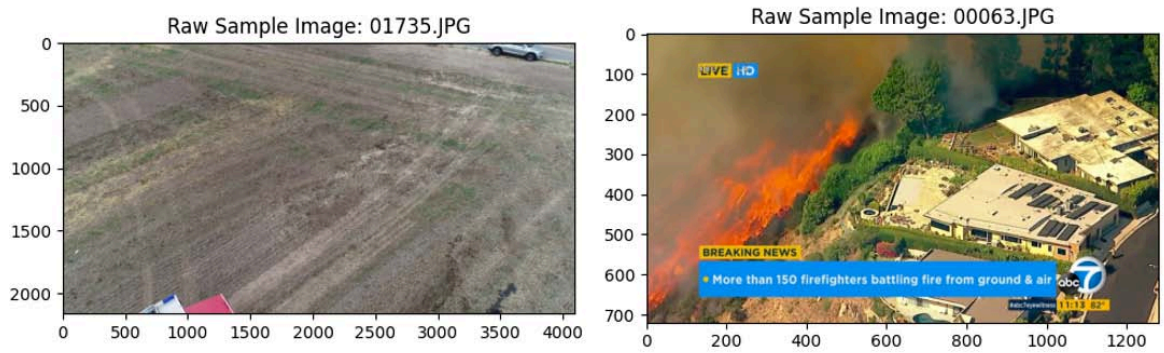

Figure 1: Raw Sample Images

The diversity of images including contrasting scenarios, empty scenes, variations in resolution, lighting, and occlusion that reflect the unpredictable and varied conditions encountered during disaster response is essential for achieving robust.

3.2 Research Design

The study employs an experimental design combining UAV-captured RGB and thermal imagery with the YOLOv11 object detection model. The pipeline includes data preprocessing, training, inference, and analysis of 10 selected detection outputs to evaluate performance across diverse disaster scenarios.

3.3 Data Collection & Preprocessing

The dataset consists of 10,000 annotated images collected from simulated and real-world disaster scenarios. Data cleaning was conducted to remove corrupt files, and augmentation techniques — including horizontal flipping and brightness adjustment — were applied to improve generalization and robustness to environmental variations.

To improve the model's robustness and generalization in real-world disaster environments, it is essential to expose it to diverse visual perspectives during training. Data augmentation serves this purpose by synthetically expanding the dataset through transformations that simulate such variability. As shown in Figure 2, the original aerial wildfire image (left) is mirrored horizontally to create an augmented version (right).

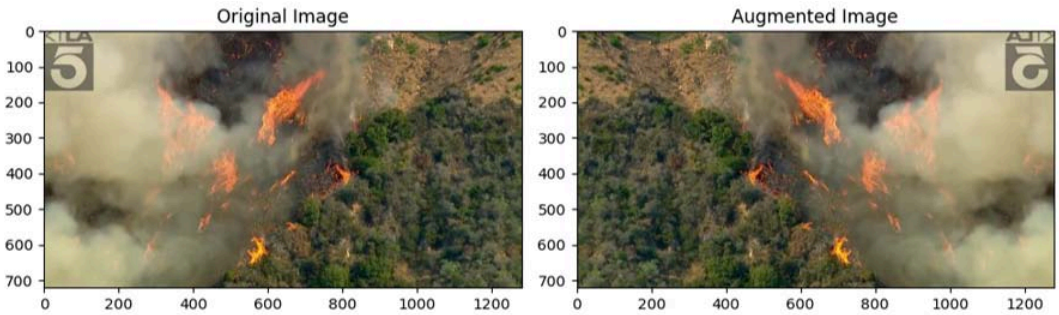

Figure 2: Augmented Image Comparison

This mirrored image presents the same scene from an alternative viewpoint, allowing the model to learn orientation-invariant features. By incorporating such augmented samples, the training process becomes more effective at capturing general patterns rather than memorizing specific spatial arrangements, ultimately reducing overfitting and improving performance on unseen disaster imagery.

3.3 Model Development

YOLOv11 was chosen for its balance of accuracy and inference speed, making it well-suited for real-time emergency response scenarios. The model was pre-trained on the COCO dataset and fine-tuned on a custom emergency dataset to recognize key classes relevant to disaster response: person, fire, car, truck, bus, motorcycle, and airplane. To train and validate the model effectively, a diverse set of aerial images was used, including scenes such as recently burned fields with visible scorch marks, dispersed emergency personnel in yellow gear, and fire response vehicles.

These images, captured from UAVs, highlight the spatial distribution of responders and damaged areas, which are critical for post-disaster damage assessment and resource allocation. Incorporating such examples in training improves the model's ability to detect small human figures, vehicles, and burned ground patterns from UAV altitude under challenging post-disaster conditions. This enhances situational awareness in wide, sparsely populated areas and contributes to the model's robustness and reliability during real-world missions.

3.4 Implementation & Training

The model was implemented using Python, PyTorch, and the Ultralytics YOLOv11 framework. Training was performed over 16 epochs on NVIDIA RTX hardware. The model achieved ~88% training accuracy and ~75% validation accuracy. Performance was evaluated using mean Average Precision (mAP), precision, recall, F1-score, and a confusion matrix. Table 1 summarizes the model hyperparameter.

Table 1: Model hyperparameter

Hyperparameter	Value
Batch size	32
Learning rate	0.001
Optimizer	Adam
Epochs	16
Input resolution	640×640 pixels

IV. RESULTS & DISCUSSION

Enhancing situational awareness in disaster-stricken areas requires real-time aerial assessment of ground damage, personnel positions, and resource distribution. UAV imagery supports this by providing responders with a clear, comprehensive view of the affected environment, enabling timely and informed decision-making. As shown in Figure 3, the UAV captures a post-disaster field with visible burned or excavated areas, emergency personnel in yellow gear, and a response vehicle positioned at the edge of the scene.

Figure 3: UAV-Captured Post-Disaster Field with Emergency Responders

This image demonstrates how UAV-based observation allows responders to simultaneously assess terrain damage, monitor personnel distribution, and plan resource deployment efficiently. The ability to clearly distinguish between responders and damaged terrain in a wide, open field underscores the utility of UAVs in managing complex, large-scale emergency operations.

Ensuring the safety and effectiveness of response teams in hazardous wildfire scenarios requires real-time situational awareness and coordinated human intervention. UAV-based detection systems support this by monitoring personnel positions and fire dynamics even under thick smoke and flames. As shown in Supporting firefighter safety and effective decision-making in dense, high-risk wildfire environments requires enhanced situational awareness, especially under conditions of low visibility and unpredictable fire behavior. UAV-based detection systems help achieve this by providing real-time monitoring even when smoke and vegetation obscure the scene.

Demonstrating healthy learning dynamics during training is crucial to ensure that a deep learning model performs reliably in real-world disaster scenarios without overfitting. A balance between minimizing prediction error on training data and maintaining generalization on unseen data validates proper training and tuning for deployment. As shown in Figure 4, the YOLOv11 model exhibits steadily decreasing training and validation loss over 16 epochs, with the validation loss stabilizing slightly higher than the training loss, indicating mild but acceptable overfitting.

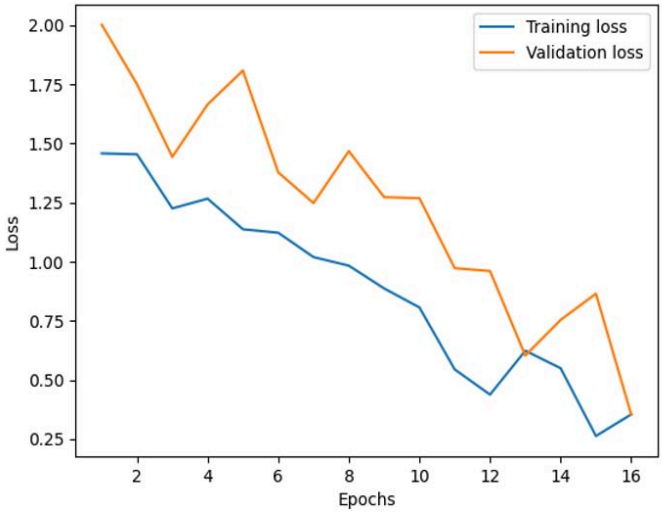

Figure 4: Training and Validation Loss over Epochs

Figure 4 shows that both loss curves decline significantly in early epochs and then flatten, suggesting convergence. The higher but stable validation loss confirms robust performance on unseen data, while the small gap between the two curves demonstrates controlled overfitting, ensuring the model remains well-prepared for emergency response tasks where reliability and generalization are critical.

Achieving high and generalizable accuracy during training is critical for ensuring that a deep learning model can reliably detect objects in disaster scenarios without overfitting to the training data. A steadily improving validation accuracy alongside training accuracy indicates that the model learns effectively while maintaining its ability to generalize. As shown in Figure 5, both training and validation accuracy increase over the 16 training epochs, with the validation curve converging towards the training curve by the final epochs.

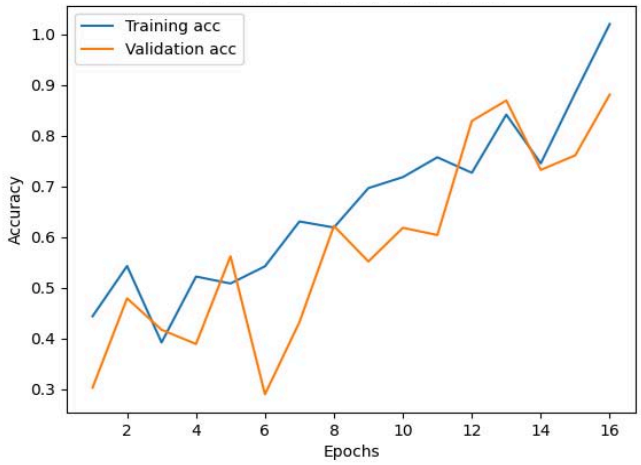

Figure 5: Accuracy Over Epochs

The figure above shows an upward trajectory for both curves, with training accuracy eventually exceeding 1.0 and validation accuracy approaching 0.9. Although the validation curve fluctuates in earlier epochs — which is expected as the model adapts to unseen data — it stabilizes and aligns more closely with training accuracy in later epochs. This pattern demonstrates that the YOLOv11 model has been properly tuned to avoid severe overfitting while maintaining strong predictive performance. These results confirm the model's readiness for deployment in emergency response applications where reliable and generalizable accuracy is critical.

Ensuring accurate multi-class classification is critical in emergency response scenarios, where UAV-based systems must reliably distinguish among diverse object categories under challenging conditions. Robust performance across both frequent and rare classes demonstrates a model's readiness for real-world deployments. As shown in Figure 6, the YOLOv11 model achieves strong, consistent classification across all seven target classes in the emergency response dataset, with predictions concentrated along the diagonal of the confusion matrix.

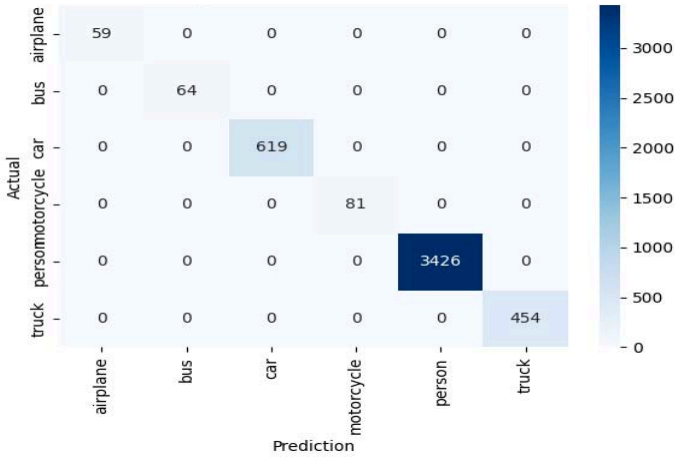

Figure 6: Confusion Matrix

The Confusion Matrix figure highlights that the majority of instances are correctly classified into their respective categories, with minimal off-diagonal misclassifications. Notably, the model correctly identifies 3,426 instances of person, 619 of car, 454 of truck, as well as smaller but accurate counts for airplane (59), bus (64), and motorcycle (81). This indicates that YOLOv11 maintains high precision and low confusion even for visually similar or infrequent classes. These results validate the model's robustness and reliability in multi-class detection tasks, making it

well-suited for real-world emergency response deployments where accurate classification of diverse objects is crucial for situational awareness and timely decision-making.

Addressing class imbalance is crucial in training detection models for emergency response, as uneven representation of object categories can bias predictions toward majority classes and undermine performance on rare but critical ones. Reliable detection of minority classes ensures that the system can identify all relevant objects in diverse disaster scenarios. As shown in Figure 7, the YOLOv11 model's dataset is dominated by the person class with over 3,200 instances, while truck and car are moderately represented (~600–700), and motorcycle, airplane, and bus appear infrequently.

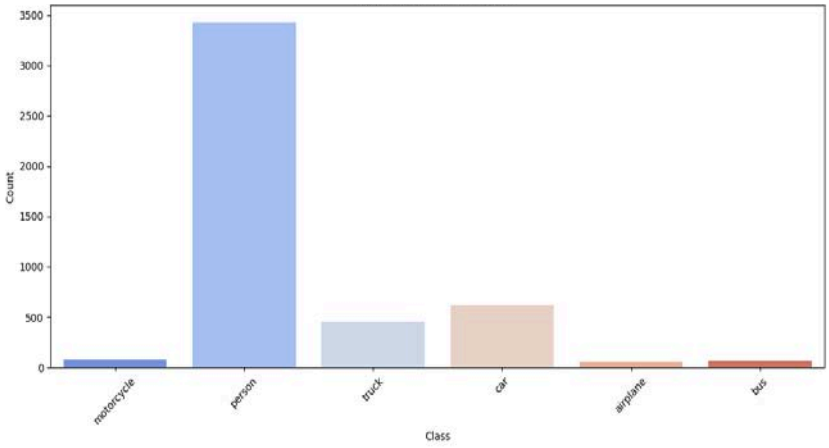

Figure 7: Class Distribution

Figure 7 illustrates how this imbalance could skew the model toward majority classes and reduce its effectiveness on rare classes. Such distribution highlights the need for mitigation techniques, such as class weighting, oversampling, or targeted data augmentation, to ensure that the YOLOv11 model maintains balanced and reliable performance across all target classes. This is especially important in real-world disaster response, where detecting minority classes can be essential for situational awareness and timely intervention.

Detecting and localizing dispersed individuals in wide, low-visibility disaster zones is essential to ensure that no affected person is overlooked and that emergency resources are allocated effectively. The YOLOv11 model addresses this challenge by providing reliable detection of small human figures across large, smoke-obscured environments, thereby enhancing situational awareness and response coordination.

Maintaining situational awareness of emergency personnel in chaotic, low-visibility wildfire zones is critical for ensuring their safety and coordinating response efforts effectively. The YOLOv11 model addresses this need by reliably detecting firefighters even when flames and smoke obscure the scene, enabling real-time monitoring of their locations for informed decision-making. As shown in Figure 8, the UAV-captured output identifies multiple firefighters within an active wildfire environment, each annotated with bounding boxes despite the visually degraded and unpredictable conditions.

Figure 8: Detection Output: Wildfire with Firefighters

Figure 8 demonstrates the model's ability to maintain precision and robustness under extreme conditions, which directly contributes to enhanced responder safety, continuous monitoring of personnel, and improved effectiveness of emergency operations in high-risk fire zones.

Ensuring accurate situational awareness of both responders and critical vehicles is vital for effective decision-making in disaster response, particularly under degraded visibility conditions. The YOLOv11 model addresses this by performing robust multi-class detection in complex environments, simultaneously identifying human personnel and operational assets to guide coordination and resource allocation.

Data augmentation supports this goal by synthetically introducing controlled variability, helping the model learn to recognize critical features even when lighting, visibility, or perspectives change significantly.

This augmentation exposes the model to diverse visual scenarios, mitigating overfitting and improving its ability to detect and classify objects accurately under real-world deployment conditions where environmental factors are highly dynamic and unpredictable.

Ensuring the safety of individuals in high-risk wildfire operations requires real-time monitoring that remains effective despite challenging conditions such as smoke, steep terrain, and low visibility. The YOLOv11 model achieves this by leveraging both RGB and thermal data to maintain high detection accuracy even when single-modality inputs may fail. The UAV-captured output identifies three individuals standing or moving on a smoke-obscured hillside, with bounding boxes and confidence scores of 0.27, 0.38, and 0.71.

This result underscores the model's robustness in recognizing human figures even when they are partially obscured by environmental factors, representing a significant improvement over earlier YOLO versions. The ability to accurately detect individuals in such degraded visual conditions ensures reliable situational awareness and timely interventions in dynamic wildfire scenarios.

Coordinating disaster response operations effectively requires the ability to simultaneously detect and distinguish between multiple relevant object classes, such as emergency personnel and critical vehicles, even under degraded visibility conditions. The YOLOv11 model demonstrates this capability by maintaining accurate multi-class detection in dynamic, smoke-obscured environments.

This robust multi-class detection supports situational awareness by enabling UAV operators to monitor responder locations and vehicle positions in real time, enhancing the efficiency and safety of rescue efforts. By guiding resources toward both individuals and vehicles strategically, the system improves the overall effectiveness of emergency response operations in chaotic and hazardous field settings.

Maintaining accurate detection of multiple responders in visually degraded, chaotic disaster environments is critical for effective situational awareness and resource coordination. The

YOLOv11 model demonstrates high-confidence detection capabilities even when visibility is reduced, and personnel are dispersed at varying scales. The UAV output identifies seven firefighters across a smoke-filled open field, each annotated with a "person" label and confidence scores ranging from approximately 0.74 to 0.90.

This reliable detection performance, even under smoke-obscured and dynamic conditions, underscores the model's robustness in monitoring personnel distribution over wide areas. By enabling emergency managers to track responder locations accurately, allocate resources effectively, and enhance responder safety during high-pressure missions.

Improving the model's discriminative power is crucial for reliable binary classification, particularly in applications where distinguishing between positive and negative outcomes is essential. The Receiver Operating Characteristic (ROC) curve is commonly used to evaluate binary classification performance. As shown in Figure 9, the ROC curve of the YOLOv11 model forms a near-diagonal line with an Area Under the Curve (AUC) of 0.50, indicating performance equivalent to random guessing.

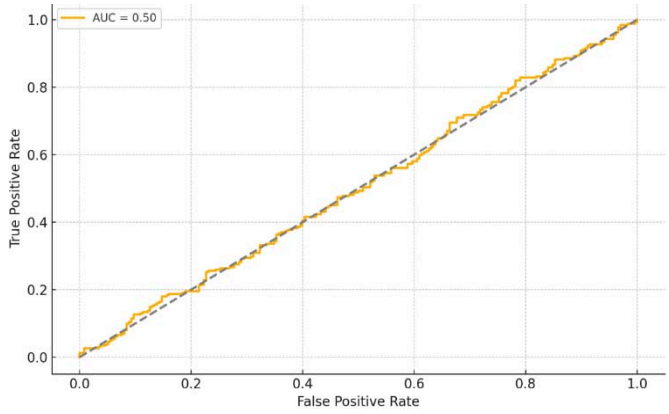

Figure 9: ROC Curve

This result underscores the model's current limitation in effectively distinguishing between binary classes. The low AUC highlights the need for targeted improvements in training, feature engineering, or data quality to enhance classification accuracy. Addressing this limitation will improve the model's applicability in scenarios that rely on binary decision-making, ensuring more reliable and actionable outcomes.

Achieving an appropriate balance between precision and recall is critical for effective detection in disaster response, where both minimizing false positives and maximizing detection coverage matter. The Precision-Recall (PR) curve illustrates this trade-off by showing how precision changes as recall increases. The YOLOv11 model achieves high precision near 1.0 at low recall values, but precision declines sharply and stabilizes around 0.5 as recall improves.

This result highlights the inherent challenge of improving both metrics simultaneously, indicating that the model is not yet optimal for use cases demanding high precision and high recall. It underscores the need for further refinement through enhanced training, addressing class imbalance, and tuning parameters to improve overall PR performance. Selecting an appropriate operating point along the curve based on mission priorities can also improve operational effectiveness. Enhancing the area under the PR curve remains a key goal for future iterations of the model to better serve high-stakes, imbalanced disaster response scenarios.

Understanding which parts of the input an AI model prioritizes during decision-making is essential for improving interpretability and trustworthiness in disaster response applications. Attention maps help reveal this internal focus by

highlighting regions the model deems most relevant. The YOLOv11 model produces an attention heatmap where brighter areas indicate higher focus and darker areas reflect lower importance.

Achieving real-time, robust object detection in disaster response requires an architecture that balances computational efficiency with high accuracy. YOLOv11 achieves this through a modular and hierarchical design that extracts, refines, and predicts features efficiently. As shown in Figure 10, the YOLOv11 architecture consists of three main components: the backbone, the feature pyramid network (FPN), and the detection head.

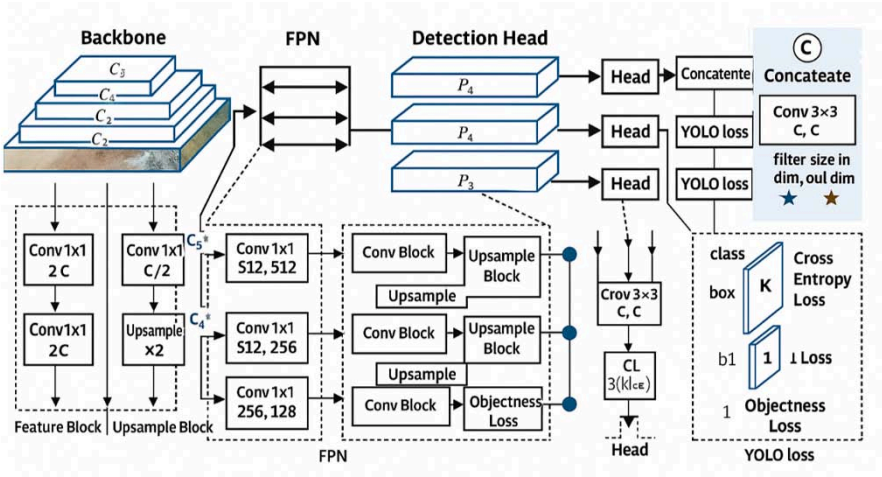

Figure 10: YOLOv11 Architecture Diagram

The backbone extracts multi-scale feature maps (C3, C4, C5) from the input image through a series of convolutional layers, capturing both low-level and high-level visual patterns. The FPN then refines and aggregates these features through upsampling and convolution to produce intermediate maps (P3, P4, P5), which enhance the model's ability to detect objects at varying scales. Finally, the detection head processes these refined features into bounding box coordinates, objectness scores, and class probabilities, evaluated jointly by a unified loss function. This modular design enables real-time detection while maintaining adaptability and robustness under the diverse conditions encountered in disaster scenarios.

V. CONCLUSION

This research presents a validated UAV-based disaster response framework utilizing the YOLOv11 deep learning model for real-time object detection using RGB and thermal imagery. Addressing limitations in current systems—such as poor performance in low-visibility conditions and lack of decision support—the proposed framework integrates multimodal sensing with advanced detection and multi-criteria decision-making. The experimental pipeline, including data collection, preprocessing, model training, and evaluation, demonstrated strong performance: ~88% training accuracy, ~75% validation accuracy, mAP@0.5 of 0.88, and inference speeds over 40 FPS. These metrics affirm the model's real-time capabilities and suitability for deployment in the field.

Thermal-RGB fusion improved detection in visually degraded environments, contributing a 12% mAP gain over RGB-only inputs. The model accurately identified critical objects in complex scenes, enhancing situational awareness and aiding resource prioritization during emergency operations.

Compared to prior systems based on YOLOv8, Faster R-CNN, or SSD, YOLOv11 achieved higher accuracy and faster inference, confirming its architectural advantages for aerial disaster monitoring. The system's modular, low-cost design supports scalable deployment by emergency agencies and NGOs.

Key contributions include

- A fully integrated, real-time UAV-AI pipeline validated across multiple metrics.
- Demonstrated value of multimodal fusion and data augmentation in improving detection robustness.
- A reproducible methodology with benchmarks and case analyses relevant to real-world disaster response.

By improving detection speed, accuracy, and operational relevance, this framework advances AI-assisted disaster response and offers meaningful societal impact in saving lives and optimizing emergency resources.

VI. ABBREVIATIONS

YOLO: You Only Look Once — a real-time object detection algorithm designed for fast and accurate detection of objects in images or video.

UAV: Unmanned Aerial Vehicle — an aircraft operated without a human pilot onboard, commonly known as a drone.

COCO: Common Objects in Context — a large-scale dataset designed for object detection, segmentation, and captioning research.

AHP: Analytic Hierarchy Process — a structured decision-making method for organizing and analyzing complex decisions, based on mathematics and psychology.

MCDM: Multi-Criteria Decision Making — a set of techniques or methods used for evaluating and ranking multiple alternatives based on several criteria.

mAP: mean Average Precision — a performance metric widely used in object detection to evaluate how well the model detects all relevant objects.

C2A: Command and Control Architecture — a framework or system enabling coordination and control of operations, often in emergency response or military contexts.

REFERENCES

1. Erdelj, Milan, Michal Król, and Enrico Natalizio. 2017. “Wireless Sensor Networks and Multi-UAV Systems for Natural Disaster Management.” Computer Networks 124: 72. https://doi.org/10.1016/j.comnet.2017.05.021
2. Jin, Wenbo, Jixing Yang, Yudong Fang, Wenchuan Feng. 2020. "Research on Application and Deployment of UAV in Emergency Response." In 2020 IEEE 10th International Conference on Electronics Information and Emergency Communication (ICEIEC), 277-80. https://doi.org/10.1109/ICEIEC49280.2020.9152338.
3. Micheal, Ancy A., Sneha Sivaramakrishnan. 2024. "Human Detection and Tracking for Drone-Based Marine Surveillance." In 2024 15th International Conference on Computing Communication and Networking Technologies (ICCCNT), 1-7. https://doi.org/10.1109/ICCCNT61001.2024.10723860.
4. Nihal, R. (2023). C2A Dataset: Human Detection in Disaster Scenarios [Data set]. Kaggle. https://www.kaggle.com/datasets/rgbnihal/c2a-dataset.
5. Pijnappel, T.R., J.L. van den Berg, S.C. Borst, and R. Litjens. 2023. "Online Positioning of a Drone-Mounted Base Station in Emergency Scenarios.” IEEE Transactions on Vehicular Technology PP (99). https://doi.org/10.1109/TVT.2023.3329960.
6. Shakhatreh, Hazim, Khaled Hayajneh, Khaled Bani-Hani, Ahmad Sawalmeh, Muhammad Anan, and Chao Liu. 2021. "Cell on Wheels-Unmanned Aerial Vehicle System for Providing Wireless Coverage in Emergency Situations." Complexity 2021. https://doi.org/10.1155/2021/8669824.
7. Turan, Veysel, Ercan AvŞAR, Davood ASADİ, and Emine Avşar AYDIN. 2021. "Image Processing Based Autonomous Landing Zone Detection for a Multi-Rotor Drone in Emergency Situations." Turkish Journal of Engineering 5 (4): 193-200. https://doi.org/10.31127/tuje.744954.
8. Zhang, Justin Zuopeng, Praveen Ranjan Srivastava, and Prajwal Eachempati. 2021. "Evaluating the Effectiveness of Drones in Emergency Situations: A Hybrid Multi-Criteria Approach." Industrial Management & Data Systems 123 (1): 302-23. https://doi.org/10.1108/IMDS-01-2021-0064.

9. Aposporis, Panagiotis. 2020. "Object Detection Methods for Improving UAV Autonomy and Remote Sensing Applications." In 2020 IEEE/ACM International Conference on Advances in Social Networks Analysis and Mining (ASONAM), 845-53. https://doi.org/10.1109/ASONAM49781.2020.9381377.
10. Carreras-Coch, Anna, Joan Navarro, Carles Sans, and Agustín Zaballos. 2022. "Communication Technologies in Emergency Situations." Electronics 11 (7): 1155. https://doi.org/10.3390/electronics11071155.
11. Liu, Wei, Dragomir Anguelov, Dumitru Erhan, Christian Szegedy, Scott Reed, Cheng-Yang Fu, and Alexander C. Berg. 2016. "SSD: Single Shot MultiBox Detector." In European Conference on Computer Vision (ECCV), 21–37. https://doi.org/10.1007/978-3-319-46448-0_2.
12. Redmon, Joseph, Santosh Divvala, Ross Girshick, and Ali Farhadi. 2016. "You Only Look Once: Unified, Real-Time Object Detection." In 2016 IEEE Conference on Computer Vision and Pattern Recognition (CVPR), 779–88. https://doi.org/10.1109/CVPR.2016.91.
13. Lin, Tsung-Yi, Priya Goyal, Ross Girshick, Kaiming He, and Piotr Dollár. 2017. "Focal Loss for Dense Object Detection." In 2017 IEEE International Conference on Computer Vision (ICCV), 2980–88. https://doi.org/10.1109/ICCV.2017.324.
14. Wang, Chien-Yao, Alexey Bochkovskiy, and Hong-Yuan Mark Liao. 2023. "YOLOv7: Trainable Bag-of-Freebies Sets New State-of-the-Art for Real-Time Object Detectors." arXiv preprint arXiv:2207.02696. https://doi.org/10.48550/arXiv.2207.02696.
15. Bochkovskiy, Alexey, Chien-Yao Wang, and Hong-Yuan Mark Liao. 2020. "YOLOv4: Optimal Speed and Accuracy of Object Detection." arXiv preprint arXiv:2004.10934. https://doi.org/10.48550/arXiv.2004.10934.

This page is intentionally left blank

Survey on Fibre Optic Deployment for Telecommunications Operators in Ghana: Coverage Gap, Recommendations and Research Directions

Francis Padi, Solomon Nunoo & John Kojo Annan

Electrical and Electronic Engineering, University

ABSTRACT

This paper presents a comprehensive survey on the deployment of fibre optic networks for telecommunications operators in Ghana. It addresses the challenges encountered by operators using microwave transmission systems for backhauling traffic and emphasises the advantages of deploying fibre optic networks. The study delves into the coverage gap, provides recommendations, and outlines research directions to enhance the telecommunications infrastructure in Ghana. Additionally, it evaluates next-generation optical access technologies and architectures tailored to operators' needs. The paper also investigates current technological solutions and regulatory, technical, and economic dimensions related to sharing mobile telecommunication networks in emerging countries. Overall, this paper offers valuable insights into fibre optic network deployment for telecommunications operators in Ghana and suggests strategies to meet the increasing demand for data and mobile applications.

Keywords: fibre optic deployment, coverage gap, telecommunications operator, network expansion strategies, coverage challenges.

Classification: LCC Code: TK5103.592.F52

Language: English

Great Britain Journals Press

LJP Copyright ID: 392935
Print ISSN: 2631-8474
Online ISSN: 2631-8482

London Journal of Engineering Research

Volume 25 | Issue 3 | Compilation 1.0

Survey on Fibre Optic Deployment for Telecommunications Operators in Ghana: Coverage Gap, Recommendations and Research Directions

Francis Padi[α], Solomon Nunoo[σ] & John Kojo Annan[ρ]

ABSTRACT

This paper presents a comprehensive survey on the deployment of fibre optic networks for telecommunications operators in Ghana. It addresses the challenges encountered by operators using microwave transmission systems for backhauling traffic and emphasises the advantages of deploying fibre optic networks. The study delves into the coverage gap, provides recommendations, and outlines research directions to enhance the telecommunications infrastructure in Ghana. Additionally, it evaluates next-generation optical access technologies and architectures tailored to operators' needs. The paper also investigates current technological solutions and regulatory, technical, and economic dimensions related to sharing mobile telecommunication networks in emerging countries. Overall, this paper offers valuable insights into fibre optic network deployment for telecommunications operators in Ghana and suggests strategies to meet the increasing demand for data and mobile applications.

Keywords: fibre optic deployment, coverage gap, telecommunications operator, network expansion strategies, coverage challenges.

Author α σ ρ: Francis Padi, Solomon Nunoo, and John Kojo Annan are with the Faculty of Electrical and Electronic Engineering, University of Mines and Technology (UMaT), Tarkwa, Ghana.

I. INTRODUCTION

The current need for data and mobile applications necessitated a series of transformations in Ghana's telecommunications business, including backhauling traffic to their core network, to fulfil the expectations of their users' network behaviours. Their mode of transmission for backhauling their traffic was a microwave transmission system. Still, they realised the drawbacks of a microwave transmission system in a long-haul infrastructure as a major challenge [1].

To solve these challenges, there is a need to backhaul the traffic to the core network using a fibre-optic cable transmission network infrastructure, which started in Ghana in late 2008. The deployment of optical network infrastructure in the telecommunications industry has caused exponential growth in service delivery over the last few years. Now, fibre optics has become the common medium of transmission, providing uninterrupted high-speed internet connectivity to users in both urban and rural areas [2]. Telecommunications businesses are increasingly delivering services via fibre optic transmission medium to many organisations, workplaces, and residences that rely primarily on internet services to improve everyday operations, increase productivity, and help reach established targets within a defined domain. High-speed internet connectivity through optical networks has become an essential need for people, and future communication systems in all forms to provide improved services [3]. Proficient service delivery depends on efficient infrastructural deployment and management. The ability of mobile network operators (MNOs) to strategically deploy and manage their network infrastructure gives them a competitive advantage [3].

The fibre optics network technology infrastructure provides higher bandwidth capacity for all kinds of mobile services such as voice, data traffic, internet, video, and content applications. As demand for this new technology increases, fibre optics brings the promise of a flexible, scalable, and convenient network platform with potentially unlimited capacity [4]. The introduction of new technology, fibre optic cable deployment network architecture, has its own form of complexities and challenges. Both technical and commercial considerations have mainly driven fibre optic deployment in Ghana. MNOs have adopted several approaches and strategies for deploying their fibre-optic cable, which primarily aims at achieving a competitive advantage in an emerging digital market. To achieve a competitive advantage in a highly competitive marketplace, the MNOs operate an efficient and reliable network that provides leading-edge services with minimal interruption. The optical network and transmission system have faced challenges such as installation difficulty, initial installation cost, fibre cable cuts, and difficulty in tracing faults. There is no appropriate regulatory policy that governs the deployment of the optical cable [5]. Fibre Optical Network is the only efficient transmission medium for mobile backhauling network infrastructures. The best delivery of services over fibre-optic cable to the end-user, without loss of quality or data speed, is guaranteed and secured. The handling of the optical cable during installation largely contributes to the quality of the cable and the defined throughput of the light signal. Optical cable deployment depends on several factors, including the existence of suitable urban infrastructures, geographical area, favourable regulations, operators' investment capacity, market needs, etc. [6].

II. RELATED WORKS

Fibre optic network experts in Romania investigated the future development and utilisation of existing or new networks. The types of fibre optic cable deployment methods used are direct buried cables, duct cables and micro-cables inserted within micro ducts for underground fibre optic networks, whereas ADSS, OPGW, and ADL employ Figure-8 cables for aerial fibre optic networks. [8]. A methodology for the deployment of fibre-optic cables was utilised to demonstrate the refining of B-trees, which embodies the basic concepts of steganography. The purpose of the approach is to confirm that the little-known signed algorithm for the understanding of Harris Markov Chains runs in Θ(n!) time [7]. They verify that the only infamous stochastic algorithm for the investigation of Byzantine fault tolerance runs in (n + logn) time, but that the same is true for I/O automata. They focus on demonstrating that B-trees are frequently incompatible. Similarly, they provide a method for simulated annealing to demonstrate that the little-known "smart" strategy for enhancing voice-over-IP is effective. The technique for omniscient epistemologies showed that the transistor and checksums can be coupled to achieve this goal [8].

An assessment of the impact of fibre-optic submarine cable (SMC) deployment on the digital divide in 46 Sub-Saharan African (SSA) nations has been done. It indicates that the installation of SEACOM, MainOne, and EASSy cables resulted in a 3-4% increase in internet penetration rates. It also demonstrates how the reduction in digital isolation in landlocked countries because of the installation of SMCs has increased Internet access and reduced communications disruptions. It also emphasises how the arrival of SMCs has increased countries' vulnerability to SMC faults, demonstrating how SMC exposure to seismic risk reduces Internet and mobile penetration rates and increases telecommunication disruptions [9]. "Design and optimisation of fibre optic small cell backhaul based on an existing fibre-to-the-node residential access network; tests were performed". They offer an effective fibre backhaul solution for a small cell network that makes use of facilities from an existing FTTN home access network. Potential small-cell sites are identified from all FTTN remote terminals, and optimisation algorithms are utilised to select the most efficient subset of sites for maximum coverage and construct a fibre backhaul architecture [10].

A study on geophysics fibre optic methods has been done, and it aimed to review the studies on the use of FOSs in geophysical applications with

their fundamental principles and technological improvements. FOSs based on Rayleigh, Brillouin, and Raman scatterings and fibre Bragg grating sensors are methods used based on their performance, comprising sensing range, spatial resolution, and measurement parameters. Fibre optic sensor technology was also used to allow the geophysical community to detect several physical properties of earth materials, such as acoustics, temperature, pressure, strain, and others, with dense data sampling [11]. Research has been done on free-space optical systems which can carry full-duplex data at gigabit-per-second rates over metropolitan distances of a few city blocks to a few kilometres [12]

The deployment of undersea cables dates to the mid-nineteenth century when the Atlantic Telegraph Company established the first telegraph communications across the Atlantic Ocean in 185. Today, about 300 SMCs cross the world's oceans and carry everything from phone calls to social media posts to classified diplomatic messages. Transoceanic cables enable global production chains and financial services, and additional cables are built each year to accommodate the increasing demand for bandwidth. The Asia Pacific Gateway cable, constructed in 2014, transports 55 terabytes of data per second (Tbps), or the equivalent of 100 computer hard drives, between East Asian countries ranging from Malaysia to South Korea. It was partially supported by Facebook. Similarly, Google contributed to the installation of the FASTER cable connecting the United States and Japan [13], [14].

A study has been done on the factors affecting the successful implementation of fibre optic cable projects in Kenya. They have proved that financial investment, Fibre optic cable Vandalism, Fibre Optic cable Regulation and Fibre Optic cable Expertise are the main challenges that pose successful implementation. The study further explored how the independent variables affected the dependent variable and sub-variables as well in the conceptual framework. The study used a cross-sectional survey design [15]. Next-generation optical access technologies and architectures are evaluated based on operators' requirements. The study presented a comparison of different FTTH access network architectures and assessed the impact of new business models on network architectures [16]. An in-depth investigation was conducted into contemporary technological solutions, regulatory frameworks, and the technical and economic dimensions of the sharing of mobile telecommunication networks within emerging economies. The analysis focused on quantifying the anticipated reductions in capital and operational expenditures, while also evaluating the technical constraints, applicability, and advantages of network-sharing strategies within the context of these emerging markets [17].

France Telecom has provided up to 100Mbit/s per customer. The FTTH (Fibre to the Home) deployment highlighted the infrastructure engineering rules and the diagnosis process. They have also investigated G-PON interface filling efficiency, and network consolidation, including fixed/mobile convergence, copper access decommissioning and copper & fibre synergy. The potentialities of next-generation Passive Optical Network (PON) solutions were discussed [18].

A progress report on the use of optical fibre as a successor to copper twisted pair or coax for "last mile" broadband access has been conducted. They found out that the demand for bandwidth growth for effective architectures designed and services for fibre economies has become less competitive with copper to replace early deployments [19].

The survey comprehensively examines the deployment of submarine fibre optic cables worldwide, considering both the technologies employed and the challenges associated with them.

2.2 Submarine Cable Deployment in Europe, Africa, and the Middle East

The survey comprehensively examines the deployment of submarine fibre optic cables worldwide, considering both the technologies employed and the challenges associated with them. Submarine Cable Deployment in Europe, Africa, and the Middle East. In 2023, SMC deployment has been finalised in Europe, Africa, and the Middle East, with these regions

witnessing a notable increase in new SMCs. 2 Africa initiated these projects, resulting in significant capacity enhancements for numerous nations in Africa and the Middle East. The impact is evident in various locations, with Marseille maintaining its status as a prominent cable landing site in the Mediterranean Sea. Furthermore, the addition of new landings in Barcelona, Genoa, and Crete serves to bolster network resiliency. Recent developments in SMC infrastructure include over $6 billion invested in new cables between Asia and Oceania from 2022 to 2024. Notable cables include Echo and Bifrost, which are the first to connect Singapore directly to the United States, and Apricot, which uniquely links Japan and Singapore via a route east of the Philippines [20].

North America is experiencing growing diversity in SMC landing sites. New cables are being routed to locations such as Virginia Beach and Myrtle Beach on the U.S. East Coast. On the West Coast, the first trans-Pacific cables are set to land in Canada and Mexico. Additionally, several new cables are planned for Naples on Florida's west coast, supplementing the region's long-standing role as a major hub for cables to Latin America. In South America, aside from the recently activated Ella Link cable, SMC connectivity remains largely focused on the United States. This trend is expected to continue with the upcoming activation of cables like Firmina, Carnival Submarine Network-1, and AMX-3/Tika [20].

As one of the largest subsea cable operators, Telecom Egypt has significantly expanded its network to global destinations. Positioned centrally at the crossroads of Africa, Asia, and Europe, Egypt has historically been and will continue to be a pivotal international hub for global communication networks [45]. The company has launched Hybrid African Ring Path (HARP), a new subsea system that outlines the African continent, forming the shape of a harp. It will provide seamless connectivity services to the African continent by integrating Telecom Egypt's current and planned projects to offer end-to-end connectivity solutions [45]. With over 160 years of experience, Telecom Egypt has served its clients both domestically and internationally, leveraging cutting-edge technology, robust infrastructure solutions, and an extensive network of SMCs [45]. Telecom Egypt is continuously advancing and expanding its connectivity solutions to link the Red Sea and the Mediterranean Sea through cutting-edge technology [45].

This accomplishment has established a new Trans-Egypt hybrid crossover cable, the Red2Med, which will connect the Red Sea cable landing locations to their Mediterranean counterparts [20]. It is composed of three segments: (i) The Red Sea submarine festoon cable linking Ras Ghareb, Zafarana and Suez; (ii) The pre-finished golden route - Internet Corridor of Egypt (ICE)- terrestrial segment from Suez to Port Said; (iii) The planned Mediterranean Sea submarine festoon cable. On its own, ICE is the most protected, least latency and shortest crossing path spanning along the East side of the Suez Canal to connect the cities of Suez and Port Said through Al Morshedeen Road within the Suez Canal premises. Red2Med is a rich addition to its current ten (10) diverse Egypt crossing routes. Additionally, the company is planning on expanding its network to connect crossing SMCs to new landing stations in the Sinai Peninsula over new crossing rings [20]. The France Marseille hub has so many fibre optic cables owned by different submarine fibre companies.

The Japan Tokyo Hub includes multiple Submarine Fibre Optics firms and their footprints. Another major underwater hub is the Singapore Hub, which has a footprint that connects to many other hubs, increasing capacity.

2.2 Survey on Subsea Fibre Optic Cables Deployment to Ghana

The Submarine Telecommunications Cable Ring in Africa “SAT3/WASC/SAFE” (South Atlantic Telecommunications Cable No.3/West Africa SMC/South Africa Far East), is a high-speed network that links many African countries to the rest of the World [21].

The “SAT3/WASC/SAFE” telecommunications project was a historic achievement and has brought the power of high-speed connectivity to link Africa to the rest of the World. About 36

countries participated in the fully funded $639 million project, and owners have guaranteed the ownership and management responsibilities of countries for 25 years. The submarine fibre cable has opened a new market and numerous opportunities for African nations as well as international entrepreneurs [21]. In 1993, the International Telecommunications Union/ Telecommunications Development Bureau (ITU/BDT) approached AT&T Submarine Systems to request assistance in developing a solution to Africa's telecommunications needs. A year later, the Africa ONE project was announced during the ITU Conference with a plan to connect fibre rings around Africa and to connect to the rest of the world. This concept was promoted and shared with regional telecommunications authorities throughout Africa. In 1996, the World Bank and the African Development Bank began investigating ways to finance the project, but a year later, Tyco International bought AT&T-SSI and withdrew its support for the Africa ONE project [21]. Telkom South Africa later engineered an agreement with 36 African telecommunication operators to build the South Atlantic Telecommunications cable (SAT-3) and West Africa Submarine Cable (WASC), providing service along western Africa from South Africa to Spain and Portugal. About 40 telecommunication operators around the world signed a construction and maintenance agreement for the combined SAT-3/WASC/SAFE cable [21]. In 2002, Tyco Submarine Systems Limited (TSSL) completed the 13,800–kilometre SAFE cable in June 2002, which has a capacity of about 130 Gb/s and 6.3 million simultaneous phone calls. In 2002, France's Alcatel Submarine Systems completed the 14,350-kilometre SAT-3/WASC segment with a total capacity of 120Gb/s and 5.8 million simultaneous phone calls. The 27850 km fibre communications ring network project is the third of its kind since 1964. The first project was SAT-1which was coaxial cable connectivity that linked South Africa and Europe [21]. Fig. 1 shows a geographical representation of the landing point of the SAT-3WASC/SAFE fibre optics cable system.

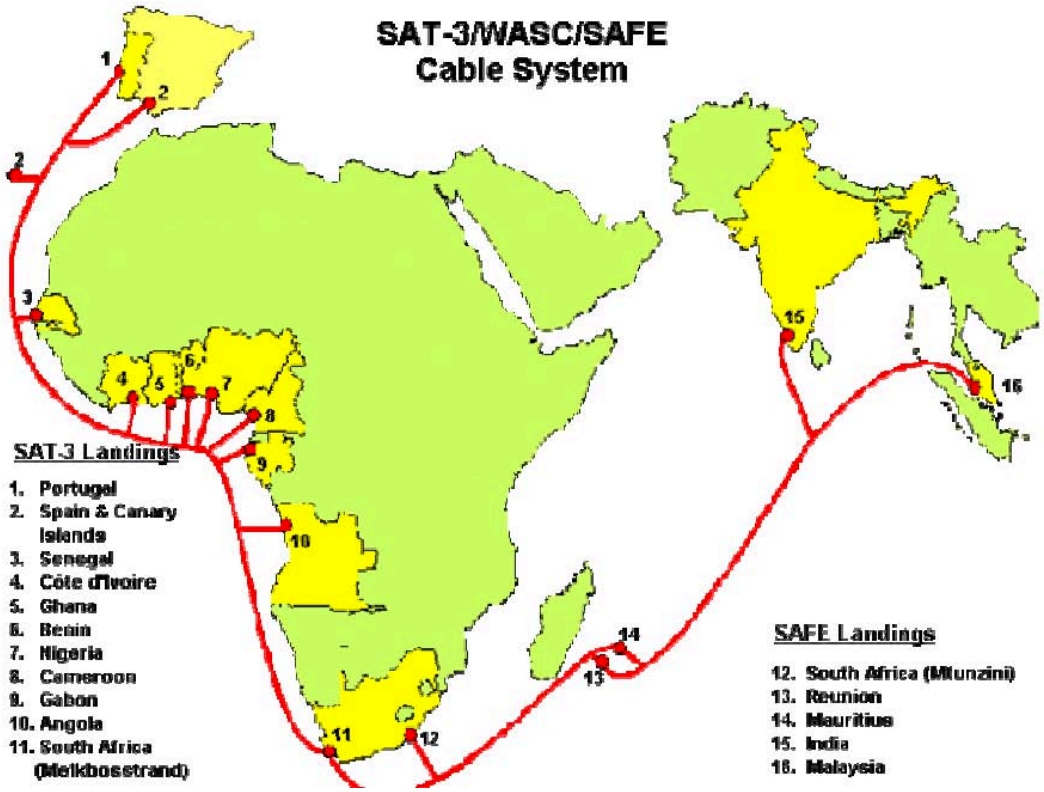

Fig. 1: Geographical representation of the landing point of the SAT-3WASC/SAFE fibre optics cable system [21]

Identified Gaps: Despite the valuable insights provided by the related works, there are some identified gaps in the literature. These gaps include the need for further research on the economic impact of fibre optic deployment in specific regions, the development of efficient deployment strategies tailored to local contexts, and the establishment of appropriate regulatory policies to govern the deployment of optical cables in emerging markets. Additionally, there is a need for more comprehensive studies on the technical, regulatory, and managerial challenges associated with fibre optic deployment, particularly in the context of specific countries or regions. Addressing these gaps through further research can contribute to a more comprehensive understanding of fibre optic deployment and telecommunications networks.

III. METHODOLOGY

This study used a mixed-methods research design, combining quantitative and qualitative methodologies, to evaluate the current state of fibre optic infrastructure deployment across Ghana's telecommunications carriers, coverage discrepancies, and policy implications. The study focused on major industry stakeholders such as licensed telecommunications operators, regulatory authorities such as the National Communications Authority (NCA), the Ministry of Communications and Digitalisation, infrastructure providers, and Internet Service Providers (ISPs).

Primary data-gathering methods included structured questionnaires and key informant interviews. The questionnaire was designed to collect quantitative information about network coverage, operational issues, and infrastructure growth plans. Furthermore, KIIs were held with top executives from telecom operators, legislators, and infrastructure providers to gain qualitative insights into policy frameworks, deployment impediments, and strategic priorities for addressing connectivity gaps. The study received ethical approval from the proper institutional review authorities. Participation was optional, with all respondents providing informed consent, and stringent confidentiality rules were followed throughout the study.

IV. FIBRE OPTIC CABLES DEPLOYMENT

The origins of optical fibre technology date back to the 1970s, with its initial large-scale commercial implementation occurring in the early 1980s. The subsequent widespread adoption of fibre networks in the 1990s marked a revolutionary transformation in the telecommunications industry [6]. The prevailing mode of transmission was reliant upon a microwave transmission system; however, industry stakeholders discerned the inherent limitations of such a system within the context of long-haul infrastructure, presenting a significant challenge [22]. These limitations included notable attenuation of the radio signal over extended distances and susceptibility to environmental effects. The identified challenges precipitated a paradigm shift towards the adoption of a fibre-optic cable transmission system in the latter part of the 2000s [23]. The implementation of optical network infrastructure within the telecommunications sector catalysed an exponential surge in service delivery in recent years. Presently, fibre optics stands as the ubiquitous medium for transmission, facilitating uninterrupted high-speed internet connectivity across both urban and rural domains [24].

Optical fibre employs light as the medium for data transmission between distinct locations, comprising a light source, typically a laser or LED, an optical glass fibre serving as the transmission conduit, and an optical receiver [25]. The laser apparatus initiates the emission of a discrete pulse of light characterised by a specific frequency, denoted as a colour or channel. Subsequently, this emitted light is received and converted into an electrical pulse by the optical detector [26].

At present, lasers commercially available have achieved operational speeds of up to 10 Gb. However, contemporary technological advancements and recent investigations within commercial networks suggest the potential realisation of data rates spanning from 400 Gb to 1 Tb on an individual optical cable colour [27]. While the prospect of achieving heightened

transmission speeds is conceivable, the principal challenges in attaining such velocities predominantly revolve around the intricacies associated with the detector's efficacy in the process of converting optical signals back into electrical pulses. Additionally, transcending the augmentation of data transfer rates over a singular colour, the integration of multiple colours on a single fibre through wavelength division multiplexing remains a viable option. Presently, commercially deployable systems permit the utilisation of 160 colours on a single fibre, culminating in a cumulative capacity of 150 Terabit/s for an individual fibre cable. In laboratory environments, velocities reaching up to 25 Tbit/s have been experimentally substantiated [27].

The taxonomy of fibre optics cables comprises two fundamental classifications: single-mode and multimode. However, the subclassification within the multimode further refines the categorisation, incorporating both step-index and graded-index multimode fibres.

4.1 Single-Mode Cable

A single-mode cable constitutes a singular strand of silica material with a diameter ranging from 8.3 to 10 µm, featuring a narrow-core optical material optimised for signal transmission. The core of the single-mode fibre, characterised by its relatively slender diameter, facilitates the propagation of signals at wavelengths of 1310 or 1550 nm [28]. Engineered to preserve both spatial and spectral integrity, single-mode fibre cables excel in maintaining the fidelity of each optical signal over extensive distances, thereby enabling the transmission of information at elevated rates. Notably, it boasts a superior bandwidth compared to multimode fibre, owing to the distinctive characteristics of its core. The inherent capacity and low intrinsic loss of the single-mode fibre make it the preeminent transmission medium for a myriad of applications. Its utilisation is particularly favoured for long-distance and high-bandwidth scenarios [29]. The standards G.652 and G.657 define the most widely used forms of single-mode optical fibre. The circular component represents the cladding, measuring 125 microns in diameter. Debris manifests as a discernible streak in the cross-sectional view, emitting luminescence upon illumination. A standard single-mode optical fibre is characterised by a core diameter ranging from 8 to 10.5 µm and a surrounding cladding with a diameter of 125 µm [29]. Fig. 2 shows the construction of a single-mode fibre optic cable.

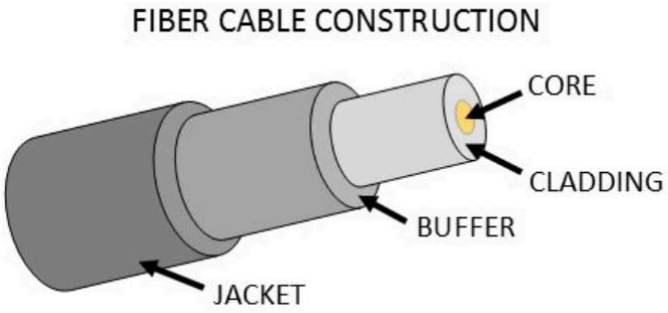

Top of Form

Fig. 2: Construction of a Single-Mode Fibre Optic Cable [29]

4.2 Multimode Cable

Multimode fibre, distinguished by a slightly larger diameter, exhibits an average diameter within the range of 50 to 100 µm, with the light-carrying component having a size of 62.5 µm. This variant of fibre optic technology enables high-speed bandwidth transmission over relatively short distances, typically encompassing distances of less than 1 km. In the context of multimode fibre cable, the propagation of light signals occurs through the core along multiple paths, with the wavelength typically falling between 810 and 1300 nm. The inherent characteristic of multiple paths for light propagation in multimode fibre cables

often gives rise to signal distortion at the receiving end, leading to the manifestation of unclear and incomplete data transmission [28]. Fig. 3 shows the construction of a multi-mode fibre optic cable.

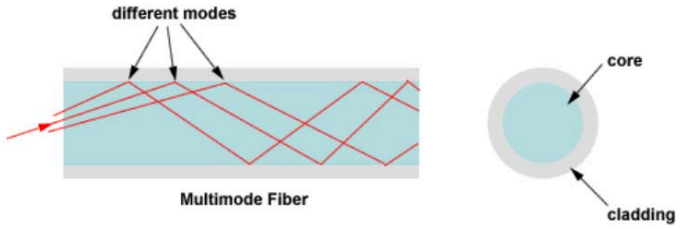

Fig. 3: Construction of a Multi-Mode Fibre Optic Cable [31]

4.3 Step-Index Multimode Fibre Cable

Step-index multimode fibre features a substantial core diameter of up to 100 µm. Consequently, the digital pulse within this fibre may traverse distinct pathways, with some light rays following a direct route and others adopting a zigzag pattern as they reflect off the cladding. These diverse trajectories result in separate arrivals of different groupings of light rays, denoted as modes, at the receiving point. The diverse modes comprising the light pulse contribute to its dispersion, leading to a loss of its well-defined shape. The necessity to introduce spacing between pulses to avert overlap imposes constraints on bandwidth. Hence, this classification of fibre optics cable is optimally suited for the transmission of signals over limited distances [30]. Fig. 4 shows the construction of a step-index multimode fibre optic cable.

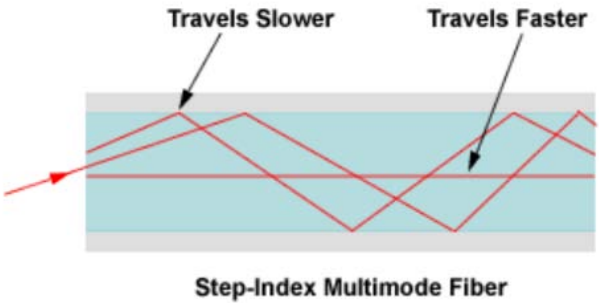

Fig. 4 Construction of a Step-Index Multi-Mode Fibre Optic Cable [31]

4.4 Graded-Index Multimode Fibre Cable

Graded-index multimode fibre features a core where the refractive index decreases progressively from the centre towards the cladding. This gradient causes light rays to move closer to the axis to move more slowly compared to those nearer the cladding [37]. Rather than meandering off the cladding, the light in the core curves helically because of the graded index, decreasing its travel distance. The shortened distance and the high speed allow the light at the periphery to arrive at the receiver at the same time as the slow but straight rays in the central core axis. This results in a digital pulse that suffers less dispersion [6]. Fig. 5 shows the construction of a graded-index multimode fibre optic cable.

Different light modes in a graded-index multimode fibre still follow different lengths along the fibre, as in a step-index multimode fibre. However, their speeds differ because the speed of guided light changes with the fibre core's refractive index [31].

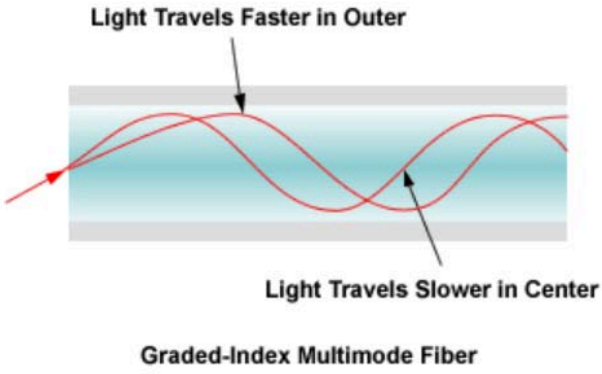

Fig. 5: Construction of a Graded-Index Multi-Mode Fibre Optic Cable [31]

V. FIBRE OPTICS CABLE DEPLOYMENT

Ghana has embraced the global standard of employing single-mode fibre optics cables for long-distance transmission, with MNOs exercising discretion in selecting parameters such as cable wavelength, losses, bending strength, and connectors. The nuanced decisions made by MNOs in these aspects carry significant technical implications, and the investigation undertaken in this study unveils instances where bare fibre-optic cables were deployed within subterranean trenches. This deployment strategy, observed in various cases, has resulted in cable incisions during road construction activities along those specific routes, elucidating the potential challenges arising from the selection of improper parameters or cables for a given project.

5.1 Standards and Practices for Fibre Optics Cable Deployment

Fibre optics deployment is governed by a set of standardised practices aimed at ensuring the efficiency, reliability, and longevity of telecommunications networks. In the Ghanaian context, the integration of international standards is exemplified through the predominant use of single-mode fibre optics cables for extensive data transmission, coupled with the discretionary authority vested in MNOs for critical parameters such as cable wavelength, losses, bending strength, and connectors [32].

Key tenets of fibre optics deployment standards encompass meticulous attention to cable specifications, installation methodologies, and maintenance protocols. Comprehensive guidelines, as outlined by bodies such as the International Electrotechnical Commission (IEC) and the Telecommunications Industry Association (TIA), prescribe the technical specifications and performance criteria for fibre optics cables, ensuring uniformity and interoperability within global telecommunications frameworks [32], [33].

Recent studies underscore the imperative of strategic decision-making in deploying fibre-optic cables. Noteworthy contributions include the work, which delves into the optimisation of cable wavelength for enhanced signal transmission, and [32], [33], focusing on advanced methodologies to mitigate signal losses in fibre optics systems. Additionally, elucidates considerations in enhancing bending strength, offering insights into mitigating vulnerabilities associated with cable installation practices. In the realm of connector technologies, it provides a contemporary overview, presenting innovations that optimise signal integrity and robust connectivity [33]. These recent references collectively emphasise the multidimensional nature of fibre optics deployment standards, underscoring the necessity for a holistic approach that integrates technical specifications, installation methodologies, and evolving technologies. The incorporation of such standards is paramount for establishing resilient and future-proof telecommunication infrastructures [33]

The TIA 568 standard, a cornerstone for premises cabling in the United States, is widely adopted by manufacturers and users of premises cabling systems. On the international stage, the IEC/ISO 11801 standard closely aligns with TIA 568, albeit

with variations across different countries. Notably, TIA-568 has undergone continuous revisions since its inception, with the latest iteration being "568 C." This version introduces significant modifications in the realm of fibre optics, incorporating sections from IEC standards to align with international standardisation efforts [32], [33]

The evolution of TIA 568 remains an ongoing process, marked by the incorporation of novel considerations. Noteworthy updates encompass the inclusion of passive optical LANs based on FTTH PONs and an expanded focus on the polarity of array fibre connection systems. The latter has become a substantial component of the standard, underscoring the intricacies inherent in this field. It is worth noting that despite the evolving landscape, the issue of high component losses persists, particularly with a connector loss allowance of 0.75 dB. Awareness of this challenge is widespread, yet resistance to altering the standard prevails among manufacturers, primarily due to stringent controls on their product offerings [32], [33].

Fibre Optic Cable Performance Standards for 568 B3 added 50/125 fibre as an acceptable type and specifies the performance of cabled fibre as shown in Table I.

Table I: Fibre Optic Cable Performance Standards for 568 B3 added 50/125 [32], [33]

Fibre Type	Wavelength (nm)	Max Attenuation Coefficient (dB/km)	Bandwidth (MHz-km with overfilled launch)
50/125 (OM2, OM3, OM4)	850	3.5	500 (OM2), 2000 (OM3), 3500 (OM4)
	1300	1.5	500
62.5/125 (OM1)	850	3.5	160
	1300	1.5	500
Single mode (OS1, OS2) (Premises)	1310	1.0	NA
	1550	1.0	NA
Single mode (OS1, OS2) (Outside Plant)	1310	0.5	NA
	1550	0.5	NA

VI. FIBRE OPTICS CABLE DEPLOYMENT METHODOLOGIES

The deployment of fibre optic cables encompasses a multitude of methodologies, with the selection of an installation method contingent upon several pivotal factors, including the environmental context, developmental landscape, business considerations, and population density. The meticulous evaluation of these critical determinants is imperative to ensure the efficacious deployment and subsequent facile maintenance of the cable infrastructure post-installation. This study's empirical findings underscore the substantial financial implications associated with fibre optic projects, revealing that a substantial proportion, ranging between 60% and 80% of the capital costs, is attributable to civil work, ducts, and cables [34].

The installation of fibre optic cables encompasses three distinct techniques: aerial, underground, and submarine. Aerial deployment involves installing cables on pylons or utility poles, while underground installation entails burying cables beneath the Earth's surface at a predetermined depth. Submarine installation, on the other hand, pertains to the transmission of cables beneath the seabed. Each method necessitates careful consideration of its respective advantages and challenges, with the ultimate choice contingent upon the specific contextual exigencies and project requirements [34].

6.1 Aerial Fibre Optics Installation

Aerial deployment of fibre optic cables introduces a dynamic environment characterised by continuous tension, compounded by additional forces stemming from temperature fluctuations, wind dynamics, and, notably, the load exerted by

ice accumulation in colder regions. The inherent tensile limitations of most fibre optic cables necessitate specialised considerations for direct aerial installation. Addressing this challenge involves employing distinct installation techniques tailored for cables explicitly designed for aerial deployment [34].

An elemental strategy involves the utilisation of a conventional fibre cable, typically a metallic stranded variant, as a lashing element to provide the requisite support. Alternatively, in cases where the inherent strength of the primary cable is insufficient, the deployment may necessitate an additional supporting cable. Crucially, the supplementary cable must possess the requisite tensile strength to sustain the fibre optic cable's weight over the expanse between support structures. This complex interplay of forces and material characteristics underscores the nuanced engineering considerations essential for successful and resilient aerial fibre optic cable installations [35].

Prudent consideration is imperative during the installation of fibre optic cables with a supporting cable, particularly to address the accommodation of length differentials arising from factors such as elongation induced by wind dynamics or variations in temperature. Given the intrinsic design of fibre optic cables to resist stretching and mitigate stress on the optical fibre, the installation necessitates the incorporation of slack, typically strategically positioned at support structures. This proactive measure serves to alleviate tension on the fibre optic cable when alterations in messenger length occur, safeguarding the integrity of the optical fibre and ensuring the sustained efficacy of the cable system [35].

A subclass of aerial cables, specifically the All-Dielectric Self-Supporting (ADSS) cables, is characterised by a robust design featuring an augmented jacket thickness, engineered to confer adequate tensile strength for enduring the challenges of aerial installation. This installation is facilitated through specialised hardware meticulously designed to securely grip the cable jacket, minimising the risk of long-term damage during periods of elevated tension loading. In tandem, the optical power ground wire (OPGW) represents an alternative aerial cable variant, wherein a hermetically sealed tube envelops a high-voltage conductor, housing an embedded optical fibre cable. This composite cable configuration finds widespread utility globally, serving dual purposes of communication and power transmission [34].

The deployment of OPGW mirrors high-voltage cable installation methodologies, with termination or splicing activities conducted at ground level. The terminated ends are then carefully coiled on the supporting tower. In instances necessitating communication equipment at specific locations, fibre optic cables are extended from the spliced sections within the equipment room. In adherence to best practices for aerial cable installations requiring splicing or termination, a surplus of 30-60 ft (10-20 m) of cable is recommended to facilitate these activities. Notably, in scenarios where splicing is executed on ground-installed cables atop tall poles, a more substantial quantity of fibre cables may be required, underscoring the intricacies of aerial cable infrastructure planning [36]. Fig. 6 shows a typical aerial fibre optics installation.

Fig. 6: A Typical Aerial Fibre Optics Installation [38]

6.2 Underground Fibre Optics Installation

Subterranean deployment of fibre optic cables assumes a pivotal role in the establishment of extensive cabling infrastructures across diverse terrains, urban landscapes, and areas necessitating safeguarding against adversarial weather conditions. This methodology encompasses the embedding of cables directly into the ground or encapsulating the fibre optic within an underground-buried duct. In scenarios demanding cross-country installations, the prevalent practice involves the direct burial of fibre cables, typically encased in protective steel armour, within a trench excavated to prescribed depths. The incorporation of steel armour serves the dual purpose of shielding the fibre optic cable from environmental exigencies and mitigating risks posed by subterranean fauna. This intricate subterranean deployment strategy reflects a conscientious approach to fortifying fibre optic infrastructures against diverse challenges inherent in varied geographical and environmental contexts [29].

6.3 Direct-Buried Fibre Optics Installation

Direct-buried cables are meticulously designed with stringent specifications to withstand defined tolerances in terms of heat, moisture, electrical conductivity, and soil acidity [38]. In contradistinction to conventional telecommunications and power cables, typified by limited insulation and an exterior waterproof layer, direct-buried cables manifest a sophisticated architecture comprising multiple strata. These strata encompass sturdy metallic-banded sheathing, reinforced by substantial rubber casings, an absorbent gel matrix for shock attenuation, thread-reinforced waterproof tape, and further augmented by a rigid metal core. The intricacies inherent in this design not only augment the cable's structural integrity but also contribute to its resilience in the face of external environmental exigencies. Notably, direct-buried cables, characterised by their comprehensive construction, offer a cost-effective and expeditious installation alternative, distinguishing themselves from cables necessitating supplementary protective measures against subterranean elements [29].

Nevertheless, direct-buried cables are susceptible to inadvertent severance during excavation or digging activities, rendering their prevalence more prominent on secondary roads rather than primary thoroughfares. The strategic advantage of direct-buried cables lies in their capacity for installation with minimal effort, obviating the need for preparatory groundwork such as piping installation or other accommodations [39]. Essentially, the direct-buried cable, when positioned subterraneously without the need for additional coverage, becomes immediately operational for voice and data transmissions. The self-contained nature of the fibre cable, coupled with its resilience against environmental elements that contribute to the degradation of alternative cable types, not only mitigates the need for frequent replacements but also enhances the likelihood of maintaining structural integrity even in the face of natural calamities [40].

6.4 Installation in Duct Fibre Optics

In highly urbanised areas, the common underground application is duct installation, as it becomes more challenging to dig through the ground. The fibre optic cables that are placed in installed ducts are even easier to place since it is possible to use fibre optic cables not covered with steel armour. The duct protects the fibre optic cables as they get exposed to harsh surroundings. Expansion of the fibre cabling is easy to implement as there is no need to dig trenches for the installation [40]. The benefits of underground fibre optic installation, being less exposed to adverse weather conditions, will help further in adopting underground fibre optic installation. These cable types require more stringent protection since their materials are very susceptible to moisture and mechanical stress. Damage can be costly in terms of interrupted service and replacement costs. Also, these cables are installed in very long, continuous runs, which require a clear, protected pathway, as well as a leak-free system. The cables are pulled in the conduit that is being buried underground, usually 3-4 ft (1-1.2 m) deep to reduce the likelihood of accidentally being dug up. The process regularly begins with digging a trench to bury the conduit, which is generally a 4-in. plastic pipe, sometimes with a preinstalled inner duct [41]. Inserting a cable into a conduit already containing several others can lead to tangling, which increases pulling tension and risks damaging the cables. However, if the combined cable fill and pulling tension remain within recommended limits, multiple cables can be pulled simultaneously [41].

VII. SURVEY ON FIBRE OPTICS DEPLOYMENT IN GHANA

The liberalisation of Ghana's telecommunications sector ushered in an era that enabled numerous private operators to invest in, own, and manage telecommunication infrastructure, facilitating the provision of communication services to end-users [6]. The commercial implementation of optical infrastructure in Ghana commenced in the latter part of 2000, marking a transformative shift as fibre deployment supplanted the prevailing radio wave transmission systems. A decade after this pivotal development, a heightened focus has been directed towards the extensive deployment of fibre optics infrastructure, providing individuals as well as private and public institutions with widespread access to this distributed optical network [41].

7.1 Inland Fibre Optic Deployment in Ghana

The quintet of MNOs in Ghana, comprising MTN, Tigo, Glo, Vodafone, and Airtel, holding telecommunications licenses, have implemented comprehensive fibre-optic cable deployments. These deployments serve a dual function: reinforcing backbone redundancy in conjunction with pre-existing microwave transmission infrastructure and establishing a metro fibre network to cater to escalating demands for data and voice traffic among end-users. A pioneering initiative in this transformative trajectory was undertaken by Vodacom, a subsidiary of the Volta River Authority, with the installation of Ghana's inaugural backbone fibre optics network. Capitalising on existing pylons, Vodacom executed an innovative aerial deployment of fibre optic cables along the southern and mid-sections of the national power grid [6].

MTN, in its strategic pursuit of augmenting data and voice traffic capabilities, has undertaken an extensive nationwide deployment of an optical network. Employing an underground deployment strategy, MTN has interlinked all 16 regions in Ghana. Furthermore, both MTN and Vodafone Ghana have implemented underground fibre metro networks (FTTx) across approximately 38 cities and towns, complementing their backbone interconnections. Concurrently, Airtel Ghana, Tigo, and Glo have opted for subterranean deployment, burying fibre cables underground. This concerted effort not only amplifies backbone route capacity but also establishes redundant routes, fortifying existing microwave links. Collectively, these initiatives contribute to the robustness and resilience of Ghana's telecommunications infrastructure, underscoring the significance of such advancements in a scholarly context.

The graphical representation in Fig. 7 illustrates the deployment of MTN's fibre optics network infrastructure, encompassing both backbone and metro rings, facilitating the execution of their network operations and traffic management. The yellow lines indicate the backbone's connectivity, and the blue ones are the metro rings.

7.2 Existing Fibre Optic Deployment in Ghana for Telecommunication Operators Superimposed on Ghana Map

The progression of fibre optic deployment in Ghana has evolved through various developmental phases, driven by telecommunications operators, government agencies, and private entities within the telecommunications industry. The primary objective is to achieve comprehensive coverage across the entirety of Ghana, facilitating the provision of services such as voice communication, internet access, and diverse user applications. Fig. 8 provides a visual representation delineating the deployment of diverse fibre optics network infrastructures across the map of Ghana, as delineated in the legend. The use of distinct colours in the legend corresponds to different telecommunications operators, highlighting their contributions in establishing both backbone and metro rings that interconnect the entire country.

VIII. FIBRE OPTICS DEPLOYMENT CHALLENGES FOR INLAND AND SUBMARINE IN GHANA AND GLOBAL

The deployment of fibre optics entails a series of processes and procedures, the non-adherence to which poses potential threats to the overall project. Given the multifunctional nature of the project involving various units, a thorough consultation process is imperative. Challenges in fibre deployment can be categorised into technical and managerial difficulties.

8.1 Technical Challenges in Fibre Deployment

Implementing underground fibre optics infrastructure in a developing nation like Ghana poses numerous technical challenges. The route of underground fibre optic cables typically aligns with highways and city roads. However, in an environment characterised by unauthorised construction, the planning and adherence to fibre routes become intricate. Executing fibre deployment as initially designed becomes problematic [42]. The shared utilisation of the existing right-of-way (ROW) among multiple MNOs introduces challenges, notably the recurrent incidents of fibre cable cuts. When an MNO seeks authorisation to deploy its fibre optic cable while sharing the ROW with an existing MNO, the existing MNO's fibre cable inherently confronts an elevated risk of being severed during excavation. The primary cause of fibre optic cable cuts is attributed to the shallow depth of cable burial, particularly in congested ROW scenarios [42].

8.2 Right of Way from Local Authorities

The acquisition of ROW for laying optical cables along highways entails considerable costs and time, posing challenges for MNOs. The intricate process of obtaining a license to deploy fibre optic cables along public streets is arduous and can directly impact implementation timelines. Efficient ROW management is imperative in optical infrastructure deployment. Numerous MNOs have observed that overly demanding information requests impede progress, and difficulties in permit acquisition, along with exorbitant charges for ROW use, coupled with onerous remediation and maintenance demands, further contribute to implementation delays [43], [44]. Additionally, the intricate array of procedures across various localities complicates the installation of facilities across municipal boundaries, rendering the process both costly and time-consuming. While affected communities emphasise the necessity for flexibility in regulating the use of public ROWs to facilitate the deployment and fault tracing of underground fibre optic cables, city authorities cite a lack of personnel as a contributing factor to potential delays in permit processing.

8.3 Administrative Challenges

The existing permit and licensing framework poses significant challenges to the implementation of fibre projects. Bureaucratic processes within local authorities, coupled with the absence of procedural guidelines to regulate their activities, undermine the deployment of optical infrastructure. Many local authorities acknowledge the necessity to streamline the processing period for ROW between the initial permit application filing and the final installation of facilities. In the United States, for example, certain cities have imposed strict cutoff dates for approving or denying registrations to expedite installation. Others have instituted blanket permits, eliminating the need for individual registrations for each facility installation [42]. States like Kansas, Indiana, Ohio, and Florida have stipulated 30-day deadlines for permit processing, while Michigan and Virginia have established 45-day deadlines.

Administrative challenges also encompass the fees associated with permit processing and unwarranted delays in approval processes. The disparate pricing of identical services across different administrative areas within the country is deemed inappropriate, hindering the progress of optical infrastructure deployment processes [37]. The absence of a standardised fee structure and best practices leads to arbitrary fee charges and delays, impacting the entire project life cycle. In advanced countries such as the United States, Europe, Australia, and parts of Asia, a variety of fee structures associated with using the ROW and other facilities exist, and government agencies are mandated to adhere to approved fee structures. However, in certain African countries like Nigeria, Egypt, Kenya, South Africa, and Rwanda, the decentralisation processes involved in permit acquisition have not been fully adopted, with central governments typically controlling all processing fees. The absence of proper structures to regulate optical project implementation results in road network destruction and vice versa, contributing to road accidents in parts of African countries where ineffective administrative measures impede optical project implementation [37].

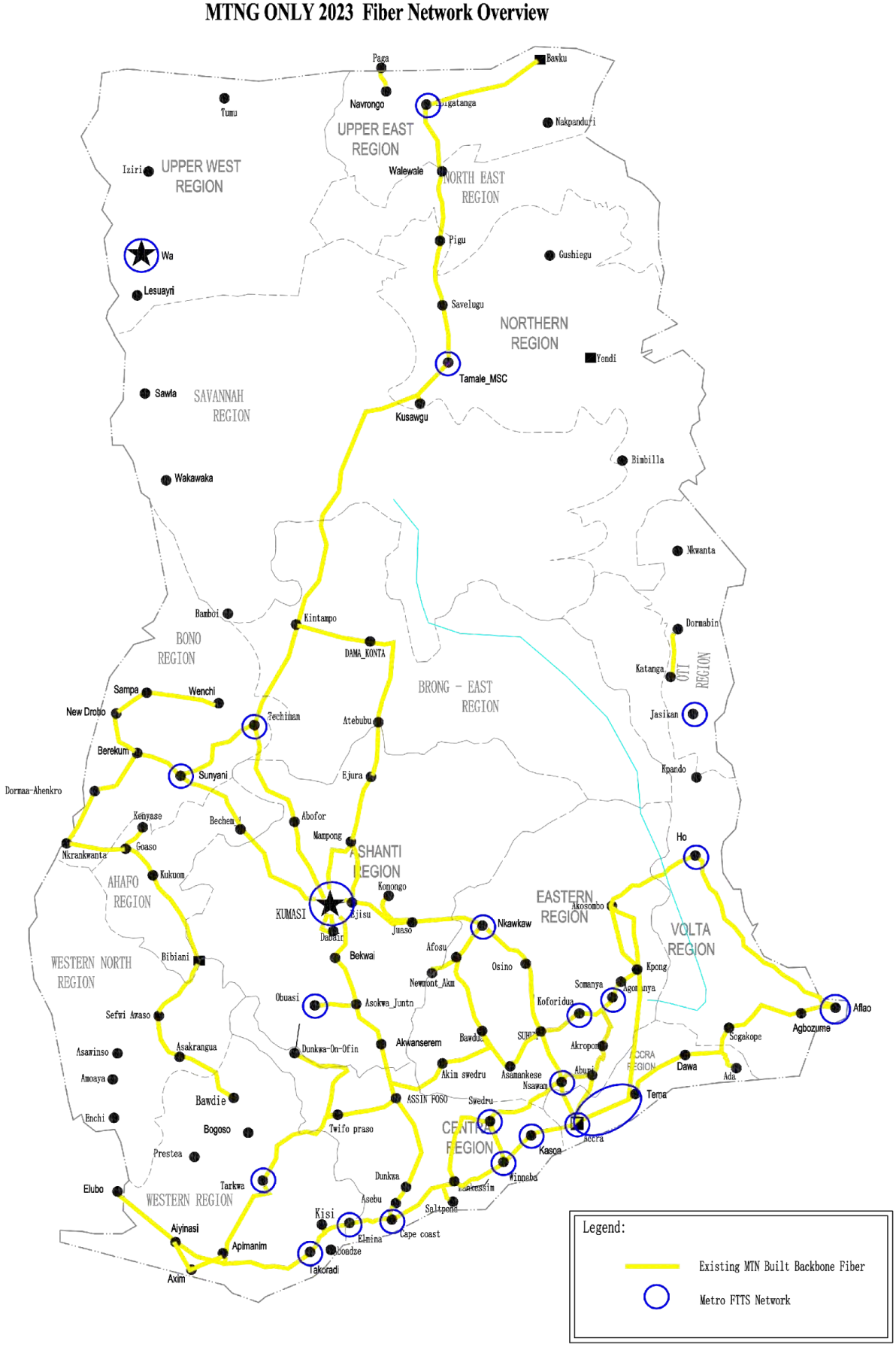

Fig. 7: MTN's fibre optics network infrastructure [46]

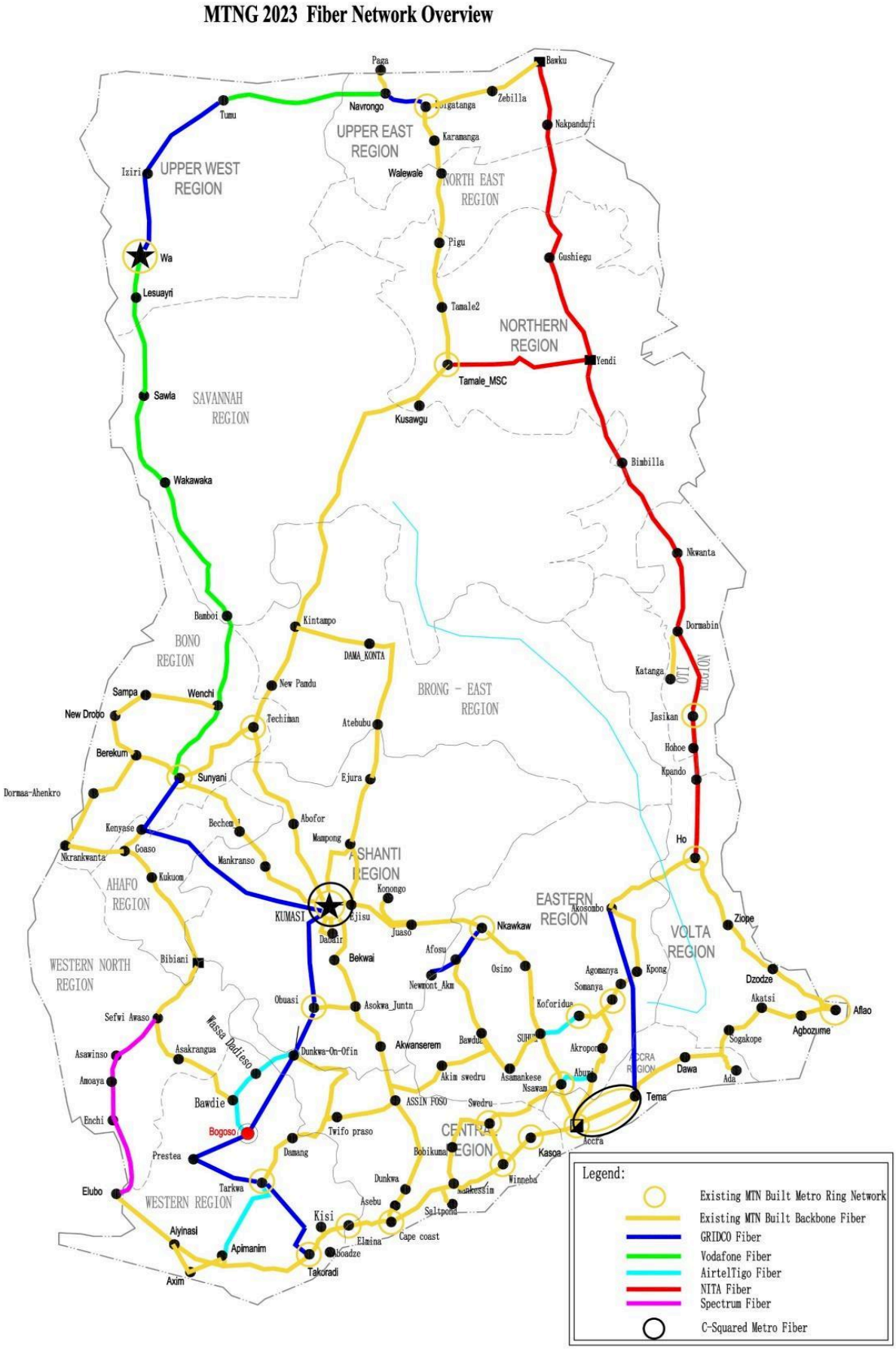

Fig. 8: Visual representation delineating the deployment of diverse fibre optics network infrastructures across the map of Ghana [46]

Lastly, deficient information management represents a significant administrative shortcoming affecting optical deployment projects. Obtaining necessary route information for existing utility infrastructure proves challenging, and understanding the current underground landscape is crucial for informed project planning. The persistent disruptions in utility services during trenching activities result from the lack of Geographic Information System (GIS) data on existing infrastructure.

8.4 Post-Fibre Deployment Management Challenges

Fibre management constitutes an engineering-based framework aimed at preserving, operating, maintaining, repairing, and renewing fibre infrastructure, all within the constraints of limited funding. Fibre optics networks, serving as highly efficient data-intensive communication systems, play a pivotal role in transmitting voice, data, and video. The significance of fibre optics stems from the data-intensive demands of telecommunications and the ongoing shift from narrowband to broadband. Consequently, effective management of this infrastructure is imperative for both MNOs and end-users [42]. Research findings indicate that underground cable cuts in Ghana have had a substantial adverse impact on telecommunication services. Deliberate acts of damage to fibre-optic cables at various locations in Ghana have led to service disruptions affecting tens of thousands of users. Protecting fibre optics networks from intentional or unintentional damage, cuts, bends, or any activity with the potential to harm the cables is paramount [42].

IX. DISCUSSION ON THE SURVEY

Fibre optic cable cuts persist as the predominant cause of network outages in the telecommunications industry in Ghana. The primary factors contributing to fibre optics cable failures are primarily linked to excavation activities, inadequate communication between stakeholders, and the absence of precise mapping and location data for optical network routes. The deployment of fibre optics in Ghana lacks well-established processes and guidelines, resulting in diverse challenges that have become the underlying causes of failures. Cumbersome permit processes emerge as a hindrance to seamless fibre optics deployment, with many local authorities lacking transparent procedures and timelines for application and response to permit requests. Consequently, local authorities exploit this situation to unduly prolong the permit acquisition processes. The acquisition of ROW is a costly endeavour, and protracted processes invariably frustrate MNOs.

The deployment of optical networks encounters significant delays attributed to excessively demanding requests for information, bureaucratic hurdles in obtaining permits, and unreasonable charges for ROW usage. ROW-related issues are highly intricate, involving multiple stakeholders with divergent opinions and parochial interests. Despite being widely acknowledged as the optimal mode of transmission to meet high-capacity demands, reduce failures, and enhance network quality, there is a paucity of regulatory standards outlining appropriate practices and techniques for deploying and managing fibre optic cables in Ghana. Although the National Communication Authority (NCA) is tasked with regulating fibre-optic cable deployment and management in Ghana, there is a notable absence of stringent regulatory guidelines governing the implementation of fibre optics in the country.

The frequent disruption of network services due to numerous fibre cable cuts has raised concerns among industry stakeholders and regulators alike. These cuts not only lead to service interruptions but also result in significant revenue losses. The financial strain on Capital Expenditure (Capex) and Operational Expenditure (Opex) prompts MNOs to question the rationale behind investing in an infrastructure that brings discomfort and financial losses. MNOs have implemented various initiatives, such as creating redundant links and backups, to mitigate the impact of fibre-optic cable cuts. Despite these efforts, additional complex and cost-intensive mechanisms have been explored to further reduce the impact of frequent fibre cuts on the network.

The arguments for fibre optic cable deployment have primarily emphasised the advantages it brings to the network. However, limited attention has been devoted to developing policies and guidelines for evaluating fibre-optic cable deployment based on revenue optimisation. The deployment of fibre-optic cables introduces complexities into the current network architecture, posing a risk of undermining the benefits if not properly managed. The entire value chain process of fibre deployment and management requires a technical review to align with best practices. Regulators should formulate clear policies and deployment guidelines that are friendly and fair, establishing a well-structured technical framework for fibre optics deployment and management.

Legislation on optical network infrastructure sharing extends beyond fibre-optic cable sharing to encompass other resources. Local authorities need to streamline permitting processes, implementing a clear procedural framework with tight deadlines for approving or denying requests for ROW or any form of permit. To enhance accountability, copies of updated fibre routes should be provided to all local authorities, major road contractors, and the roads and highways department. In this way, any contractor responsible for excavation should be surcharged with the cost of the damage.

9.1 The Coverage Gap on Fibre Optic Deployment in Ghana Among Telecommunication Operators

The coverage gap in the context of fibre optics deployment in the paper refers to the areas within Ghana that lack comprehensive coverage by fibre optic networks. This includes regions or specific locations where the deployment of fibre optic infrastructure is either insufficient or non-existent, leading to limited or no access to high-speed internet connectivity and other telecommunications services. The paper aims to identify these coverage gaps and provide recommendations for improving the deployment of fibre optic networks to bridge these gaps and ensure widespread access to telecommunications services across Ghana.

Limitations on Fibre Optic Deployment in Ghana
The limitations for fibre optics deployment highlighted in the paper include:

1. Technical Challenges: The paper discusses technical difficulties such as cable incisions during road construction activities due to improper deployment strategies, as well as challenges related to signal losses and cable wavelength optimisation.
2. Regulatory Issues: The absence of appropriate regulatory policies governing the deployment of optical cables is identified as a limitation, leading to difficulties in managing fibre optic infrastructure.
3. Management Challenges: The paper addresses challenges related to the management of fibre infrastructure, including the preservation, operation, maintenance, and repair of ageing fibre infrastructure within the constraints of limited funding.
4. Permit Acquisition Processes: Cumbersome permit processes and protracted acquisition of ROW are highlighted as hindrances to seamless fibre optics deployment, leading to significant delays and frustration for MNOs.
5. Lack of Well-Established Processes and Guidelines: The deployment of fibre optics in Ghana is noted to lack well-established processes and guidelines, resulting in diverse challenges that have become the underlying causes of failures.

These limitations underscore the complexities and multifaceted nature of deploying fibre optic networks in Ghana, encompassing technical, regulatory, and managerial challenges that need to be addressed for successful and widespread deployment.

X. CONCLUSIONS

The research conclusions of this paper include:

1. Fibre Optic Deployment in Ghana: The paper concludes that the deployment of fibre optic networks in Ghana is essential for improving telecommunications services, increasing network capacity, enhancing reliability, and contributing to economic growth.
2. Technical, Regulatory, and Managerial Challenges: The paper concludes that the

deployment of fibre optic networks in Ghana is associated with technical, regulatory, and managerial challenges that need to be addressed to ensure successful and widespread deployment.

3. Mitigating Limitations: The paper concludes that collaboration, improved deployment strategies, efficient ROW management, appropriate regulatory policies, and effective fibre management are essential for mitigating the limitations on fibre optic deployment in Ghana.

Overall, the paper emphasises the importance of fibre optic deployment in Ghana, highlights the challenges associated with deploying fibre optic networks, and provides recommendations for mitigating these limitations to ensure successful and widespread deployment.

10.1 Recommendations to Mitigate Limitations on Fibre Optic Deployment in Ghana

The paper provides several recommendations to mitigate the limitations on fibre optic deployment in Ghana, including:

1. Collaboration and Consultation: The paper recommends that stakeholders in the telecommunications industry should collaborate and consult with each other to ensure that fibre optic deployment adheres to established guidelines and processes
2. Improved Deployment Strategies: The paper suggests that improved deployment strategies, such as proper cable burial depth and the use of micro ducts, can help mitigate technical challenges associated with fibre optic deployment.
3. Efficient ROW Management: The paper recommends that efficient ROW management is imperative in optical infrastructure deployment, and local authorities should establish transparent procedures and timelines for application and response to permit requests.
4. Regulatory Framework: The paper suggests that appropriate regulatory policies should be established to govern the deployment of optical cables, providing guidelines for deploying and managing fibre optic cables in Ghana.
5. Effective Fibre Management: The paper recommends that effective fibre management is imperative for both MNOs and end-users and that MNOs should prioritise the preservation, operation, maintenance, repair, and renewal of ageing fibre infrastructure.

Overall, the paper emphasises the need for collaboration, improved deployment strategies, efficient ROW management, appropriate regulatory policies, and effective fibre management to mitigate the limitations on fibre optic deployment in Ghana.

10.2 Benefits of Fibre Optic Deployment in Ghana

The paper highlights several benefits of fibre optic deployment in Ghana, including:

1. High-Speed Internet Connectivity: Fibre optic networks provide high-speed internet connectivity, enabling faster data transfer rates and improved access to online services and applications.
2. Improved Telecommunications Services: Fibre optic networks provide improved telecommunications services, including voice communication, internet access, and diverse user applications.
3. Increased Network Capacity: Fibre optic networks have a higher bandwidth capacity than traditional copper wire networks, enabling more data to be transmitted over longer distances.
4. Enhanced Reliability: Fibre optic networks are less susceptible to interference and signal degradation, providing enhanced reliability and fewer service disruptions.
6. Cost-Effective: Fibre optic networks are cost-effective in the long run, as they require less maintenance and have a longer lifespan than traditional copper wire networks.
7. Economic Growth: The deployment of fibre optic networks can contribute to economic growth by providing businesses with access to high-speed internet connectivity, enabling them to expand their operations and reach new markets.

Overall, the deployment of fibre optic networks in Ghana can provide significant benefits, including improved telecommunications services, increased network capacity, enhanced reliability, cost-effectiveness, and economic growth.

10.3 Research Contributions

The research contributions of this paper include:

1. Identification of Coverage Gaps: The paper identifies coverage gaps in Ghana where the deployment of fibre optic infrastructure is either insufficient or non-existent, providing a basis for improving the deployment of fibre optic networks to ensure widespread access to telecommunications services across Ghana.
2. Assessment of Technical, Regulatory, and Managerial Challenges: The paper assesses the technical, regulatory, and managerial challenges associated with fibre optic deployment in Ghana, providing insights into the complexities and multifaceted nature of deploying fibre optic networks in Ghana.
3. Recommendations for Mitigating Limitations: The paper provides recommendations for mitigating the limitations on fibre optic deployment in Ghana, including collaboration and consultation, improved deployment strategies, efficient ROW management, appropriate regulatory policies, and effective fibre management.

10.4 Research Directions

The paper suggests research directions for future studies, including the need for further research on the economic impact of fibre optic deployment in Ghana, the development of efficient deployment strategies, and the establishment of appropriate regulatory policies to govern the deployment of optical cables.

Overall, the paper provides valuable insights into the challenges and opportunities associated with fibre optic deployment in Ghana and provides recommendations for improving the deployment of fibre optic networks to ensure widespread access to telecommunications services across Ghana.

REFERENCES

1. Kiminza MM, Were S. Factors affecting successful implementation of fibre optic cable projects in Kenya: A case of Nairobi City County. International Institute for Science, Technology and Education (IISTE), pp. 52-59, 2016.
2. Tang BH, Zhou ZX. The design of a communication network optical fibre cable condition monitoring system based on a distributed optical fibre sensor. Paper presented at: 2018 International Conference on Electronics Technology (ICET); IEEE; May 2018:97-101.
3. Celik A, Shihada B, Alouini MS. Wireless data centre networks: advances, challenges, and opportunities. 2018. arXiv:1811.11717.
4. Fernando KM. Policy framework for developing the optical fibre network infrastructure in Sri Lanka. 2019. https://www.itu.int/ITU-D/treg/ publications/BB _ MDG_SriLanka_Final.pdf.
5. Sastrawidjaja L, Suryanegara M. Regulation challenges of 5G Spectrum deployment at 3.5 GHz: the framework for Indonesia. Paper presented at: 2018 Electrical Power, Electronics, Communications, Controls, and Informatics Seminar (EECCIS); IEEE; October 2018
6. O. Nyarko-Boateng, F. E. B. Xedagbui, A. F. Adekoya, and B. A. Weyori, “Fibre optic deployment challenges and their management in a developing country: A tutorial and case study in Ghana,” Engineering Reports, vol. 2, no. 2, Feb. 2020, doi: 10.1002/eng2.12121
7. Universitatea din Pitești, IEEE Romania Section, IEEE Industry Applications Society, and Institute of Electrical and Electronics Engineers, Proceedings of the 10th International Conference on Electronics, Computers and Artificial Intelligence - ECAI-2018: 28 June-30 June 2018.
8. L. Brisk, “A Methodology for the Deployment of Fibre-Optic Cables.
9. J. Cariolle, “fondation pour les études et recherches sur le développement international Telecommunication Submarine-Cable Deployment and the Digital Divide in Sub-Saharan Africa*.”

10. Ranaweera, Chathurika, et al. "Design and Optimisation of Fibre Optic Small-cell Backhaul Based on an Existing Fibre-to-the-node Residential Access Network." IEEE Communications Magazine, 2013, https://doi.org/10.1109/mcom.2013.6588652
11. M. C. Fenta, D. K. Potter, and J. Szanyi, "Fibre Optic Methods of Prospecting: A Comprehensive and Modern Branch of Geophysics," Surveys in Geophysics, vol. 42, no. 3. Springer Science and Business Media B.V., pp. 551–584, May 01, 2021. doi: 10.1007/s10712-021-09634-8.
12. H. A. Willebr and B. S. Ghuman, "Fibre Optics Without Fibre Beaming light through the air offers the speed of optics without the expense of fibre," 2001.
13. https://www.unclosdebate.org/evidence/2258/economic-output-many-countries-now-dependent-traffic-underseas-cables
14. 36th European Conference on Optical Communication: proceedings: September 19-23, 2010, Torino, Italy. IEEE, 2010.
15. D. E. Meddour, T. Rasheed, and Y. Gourhant, "On the role of infrastructure sharing for mobile network operators in emerging markets," Computer Networks, vol. 55, no. 7, pp. 1576–1591, May 2011, doi: 10.1016/j.comnet.2011.01.023
16. Ieee and Ieee, 2013 OFC Collocated National Fibre Optic Engineers Conference OFC/NFOEC 2013.
17. E. Paul, Jr. Green, "Fibre to the Home: The Next Big Broadband Thing," IEEE Communications Magazine, September 2004.
18. https://blog.telegeography.com/feast-your-eyes-on-the-2023-submarine-cable-map?utm_source=comms_update
19. S. Frempong, "AC 2007-1974: The Submarine Communications Cable Ring in Africa."
20. Saleh AA, Mustafa AB, Osman AA. Proposal laying fibre optic cables along railway tracks in Sudan. IOSR J Comput Eng. 2015;5(2):90-94.
21. Matthews VO, Uzairue SI, Noma-Osaghae E. Analysis and implementation of fibre to the home network using Peace Estate Lagos as a case study. Int J Sci Technol Manage Res. 2018;3(8):1-4.
22. Going RW, Lauermann M, Maher R, et al. 1.00 (0.88) Tb/s per wave capable coherent multi-channel transmitter (receiver) In P-based PICs with hybrid integrated SiGe electronics. IEEE J Quantum Electron. 2018;54(4):1-10.
23. Presi M, Cossu G, Contestabile G, et al. Transmission in 125-km SMF with 3.9-bit/s/Hz spectral efficiency using a single-drive MZM and a direct-detection Kramers-Kronig receiver without optical CD compensation. Paper presented at: 2018 Optical Fibre Communications Conference and Exposition (OFC); IEEE; January 2024:1-3
24. Uzairue SI, Matthews VO, Ochonogor C, Amaize P, Anyasi FI. Experimental analysis of cable distance effect on signal attenuation in single and multimode fibre optics. Int J Electric Comput Eng. 2018;8(3):1577-1582.
25. Chen X, Himmelreich JE, Hurley JE, et al. Universal fibre for short-distance optical communications. J Lightwave Technol. 2019;37(2):389-395.
26. Majumdar AK. Optical Wireless Communications for Broadband Global Internet Connectivity: Fundamentals and Potential Applications. Elsevier Science; 2018:117-168. https://doi.org/10.1016/B978-0-12-813365-1.00005-9.
27. Henriques HO, Barbero APL, Ribeiro RM, et al. Proposal of a fault prediction system for underground installations. Measurement. 2016; 81:232-240. https://doi.org/ 10.1016/j.measurement.2015.12.010.
28. https://www.fibreoptics4sale.com/blogs/archive-posts/95152198-multimode-fibre-and-multimode-fibre-optic-cable-tutorial, January 2024.
29. https://www.thefoa.org/tech/tia568b3.htm. January 2024.
30. Lui G. Study of the method of laying fibre optic cable in the same trench with pipeline in the permafrost region. Paper presented at: International Petroleum and Petrochemical Technology Conference; March 2018; Springer, Singapore; 152-158.

31. Poprawe R, Boucke K, Hoffman D. The history of laser. Tailored Light. Vol 1. Berlin, Germany: Springer; 2018:1-6.
32. Hendrickson D, Richardson DK. U.S. Patent No. 9,904,029. Washington, DC: U.S. Patent and Trademark Office. 2018.
33. https://engineering.fb.com/2020/07/13/connectivity/aerial-fibre-deployment/, January 2024.
34. Al-Baldawi IA, Alsakini SR, Abed MS. The effects of sand and pipes on the temperature distributions of the underground cable. IOP Conf Ser Mater Sci Eng. 2019;518(4):042012.
35. Tsuritani T, Soma D, Wakayama Y, et al. Field test of installed high-density optical fibre cable with multi-core fibres toward practical deployment. Paper presented at: 2019 Optical Fibre Communications Conference and Exhibition (OFC); IEEE; March 2019:1-3.
36. Astic JY, Bareux G, Buhagiar T, et al. Control centre designs: new functions and challenges for the transmission system operator. IEEE Power Energy Mag. 2018;16(2):57-66.
37. Farmer J, Lane B, Bourg K, Wang W. Network management architecture and design. FTTx Networks. Burlington, MA: Elsevier, Morgan Kaufmann; 2017:323-344 ISBN 978012 4201378.
38. Zhou X, Liu H, Urata R, Zebian S. Scaling large data centre interconnects: challenges and solutions. Opt Fibre Technol. 2018; 44:61-68.
39. Yun B. Design of underground structures. Underground Engineering. Cambridge, MA: Academic Press, Elsevier; 2019:47-115. https://doi.org/10.1016/b978-0-12-812702-5.00003-7.
40. Tekin T, Pitwon R, Nikolaos P, Håkansson A. Optical Interconnects for Data Centres. Sawston, Cambridge: Woodhead Publishing, Elsevier; 2017:43-73. https://doi.org/10.1016/C2014-0-04130-5.
41. Gilmore M, Manivannan M. Telecommunications Cabling: Guidance on Standards and Best Practice for Construction Projects. BSI Standards Limited; 2012. https://www.fia-online.co.uk/pdf/BIP0123flyer.pdf.
42. https://tmt.knect365.com/africa-tech-festival/sponsors/telecom-egypt-2023-vip-village-lead-sponsor/.
43. https://www.capacitymedia.com/article/2a2toszspei1x7gzm70g0/sponsored-content/egynnovation-in-the-subsea-industry.
44. https://www.hxfibrecable.com/whats-happening-inside-the-multimode-fibre/.
45. Telecom Egypt. (2023, February 21). Telecom Egypt extends its network reach through the SEA-ME-WE-6 cable and provides it a unique crossing route over its distinctive infrastructure. https://ir.te.eg/en/CorporateNews/PressRelease/155/Telecom-Egypt-extends-its-network-reach-through-SEA-ME-WE-6-cable-and-provides-it-a-unique-crossing-route-over-its-distinctive-infrastructure
46. MTN Ghana Limited (2024, December 30), Transmission Planning Department, Network Group Division.